A STUDY ON PHYSICAL AND DOSIMETRIC ASPECTS OF IMAGE GUIDED RADIATION THERAPY

Thesis submitted to the
University of Calicut in partial fulfillment of the
requirements for the degree of

DOCTOR OF PHILOSOPHY IN PHYSICS

SILPA AJAYKUMAR

DEPARTMENT OF PHYSICS
UNIVERSITY OF CALICUT
KERALA, INDIA 673 635

2021

CERTIFICATE

Certified that the work presented in this thesis entitled **A Study on Physical and Dosimetric Aspects of image Guided Radiation Therapy** is a bonafide work done by Mrs. Silpa AjayKumar, under my guidance in the Department of Physics, University of Calicut and that this work has not been included in any other thesis submitted previously for the award of any degree. I also certify that all the corrections/suggestions recommended by the adjudicators have been incorporated in the revised thesis

University of Calicut
September 2021

Prof. M.M Musthafa
(Supervising Guide)

DECLARATION

I hereby declare that the work presented in this thesis entitled '**A Study on Physical and Dosimetric Aspects of image Guided Radiation Therapy**' is based on the original work done by me under the guidance of Prof. M.M Musthafa, Department of Physics, University of Calicut, and has not been included in any other thesis submitted previously for the award of any degree.

University of Calicut
September 2021

Silpa Ajay Kumar

ABSTRACT

Cancer is a disease, characterized by uncontrolled growth of cells. Surgery, chemotherapy and radiotherapy (RT) are the common methods of treating cancer or malignancy. Radiotherapy is a clinical modality dealing with the use of ionizing radiations to treat malignant diseases. Modern radiotherapy assures high level of accuracy and precision throughout the treatment delivery. The high level of accuracy is achieved through image guidance which ensures delivery of highly conformal dose to the tumour. During IGRT, untargeted areas are also exposed with low dose radiation, termed as out of field dose. This needs to be estimated accurately for minimizing secondary cancer risk. Keeping this in view, a systematic measurement of out of field dose is performed and a mathematical model is developed on the basis of Moliere multiple scattering theory. The work undertaken is divided in to 6 chapters. Chapter 1 introduces details on radiotherapy, delivery techniques, problems associated with out of field dose and over view of the thesis. Chapter 2 includes the literature review . Chapter 3 elaborates on the equipment, methods, treatment planning systems (TPS), phantoms and detectors. Chapter 4 contains, different measurement methods adopted for out of field dose measurements. Since modern radiotherapy treatment modalities are highly depend on generating complex treatment plans, accuracy of treatment planning system is checked in predicting the out of field dose. Further small field dosimetry was analysed with different detectors andresults are summarized in Chapter 5. Realizing the requirement of fine accuracy in measurement, films were included in measurement for small field sizes and the mathematical models are developed on the basis of this measurement. The details of these measurements and analysis as well as the mathematical modeling is are explained in Chapter 6. This model will help in estimating the out of field doses accurately by incorporating in the treatment protocol. The summary of the work and future perspective are also discussed separately in this chapter.

Key words

Out of field dose, small field detectors, dosimetric Films, treatment planning system, Moliere multiple scattering.

സംഗ്രഹം

കോശങ്ങളുടെ അനിയന്ത്രിതമായ വളർച്ച കാരണം ഉണ്ടാകുന്ന ഒരു രോഗമാണ് കാൻസർ. ശസ്ത്രക്രിയ, കീമോതെറാപ്പി, റേഡിയേഷൻ തെറാപ്പി (RT) എന്നിവയാണ് കാൻസർ ചികിത്സയ്ക്കുള്ള സാധാരണ രീതികൾ. അയോണൈസിംഗ് വികിരണങ്ങൾ ഉപയോഗിച്ച് ക്യാൻസർ രോഗത്തെ ചികിത്സിക്കുന്ന വിഭാഗമാണ് റേഡിയോ തെറാപ്പി. ചികിത്സയിലൂടനീളം ഉയർന്ന കൃത്യത ഉറപ്പു നല്കാൻ ആധുനിക റേഡിയേഷൻ തെറാപ്പി ചികിത്സ വഴി സാധിക്കുന്നു. ഇമേജ് ഗൈഡൻസ് ഉപയോഗിച്ചാണ് ഉയർന്ന തലത്തിലുള്ള കൃത്യത നിലനിർത്താൻ. ഇമേജ് ഗൈഡഡ് റേഡിയേഷൻ തെറാപ്പി (IGRT) എന്നത് ഇമേജ് ഗൈഡിംഗും ട്യൂമറിലേക്ക് ഉയർന്ന ഡോസ് ഡെലിവറിയും ഉൾക്കൊള്ളുന്ന ഒരു സംവിധാനമാണ്. IGRT ചികിത്സ സമയത്ത്, ചികിത്സ നല്കാൻ ഉദ്ദേശിക്കുന്ന കോശങ്ങൾക്ക് (target) പുറത്തുള്ള സ്ഥലത്തെ കോശങ്ങൾക്കും ചെറിയ അളവിലുള്ള അണു വികിരണം (low dose) ഏൽക്കാൻ ഇടയാകുന്നു. ഈ അനാവശ്യമായ അണുവികിരണത്തെ അഥവാ റേഡിയേഷൻ ഡോസിനെ ഔട്ട് ഓഫ് ഫീൽഡ് ഡോസ് എന്ന് വിളിക്കുന്നു. ദ്വിതീയ കാൻസർ (secondary malignancy) സാധ്യത കുറയ്ക്കുന്നതിന് ഇത് കണക്കിലെടുക്കേണ്ടതുണ്ട്. ഇതിന്റെ അടിസ്ഥാനത്തിൽ, ഔട്ട് ഓഫ് ഫീൽഡ് ഡോസിന്റെ ചിട്ടയായ അളവെടുപ്പ് നടത്തുകയും ഔട്ട് ഓഫ് ഫീൽഡ് ഡോസ് കണക്കാക്കുന്നതിനായി മോലിയറെ മൾട്ടിപ്പിൾ സ്കാറ്ററിംഗ് തിയറിയുടെ അടിസ്ഥാനത്തിൽ ഒരു ഗണിതശാസ്ത്ര മാതൃക അവതരിപ്പിക്കുകയും ചെയ്തു. മേൽപ്പറഞ്ഞ കാര്യങ്ങൾ ഉൾക്കൊള്ളിച്ചു പ്രബന്ധത്തെ ആറ് അധ്യായങ്ങളായി വിഭജിച്ചിരിക്കുന്നു. അദ്ധ്യായം ഒന്നിൽ റേഡിയോ തെറാപ്പി, വിവിധ റേഡിയോ തെറാപ്പി ചികിത്സാ രീതികൾ, ഔട്ട് ഓഫ് ഫീൽഡ് ഡോസുമായി ബന്ധപ്പെട്ട് നിലവിലുള്ള പ്രശ്നങ്ങൾ, പ്രബന്ധത്തെ കുറിച്ചുള്ള പൊതുവായ അവലോകനം എന്നിവ അവതരിപ്പിച്ചിരിക്കുന്നു. രണ്ടാം അധ്യായത്തിൽ ഔട്ട് ഓഫ് ഫീൽഡ് ഡോസിനെ സംബന്ധിച്ച ഇതുവരെയുള്ള പഠനങ്ങളുടെ അവലോകനം ഉൾപ്പെടുത്തിയിരിക്കുന്നു. വ്യത്യസ്ത ചികിത്സാ യന്ത്രങ്ങൾ, ചികിത്സാ ആസൂത്രണ സംവിധാനങ്ങൾ, ശരീര മാതൃകകൾ (phantoms), ഡിറ്റക്ടറുകൾ എന്നിവ ഉൾപ്പെടുന്ന വിവിധ സാമഗ്രികളെക്കുറിച്ചും പഠനത്തിനായി ഉപയോഗിക്കുന്ന രീതികളെക്കുറിച്ചും അധ്യായം മൂന്നിൽ വിശദീകരിക്കുന്നു. ഫീൽഡിന് പുറത്തുള്ള ഡോസ് തിട്ടപ്പെടുത്തുന്നതിനായി സ്വീകരിച്ചിരിക്കുന്ന വ്യത്യസ്ത അളവെടുപ്പ് രീതികൾ അധ്യായം നാല് ഉൾക്കൊള്ളുന്നു. ആധുനിക റേഡിയോതെറാപ്പി ചികിത്സാ രീതികൾ സങ്കീർണ്ണമായ ചികിത്സാ പദ്ധതികൾ (treatment plan) സൃഷ്ടിക്കുന്നതിനെ ആശ്രയിച്ചിരിക്കുന്നതിനാൽ, ഔട്ട് ഓഫ് ഫീൽഡ് ഡോസ് പ്രവചിക്കുന്നതിൽ ട്രീറ്റ്മെൻറ് പ്ലാനിംഗ് സിസ്റ്റത്തിന്റെ (TPS) കൃത്യത പരിശോധിക്കേണ്ടത് പ്രധാനമാണ്. തുടർന്ന് ചെറിയ ഫീൽഡ് ഡോസിമെട്രിയ്ക്ക് പര്യാപ്തമായ ഡിറ്റക്ടറുകളുടെ കൃത്യത പരിശോധിച്ച് നിഗമനം ചെയ്തു, ഇത് അദ്ധ്യായം അഞ്ചിൽ സംഗ്രഹിച്ചിരിക്കുന്നു. അളവെടുപ്പിൽ സൂക്ഷ്മമായ കൃത്യതയുടെ ആവശ്യകത മനസ്സിലാക്കി, ചെറിയ ഫീൽഡുകളെ സംബന്ധിച്ച പഠനത്തിൽ ഫിലിമുകൾ ഉൾപ്പെടുത്തി. ഈ അളവെടുപ്പിന്റെ അടിസ്ഥാനത്തിൽ ഗണിതശാസ്ത്ര മാതൃകകൾ വികസിപ്പിക്കുകയും അവയുടെ വിശദാംശങ്ങളും ഗണിതശാസ്ത്ര മോഡലിംഗും അദ്ധ്യായം 6-ൽ വിശദീകരിക്കുകയും ചെയ്തിട്ടുണ്ട്. ഈ മോഡൽ ചികിത്സാ പ്രോട്ടോക്കോളിൽ ഉൾപ്പെടുത്തുന്നത് വഴി, ഔട്ട് ഓഫ് ഫീൽഡ് ഡോസ് കൃത്യമായി കണക്കാക്കാൻ സാധിക്കും പഠനത്തിന്റെ സംഗ്രഹവും ഭാവി കാഴ്ചപ്പാടും എന്നതും ഈ അധ്യായത്തിൽ പ്രത്യേകം ചർച്ചചെയ്യുന്നു.

താക്കോൽപദങ്ങൾ

ഔട്ട് ഓഫ് ഫീൽഡ് ഡോസ്, ചെറിയ ഫീൽഡ് ഡിറ്റക്ടർ, ഡോസിമെട്രിക് ഫിലിം, ട്രീറ്റ്മെന്റ് പ്ലാനിംഗ് സിസ്റ്റം, മോലിയെരെ മൾട്ടിപ്പിൾ സ്കാറ്ററിംഗ് തിയറി

ACKNOWLEDGMENT

I would first like to thank my supervisor **Dr. M. M MUSTHAFA** for his help in all aspects of this project. This project could not have been accomplished without his guidance and assistance throughout the course of the thesis work.1would like to express my gratitude to **Dr.PRABHAKAR RAMACHANDRAN**, Director of Medical Physics, and Princess Alexandra Hospital, Australia for his support in the initial stages of the work.

I am grateful to **Dr. B. SATHEESAN**, Director, Malabar Cancer Centre for his encouragement and for providing me an opportunity by granting permission to carry out my research work at Malabar Cancer Centre. I record my intense sense of thankfulness to **Mr.MIDHUN C.V,** Research Scholar, Calicut University for his support throughout the thesis work.

I extend my gratitude to **Dr. GEETHA.M, Head, Radiation Oncology** and my **DEAR COLLEGUES at Malabar Cancer Centre, Thalassery,** for their great co-operation for my entire work. 1 am grateful for the help from **Dr. RAJESH K.R, Dr. SIJI CYRIAC, Dr. ABDUL HANEEFA K and Dr. MUHAMMED SHAN** for their suggestions and help. I sincerely thank all teachers and staffs at the department of physics of Calicut University, for their help and support during the thesis.

I take this opportunity to express my regards to my friends and family for helping me through this time. There is no way I would have finished this thesis without their assistance, especially to my mother **Mrs. SOBHANA** my father **Mr. PADMANABHA KURUP,** my sister and my in laws for supporting me in many ways throughout my life and for their co-operation, understanding, and constant encouragement which were the sustaining factors in carrying out the work successfully.

Silpa Ajay Kumar

TABLE OF CONTENT

LIST OF FIGURES

LIST OF TABLES

LIST OF SYMBOLS AND ABBREVIATIONS

RT	Radiotherapy
IGRT	Image Guided Radiation Therapy
VMAT	Volumetric Modulated Arc Therapy
IMRT	Intensity Modulated Radiation Therapy
SRS	Stereotactic Radiation Surgery
3DCRT	3D Conformal Radiation Therapy
SBRT	Stereotactic Body Radiation Therapy
LINAC	**L**inear **A**ccelerator
MLC	**M**ulti **L**eaf **C**ollimator
CT	Computed Tomography
MRI	Magnetic Resonance Imaging
PET	Positron Emission Tomography
GTV	Gross Tumor Volume
CTV	Clinical Target Volume
mSv	**M**illi**Si**evert
µSv	**M**icro **Si**evert
MU	**M**onitor **U**nits
PMMA	**P**oly **M**ethyl **M**eta **A**crylic
PTV	**P**lanning **T**arget **V**olumes
CSDA	Continous Slowing Down Approximation

LIST OF PAPERS PUBLISHED/PRESENTED BASED ON THESIS

1. Silpa Ajay Kumar, MM Musthafa, Jaya Prasad Tripathy, Karthickeyan Duraisamy, Resmi K Bharathan, Suja Cheruliyil Ayyappan, Geetha Muttath; july(2019), "Accuracy of Out of Field Photon Dose Calculations by a Treatment Planning System", Indian Journal of Public Health Research & Development, Volume 10, No. 7, pp.19-25.

2. Silpa Ajay Kumar, Musthafa M M, Suja CA, Resmi KB, Lisha Jose, Geetha Muttath, Shahirabanu KP, (2021), "Dosimetric comparison of FF and FFF beams in VMAT treatment plans of head and neck cancers.", Oncology and Radiotherapy,Vol.15 Iss.6: 001-006.

3. Silpa Ajay Kumar (2017), Detector Accuracy comparison for point dose measurements in small fields., 17*th* Asia Oceania Congress of Medical Physics & 38*th* Annual Conference of Association of Medical Physics of India, Organized by Department of Radiological Physics, SMS Medical College, Jaipur.

4. Silpa Ajay Kumar, M.M Musthafa, K.V Anju, C.A Suja, K.B. Resmi (2018), Dosimetric Evaluation of Out of field photon Measurement, Conference Proceedings, 39*th* Annual Conference of Association of Medical Physics of India(AMPI), Organized by Association of Medical Physicist of India Tamil Nadu and Puducherry Chapter(TN&PY-AMPI).

5. Silpa Ajay Kumar, Anila Sagar, Resmi K bharathan, Suja C.A, Musthafa M.M (2021), Assessment of depth dose variation due to introduction of inhomogeneous material. 42nd Annual Conference of Association of Medical Physics of India (AMPI), at NIMHANS Convention Centre, Bangalore.

6. Silpa Ajay Kumar, Midhun C.V, M.M Musthafa, Rijin N.T. 'Moliere weighted Multicomponent Analysis of Flat Top Gaussian Radiotherapy

beam for small fields', Conference proceedings NSRP-23 held at the University of Mysore, Mysuru, Karnataka State, India during 19 - 21 January, 2023.

7. Silpa Ajaykumar, Arathi C, Resmi k. B, Suja c.A, Lisha Jose, Vinin N. V, Geetha Muttath, M.M Musthafa (2023), "Beam Focal Spot Offset Determination for Linear Accelerators: A phantomless method". Gulf Journal of Oncology, Issue 43.

LIST OF PAPERS/ PRESENTATIONS CO-AUTHORED

8. Arun P.V, Midhun C.V, M.M Musthafa, Silpa AjayKumar, Sreena.M, Keerthi E.S, Rijin.N.T, Swapna B (2022), Antony Joseph. 'Neutron Spectroscopy in High Gamma Background using Solid State Nuclear Track Detectors'. Conference proceeding, 66^{th} DAE Symposium, Nulear Physics.held at Assam, India.

9. Arun P.V, c, M.M Musthafa, Silpa A, Naiby Joseph, Sreena.M, Farhana Thesni.M.P, Keerthi E.S, Deepthi M.V (2023), Antony Joseph. "Spectroscopic analysis of photoneutron in intense γ-ray backgroud , Applied Radiation and Isotopes.

CHAPTER 1
INTRODUCTION

1.1 Radiotherapy (RT) and Cancer

Radiation therapy or Radiotherapy is one of the most important fields of application of physics in medical science which uses ionizing radiation for the treatment of cancer. Radiation therapy works on the principle of ionization. Ionizing radiation deposits energy into a medium directly or indirectly when they are passing through the medium. Charged particles are able to do direct ionization, while neutral particles like photons transfer part of their energy to charged particle which further ionizes the medium and is called indirect ionization. From this energy is deposited in the medium. Usually interaction is with water in the body resulting free radicals which leads to gene mutation and cell death. Mainly Radiotherapy is delivered as External beam radiation therapy (EBRT) is a subset of radiation therapy that delivers high energy radiation to a targeted area from an external source, where treatment is delivered by keeping the source at a distance from the tumor. Another method is Brachytherapy (BT), where treatment is delivered by keeping the source very near to the tumor. In EBRT treatment using linear accelerators a treatment distance of 100 cm is used. Radiotherapy uses mega electron volt energy for the treatment of cancer. And the intension is to deliver maximum amount of dose to the tumor while sparing the adjacent normal tissues.

Cancer is a disease that is characterised by uncontrolled growth of cells which have the ability to infiltrate through and destroy normal cells. Ionizing radiation causes damage to Deoxyribonucleic Acid (DNA) of cancerous tissues leading to cellular death.

As per the statistical reports from National Cancer Registry Programme in India, for the year 2020, the common 5 leading sites are breast, lung, oral cavity, cervix uteri, and tongue. Trends in cancer incidence rate showed an increase in malignancy in all sites of cancer in both genders. The majority of the patients with

cancer were diagnosed at the locally advanced stage for breast (57.0%), cervix uteri (60.0%), head and neck (66.6%), and stomach cancer (50.8%). In the Indian subcontinent approximately 70% of cancers were potentially preventable through modifiable risk factors [1].

Cancer treatments depend on type, characteristics, staging and patients' physical condition. Surgery, chemotherapy and radiotherapy are the methods adopted for the treatment of cancer. Among this, surgery is the first priority for majority of isolated solid tumors where cancerous tissue is completely removed. This method is successful for early stage disease and when there is no spread. Adjuvant radiotherapy is given in selected cases targeting the microscopic spread after surgery. Chemotherapy can be an effective treatment on its own or used in combination with surgery and/or radiotherapy. Sometimes when a tumor size is large, chemotherapy or radiotherapy can be used to shrink the tumor to an adequate size to enable surgery. This thesis used head and neck cancers for clinical implementation of out of field dose measurement. Selection was based on the complex nature of the site as a greater number of critical organs were involved. Head and neck is an area where high accuracy and precision is required in patient setup. Out of field dose which is not accounted properly by the treatment planning system can enhance this critical organ dose.

1.2 Head and Neck Cancers

In India cancer of the lip and oral cavity ranks first in incidence in males and second to breast cancer in incidence when both genders taken together, according to global cancer registry 2020 [2] (Fig-1.1 and Fig- 1.2) Head and neck cancer comprises a heterogeneous group of tumors arising from the upper aero digestive tract, Para nasal sinuses, and salivary and thyroid glands. Cancers of the head and neck are generally reported with delayed diagnosis and worse outcomes [3]. Oral cavity and lip cancers among head and neck site are reportedly have more incidence. Cure and control rate is comparatively high in head and tumours.

According to the part of the body where they develop, head and Neck cancer can be divided in to five types,

1. Oral and oropharyngeal cancer: The oral cavity includes mouth and tongue. The oropharynx includes the middle of the throat,from the tonsils to the tip of the voice box.

2. Nasal Cavity and paranasal sinus cancer: nasal cavity is the air passage just behind the nose through which air passes to throat. Paranasal sinus are the air filled areas that surrounds the nasal cavity.

3. Nasopharyngeal cancer: Nasopharynx is the air passage at the upper part of the throat behind the nose.

4. Laryngeal and hypopharyngeal cancer: Larynx is the voice box and hypopharynx is the lower part of the throat that surrounds the larynx.

5. Salivary gland cancer: salivary gland produces saliva which helps to keep mouth moist.

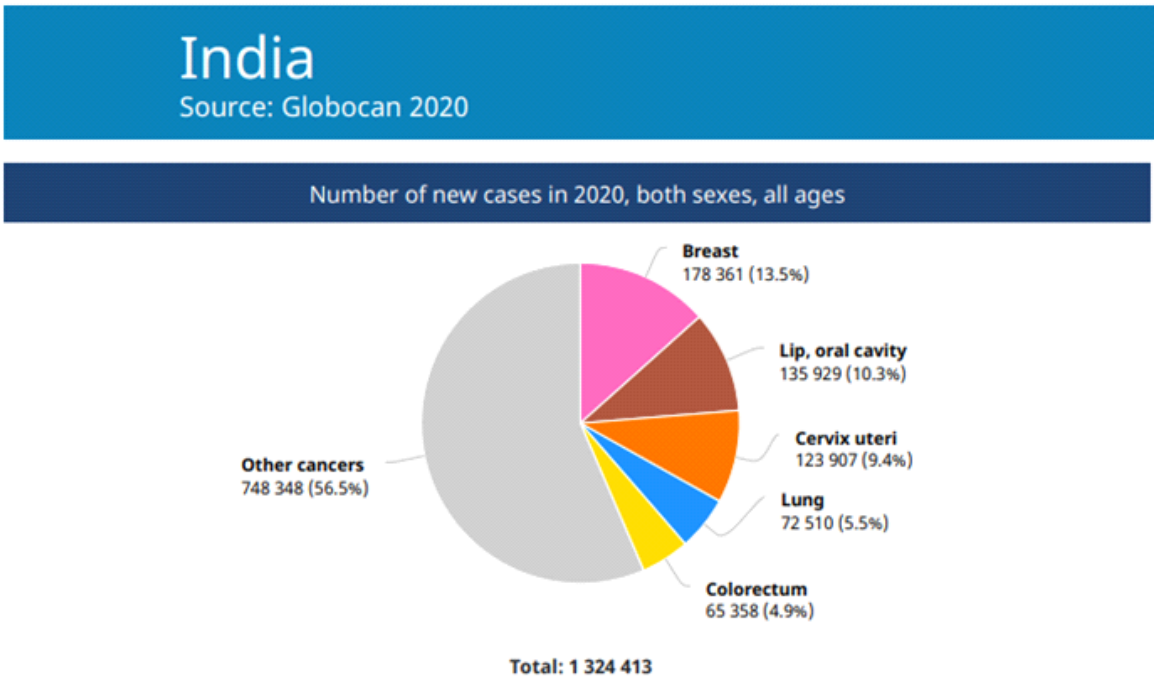

Fig 1.1 Number of new cancer cases in 2020, both sexes, all age

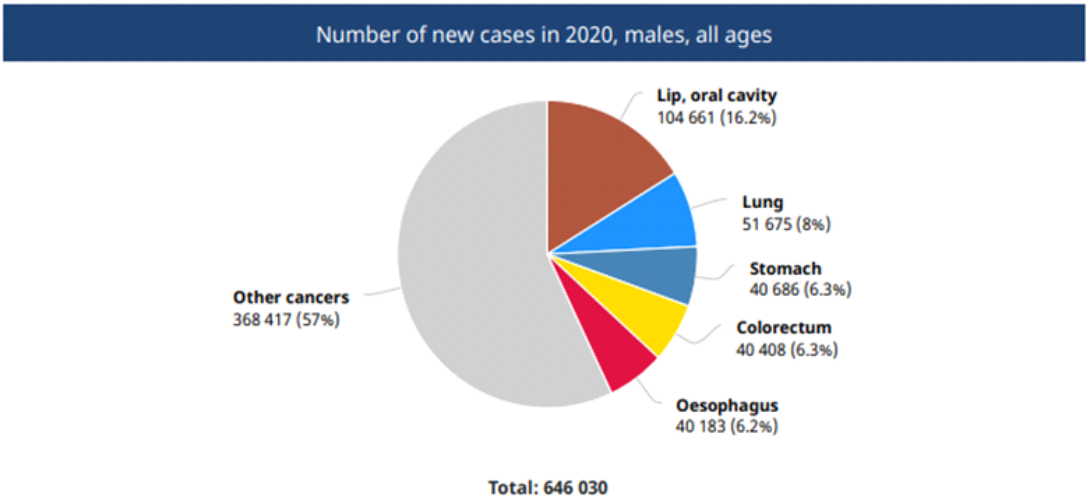

Fig1.2 Number of new cases in 2020, males, all ages

Based on the patients' health, age, and stage of cancer, the treatment varies. In many cases, surgery is the only method of treatment for early cancers where the tumor is small and has not spread. Usually large size tumors are made to shrink using chemotherapy and radiotherapy before surgery to get the intended result. Surgery and radiotherapy are the major treatment modalities in the optimal management of head and neck cancer. Further technical complications arise due to the surface contour geometries and tissue density heterogeneities typical of this physiological site. For initial stage and small volume tumours surgery is the primary choice, in such cases also adjuvant radiotherapy is delivered considering the microscopic infiltrations and other spread. Thus in the management of head and neck cancer radiotherapy has an important role.

Radiation is a double edged weapon as it cures as well as induces cancer. Due to this radiation protection is very important in Radiotherapy, so that its use is controlled. Generally Radiotherapy treatments can be divided into 'curative' and 'Palliative' A treatment with curative intent controls a tumor by removing it and preventing recurrence. While palliative treatment is given to relieve symptoms. Both are achieved with combination treatments like, surgery, chemotherapy and Radiotherapy.

Highly concentrated dose deliveries to the tumor are now possible. Improper

knowledge of the patient's anatomy and positioning of patient during the course of therapy has always been a major source of concern in radiation therapy. This may cause potential variation in clinical results by insufficient dose coverage of the target volume and over dosage of normal tissues. Respiratory-induced organ motion is a major problem in RT which results in imaging artifacts and positional uncertainty that compromise the accuracy of target delineation and treatment delivery. In modern radiotherapy treatment techniques, like volumetric modulated arc therapy (VMAT), 3D-conformal radiation therapy (3D-CRT) and Intensity-Modulated Radiation therapy (IMRT), planning and delivery, permit much more conformal dose distributions with sharper dose gradients. This high level of accuracy and precision throughout the process of treatment delivery can be achieved only with image guidance. Image-guided radiation therapy (IGRT) is a system that incorporates both image guiding and delivery of highly conformal and high dose to the tumor.

1.3 Image Guided Radiation Therapy (IGRT)

IGRT is a process that helps to maximize the accuracy and precision of radiotherapy treatment. It uses image guidance at various stages of its process like data acquisition, treatment planning, treatment simulation, patient setup, and target localization before and during treatment. Radiation therapy that employs imaging to maximize accuracy and precision throughout its entire process. This process includes target and normal tissue delineation, radiation delivery, and adaptation of therapy to anatomic and biological changes over time in individual patients. Radiation therapy has long been image-guided. In the earlier period imaging was done using megavoltage port films, which lacks 3D visualization of soft tissue targets. In the current procedure, IGRT helps to reduce the uncertainty in locating the tumor and treatment delivery. The accelerator mounted imaging systems are called on-board imagers. Modern accelerators are equipped with two kinds of imaging systems, kilovoltage (KV) imaging system and megavoltage (MV) imaging system. In the case of kilovoltage imaging system conventional x-ray tube is mounted on the gantry with an opposing flat panel detector. In the case of a megavoltage imaging system, a megavoltage electronic portal imaging device, with

its own flat panel image detector, is employed (Fig-1.3).

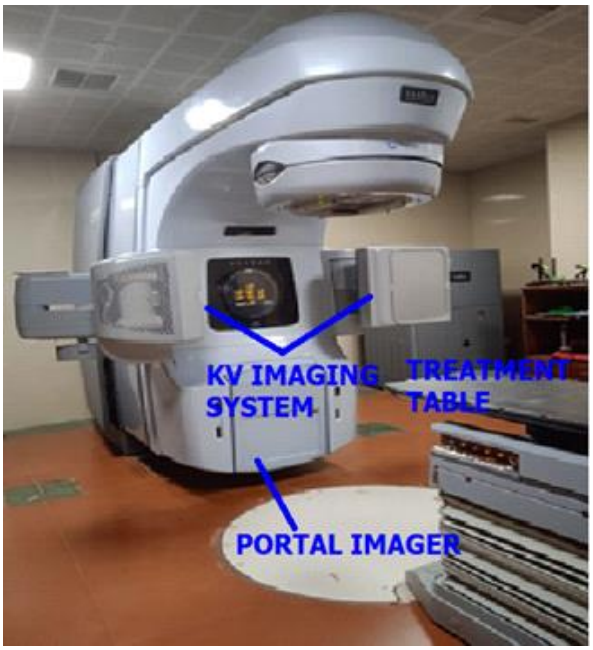

Fig 1.3 Linac mounted Imaging systems

The target location may be determined by a range of methods for soft tissue volumetric imaging such as, KVCT, MVCT, ultrasound, magnetic resonance imaging. If any discrepancy between the simulated location and the live image is observed, a correction is applied by repositioning of the patient, movement or reshaping of the radiation beam to match the target position, or holding the beam until the target falls in the correct location (eg, respiratory gating). In this way, the treatment will be delivered precisely and accurately according to the treatment plan.

1.4 Radiotherapy Process

EBRT is delivered using linear accelerators (ie, by using high energy X-rays or electrons) or with radioactive sources like Cobalt 60. The major goal of radiotherapy is to achieve local control of the tumor while minimizing damage to the critical organs. In the ideal case, radiation can kill cancers and cure patients. In addition, it can also be used to relieve the pain and discomfort of cancer patients (palliative treatment). The process of Radiotherapy treatment starts with imaging. Computed tomography, Magnetic Resonance Imaging (MRI) and Positron emission

tomography (PET) modalities are mostly used for imaging. Images are then sent to Treatment Planning system, where Gross Tumor Volume (GTV), Clinical Target Volume (CTV), gives margin to GTV accounting the microscopic infiltrations of the tumor, Planning Target Volume (PTV), gives margin to CTV accounting patient setup errors and organs at risk are contoured. Further adequate beams are placed to generate a good plan. Approved plans from the treatment system are then transferred to Treatment machines (Medical Linear Accelerator) where treatment setup is verified by imaging and finally treatment. Pre-treatment quality assurance is performed before each treatment delivery. Dedicated instruments are commercially available for the same.

1.5 Modern treatment techniques in Radiotherapy

The majority of cases are reported with locally advanced disease necessitating multi-modality treatment. Radiation therapy provides a functionally conservative approach to treatment of cancer by the increased efficacy of modern techniques in the head and neck region. Modern treatment methods like Intensity modulated Radiation therapy(IMRT), Volumetric modulated Radiation therapy(VMAT) are widely used in treatment of head and neck cancers, by ensuring good Planning Target Volume coverage and critical organ sparing. Main issue with such technique is the comparatively higher integral dose, which unfortunately not been accounted accurately. In our department most of the head and neck plans are delivered using VMAT technique. VMAT techniques usually generate homogeneous distribution with effective organ at risk sparing. Also the delivery time is comparatively less. In this gantry of the linac rotates around the patient meanwhile dose rate changes and multi leaf collimator (MLC) shape changes hence delivering beams of modulated intensities. In linac collimator jaws and MLC helps to shape the beam.

1.6 Small fields in Radiotherapy

With the advent of new techniques like IMRT, VMAT, SBRT, and SRS, it is important to apply comparatively smaller dynamic and static fields. Field sizes lesser than 4x4 cm^2 is generally accounted in the definition of small fields. And is

different from the traditional therapy field size in terms of its characteristics and needs careful consideration in both dose estimation and calculation [4]. Dosimetry of small fields plays a significant role for several purposes in modern radiation therapy. For small fields, the physics of the transmission of radiation varies from that of large fields, and some characteristics of conventional dosimetry starts to fail [4-6]. Therefore, it is important to carry out precise quality assurance for these small fields to guarantee the safety and efficacy of the treatment.

Small fields are progressively utilized in modern radiation treatment particularly in volumetric modulated arc treatment and stereotactic radiosurgery therapies. Dose confirmation is significant in these intensity modulated techniques. The appropriate detector for small field dosimetry must have some features such as higher spatial resolution, tiny volume, energy, dose rate-independence, linearity, reproducibility, and stability [8-9]. The dose uncertainty in small fields is much complex than usual. Hence it is also important to analyze the effect of sensitive volume and cross section area of the performance of the detector for reducing measurement uncertainty.

1.7 Out of field Dose Production

Image guided radiotherapy is always accompanied with low dose deposition outside the target. Dose outside the target or the field of interest or the planning target volume (PTV) is referred to as non- target dose or out of field dose [10]. Regardless of the delivery modality the radiation dose, inevitably deposited, in healthy tissues outside the clinical target has been linked to detrimental late effects and second tumors [11-15]. The patient receives dose outside of the primary radiation field, due to, secondary radiation, includes photon leakage through the treatment head of the accelerator, scattered radiation from collimators, beam modifiers and internal patient scatter. From the survivors of war (Hiroshima,Nagasaki) and other different radiation accidents, it is evident that even low doses of ionizing radiation induces cancer (ICRP Publication 99,2005) [16].

Earlier studies on out of field dose starts about 1970 from the introduction of linear accelerator machine. There have been many number of studies conducted over

the past several decades and the majority of these involve measurement of out of field doses using different types of detectors, many opted Monte Carlo radiation transport simulation for calculation of doses, and many came with analytical approaches, or combinations of these. Even after introduction of modern techniques, concern in the out of field dose still remains important as indicated by the increasing number of publications in this field. Working Group 9 (WG 9: Radiation Protection Dosimetry in Medicine) of the European Radiation Dosimetry Group (EURADOS) had been carried out on out of field neutron measurement [17]. The motivation was to assess undue, non-target patient doses in radiotherapy and the related risks of second malignancy.

Low doses in the out of field region are not generally been considered during treatment planning, as it is difficult to measure, characterize, or model low doses in the planning system. The accuracy of treatment planning system in determining the dose beyond a few centimeters outside the treatment field edge is usually poor as reported by many studies [18-20]. Larger target volumes like head and neck will cause more patient scatter and therefore higher out-of-field doses, particularly near the treatment field. Out of field dose in head neck region is of more importance as it consists of more number of critical organs. The flattening filter-free (FFF) modality used in modern treatment planning system helps in reducing the out-of-field dose [21-24]. Collimator scatter is reduced when flattening filter free beams are used.

Over the past 35- years numerous studies have conducted on out of field dose as reported by the review articles [25-27]. Even though there are many studies carried out for out of field dose measurements from early 80's to the present, the topic is still hot. The researchers are holding to some comparisons only and not any relevant conclusion that is enough to predict out of field dose has been achieved. The total Monte Carlo methods are also inappropriate due to lack of point-point validation. Most of the Monte Carlo approach is based on the total energy released in the medium followed by electron -electron scattering problem, solved through iterative random distribution of particle interactions. The observed out of field dose measurements are reproduced by the optimization to the individual point doses. The point-to-point validation requires an analytical formalism in the form of likelihood

function, to perform the validation of Monte-Carlo results. As not any successful analytical formalism is available, the topic is important to generate much data and perform fits for analytical formalism. Also analytical models developed by many authors are limited to some empirical formalism. Hence the compound of multiple scattering is generally neglected. Recent studies [28] suggest further development of analytical models, which should consider the current RT techniques and must be implemented as a clinical tool. Roger Harrison suggests experimentally verified out of field models to overcome the limitations in the out of field measurements [29]. In the present work, we derived an analytical formalism for dose distribution, from the diffusion equation, with diffusion operator from Moliere scattering cross sections. This will take in to account multiple scattering within the medium and hence better representation of data.

1.8 Problems associated with out of field dose measurements

Many analytical models are available for calculation of out of field dose from photon therapies like data from AAPM report TG 36, which has been used in combination with mathematical phantom to determine the out of field dose for different organs in a patient. Software programs are also developed to calculate the out of field doses. All the models show accuracy between 30%-60%, although much larger errors are possible Analytical models developed recently, independently, by Haurietal, and Jagetic et al offers more accuracy but increased complexity [30,31]. Also the contribution from multiple electron scattering towards the out of field dose has not been well studied. Further, there is no satisfactory mathematical modeling, representing the actual physics, is available for prediction of out of field dose contribution. Hence a mathematical model, with specific physics of interacting primary and secondary particle, that can represent the data with accuracy of mean free path of interacting particles, that can represent the data with accuracy of mean free path of interacting particles, need to be developed.

1.9 Present work

In order to develop precise theory measurements have to be performed with resolution better that the mean free path of the scattering of secondary electrons,

which is actually responsible for the energy deposition and biological effects. Hence to optimize the resolution of the measured out of field dose distribution it is decided to perform the measurements using film [66,67]. For a broader primary estimation of out of field doses, the out of field doses were measured using different detectors applying different conditions, for case of head and neck cancer. 6MV , 10 MV and 15MV photon beams from Elekta Versa HD machine and 6MV photon from Varian Clinac iX were used for the measurements. For high accuracy film dosimetry 6MV photon beam from Varian Clinac iX was used.

In Linear accelerators, predominant mode of interaction of photons with patient body is by Compton interaction. Both these ejected electrons and scattered photons are capable of producing further scattering. Although initial interaction is with photons, finally it is this multiple scattered electrons contribute to the absorbed dose. All these types of electron interactions and its multiple scattering are treated by Moliere through diffusion equation in terms of multiple scattering. Further a phenomenological model has been developed by solving diffusion equation for electrons in terms of Moliere scattering approach in which, we derived an analytical formalism for dose distribution, from the diffusion equation, with diffusion operator from Moliere scattering cross sections. This will take in to account multiple scattering within the medium.

1.10 Overview of the thesis

Thesis discuss on out of field photon dose measurement and treatment planning system accuracy in predicting the same. Out of field measurements were done using different detectors and mediums. Review on the topic of out of field dose clearly shows a lack of accurate theory and experimental based model to predict the out of field dose. A detailed review if literature and current status of the issue is presented in **Chapter 2. Chapter 3** describes the materials and methods used in this thesis and provide detailed description of various equipment, modalities and detectors used in the measurement. **Chapter 4** gives details of out of field measurement using 2D-array detector with its result and discussion. Analysis of the relative contribution of FF and FFF in out of field dose, done in a treatment planning

system, for fifty head and neck oral cavity cases, is also included in this chapter. **Chapter 5** describes the measurement and analysis of small field doses using various detectors and efficacy of each detector for small field measurements.

Chapter 6 presents the out of field dose measurement using films and details of mathematical model developed for determining the out of field dose using Moliere multiple scattering theory. Analysis of the same is explained with promising results and highlight for future studies in this field.

CHAPTER 2

REVIEW OF OUT OF FIELD DOSE MEASUREMENTS

2.1 Introduction

The intension of radiotherapy is also to increases the efficacy of life of the patients. But incidence of secondary cancer risk is becoming a concern due to this out of field dose. The incidence of cancer depends on several parameters like, type of treatment, Linear accelerator used, Field size etc. Even though many studies have been conducted about the origin of out of field but very less has come out with the exact picture and failed to implement the solution in out of field dose reduction especially in the case of small fields. The present chapter reviews some of the attempts related to the out of field dose measurement and related works.

2.2 Out of field dose measurement in early period.

Initial studies on out of field measurements were conducted using air as the medium of measurement. Greene et al [32] have measured the leakage and scatter radiation from one x-ray unit and two linear accelerators in air and phantom. They observed that up to a distance of 50-60 cm from the central axis leakage radiation dose is considerably higher than that in the open field. In a technical note by Greene et al in 1985 found that the principal source of radiation outside the main beam is scatter from the collimator system rather than head leakage or scatter from the irradiated tissue in the treatment volume. Kase et al. [33] estimated the dose from secondary radiation outside a treatment field. It is reported that collimators contributes 20-40% dose to the patient outside the treatment volume, while leakage has very small contribution but is the major source of radiation at distances beyond 40cm as observed by Greene et al. Van der et al [34] developed a model to calculate dose at any point in the body outside the primary beam using experimentally determined data. This model allows calculating photon dose outside the primary

beam with an accuracy of ±50%. He also found at larger distances the leakage radiation contributed higher.

B.A.Fraass and J.van de Geijn [35] investigated the peripheral dose for a Co-60 beam, 4-MV, 6-MV and 8-MV photon beams for different field sizes and distances from field edge in a water phantom. Transmission and in-patient scatter were found to be of similar in magnitude. Francois et al.[36] measured dose distributions as a function of depth, distance from the edge, field size and shape for different beam energies employing a large water phantom, anthropomorphic phantom using TLD. An algorithm was developed to determine the dose to organs outside the beam at a distance of 10-50 cm from the field edge. Niroomad et al.[37] measured dose to ovaries and testes from Hodgkin's fields. They have studied potential Genetic hazard of medical radiation exposure. For cobalt, they obtained a dose of 0.13% to the testis from the mantle field and 0.48% for the Para-aortic field. In the case of ovaries they reported a dose of 0.44% and 2.30 % respectively.

2.3 Out of Field Dose in Modern Treatment Techniques

Measurement medium and detectors are important in determining the accuracy of measurements. Modern treatment techniques like IMRT, VMAT and SRT modalities help in lengthening patient's lifetimes. In contrary, this increases risk of manifesting other health risks like secondary cancer. These techniques use very small fields for treating the tumor. Hence out of field dose measurement in such fields needs special attention.

Monitor unit is high in modern techniques compared to conventional techniques. Hall and Wu [38] found that IMRT of prostate cancer rather than conventional radiotherapy resulted in double the risk of fatal secondary cancer. Similar observation was made by Wang and Xu et al [39].

Followill et al [40] measured out of field doses for IMRT case for three energies 6, 18 and 25MV beams .The photon equivalent doses obtained were 80 μSv, 6.5 μSv and 10 μSv, respectively. They have calculated worst-case scenario, using risk values recommended by the National Council on Radiation Protection and

Measurements (NCRP). Risk of cancer is found be between 0.4% (for conventional 6-MV beam) and 24.4% (for 25-MV tomotherapy beam),

Ruben et al. [41] compared IMRT with 3DCRT in terms of carcinogenic risk. The risk of radiation-induced malignancies in organs outside the target volume was found to be comparable for the two methods.

Kry et al performed a number of studies on the out of field dose. A Monte Carlo model for out of field dose calculation from high energy photon therapy has been presented by Kry et al.[42]. The simulated dose was compared with measurements made using TLD in an acrylic phantom up to 55 cm from the central axis. They have observed that out of field photon dose varied substantially with field size and distance away from field edge,

Kry et al. [43] measured the photon and neutron out-of-field dose equivalents to various organs using different treatment strategies, energies and accelerators. Photon dose decreased exponentially away from primary field; neutron dose was found to be independent of the distance from treatment field. Neutrons were found to have significant contribution to out of field dose. Kry et al [44] in another study, investigated out of field dose and calculated the maximum risk of fatal secondary malignancy. It was found to be 1.7% for conventional radiation, 2.1 % for IMRT with 10-MV x-rays and 5.1% for IMRT with 15-MV x-rays. Clearly indicating higher out of field dose contribution and fatality rate for IMRT Plans. Again in 2007 Kry et al. [46] pointed out the large uncertainty in risk estimates relating to out-of-field doses.

Klein et al [46] performed peripheral data estimation of Pediatric IMRT using a phantom mimicking a three year old. 0.125cc and 0.6cc ionization chambers were used for measuring out of field dose at locations corresponding to thyroid, breast, ovaries, and testis. Distant peripheral dose (dominated by head scatter) was higher than predicted. Doses to the testes were reported to be 3 to 5 times higher for IMRT compared to conventional treatment.

Out of field dose is influenced by treatment unit, field size and beam quality. It can be reduced by selecting appropriate treatment arrangement. AAPM TG 36[1995] describes on the peripheral dose distribution for the same in which data of tertiary MLC was not available.

Mutic and Klein [47] calculated the peripheral dose with the introduction of a tertiary MLC. Ion chambers and water equivalent plastic phantoms were used for the study. It is found that peripheral dose distributions with the MLC for fully retracted and collimator rotated to 180° were comparable with the TG-36 data. Lower Peripheral dose was observed with MLC shaped fields. Also rotating the collimator to 90° with full MLC retraction reduced the peripheral dose up to a factor of 3. Vlachopoulou V et al. [48] studied on peripheral dose (PD) from high-energy photon beams in radiotherapy using dose verification system (MOSFET). Measurements were carried out for different field sizes and for various depths with the source to surface distance of 100 cm. It is observed that PD is higher near the phantom surface and drops to a minimum at the depth of dmax, and then tends to become constant with depth. Taylor et al. [49] investigated out of field doses from mini multileaf collimator-shaped fields, suggested some techniques for the minimization of out of field dose and associated risks. Kaderka et al. [50] investigated the out of field for photons, protons and carbon ions. Measurements were done using water phantom and different detectors. The peripheral dose delivered by photons is significantly higher compared to both protons and carbon ions. Photon dose is found twice the order higher than carbon ion at 50 am away from field edge. Charged particles show superiority in sparing the organs at risk.

Ahammed M et al. [51] Calculated out of field dose using the Markus detector for different field size and depth. They found an increase in out of field dose with increase in field size. The measured mean out-of-field dose overestimated in the calculated at different field sizes by 14% at field size of 10×10 cm^2 and by 15% at field size of 30×30 cm^2. Measured and calculated doses decreased approximately exponentially as a function of distance from the field edge at peripheral regions. An under estimation of TPS is reported in calculating the out of field dose for IMRT and 3DCRT.

Jihyung Yoon et al. [52] investigated post-mastectomy radiotherapies (PMRT). According to them Patient dose reconstruction is challenging for these advanced techniques because they increase the low out-of-field dose area. PMRT treatment plans for an anthropomorphic phantom were generated. FF and FFF beams were used in the study. Volumetric modulated arc therapy, mixed beam therapy, 4-field intensity modulated radiation therapy (IMRT), and tomotherapy were done. Study found that the TPS calculated doses were lower than 5% of the prescription dose using thermoluminescent dosimeters (TLD).

Garrett et al.[53] studied on out of field dose from a Peadiatric anthropomorphic phantom using FF and FFF photon beams. FFF beams resulted in reduced out-of-field doses for all field sizes when compared to flattened beams. Out of field doses for both energies found to converge at large distance away from the central axis. Also leakage is found to contribute more for out of field dose. Study concludes use of FF beams and tertiary shielding in reducing out of field dose in pediatric patients settings. Shine et al. [19] checked the out of field calculation accuracy of an Eclipse (versionn13.7) treatment planning system (TPS) used with a True Beam (TB) linear accelerator. They have measured the out of field dose and compared with TPS calcuted and Monte Carlo simulated values. In the study, the TPS underestimated the dose by around 45% on an average for the off-axis-distance range. As the off-axis distance increased, the underestimation of the dose also increased.

Roger Harrison [29] discussed on the epidemiological studies and dose-risk models on out of field dose, suggests that general strategy for out-of-field dose estimation requires development and improvement in several areas including (i) dosimetry in regions of steep dose gradient close to the field edge (ii) experimentally verified analytical and Monte Carlo models for out-of-field doses (iii) the validity of treatment planning system algorithms outside the field edge (iv) dosimetry of critical sub-structures in organs at risk (v) mixed field (including neutron) dosimetry in proton and ion radiotherapy and photo neutron production in high energy photon beams (vi) the most appropriate quantities to use in neutron dosimetry in a radiotherapy context and (vii) simplification of measurement methods in regions

distant from the target volume. Because of the limitations in the out of field measurement widely applicable and experimentally verified out-of-field models needs to be developed. Also there is a need for refinement and extension of TPS algorithms within a few centimetres of the field edge. Farhood.B and Ghorbani Man [54] review on the dose calculation accuracy of radiotherapy treatment planning systems in out-of-field region. They suggested that as the assessment of dose at out-of-field regions should not, generally, relied on TPS calculations and for accurate evaluation of out-of-field dose values other dose reconstruction methods including Monte Carlo simulations or other analytical method should be utilized to reveal accurate evaluation of it.

TG 158 [10] was formed to provide guidance for physicists in terms of assessing and managing non targeted doses. Since outside the treatment field, the photon energy spectrum, dose rate, and general shape of the dose distribution are very different and often require special consideration. Same concern is expressed in case of neutron dosimetry.

2.3.1 Small field dosimetry

Schonfield et al.[55] conducted study on dosimetric properties of microSilicon diode detector and compared with Diode E and microDiamond detector. microSilicon was found comparable with microDiamond and showed an improved behavior over diode.

Barnett et al.[56] measured the IMRT point dose measurement using diamond detector, extradin A12 ion chamber, pinpoint chamber and a Varian aS500 EPID. Measured doses were compared with HELAX-TMS calculated dose, and the results suggest diamond detector is extremely sensitive to positioning in high dose gradient regions. Avoidance of high dose gradient regions improve agreement between measured doses. The study recommends 2D dose verification as a better option for IMRT plans.

Martens [4] compared the efficiency of pinpoint chamber with Markus ion chamber and diamond detector in IMRT fields. Study suggested pinpoint chamber as an excellent detector for small field output measurement.

Poppinga et al. [57] analyzed three dimensional characteristics of active volumes of PTW microDiamond, microSilicon and diode E dosimetry using, a 10 MV proton beam. Two dimensional maps of the detectors were analyzed , The active areas where found to be 1.18 mm^2 for diode, 1.75mm^2 for microSilicon and 3.91mm^2 for the microDiamond detector

Zacharia et al. [58] compared the similarities and differences of three dosimetric protocols, IAEA code of practices 398 (2000), German dosimetry protocol DiN 6800-2(1997) and its revised version DiN 6800-2(2006). Discrepancies in the absorbed dose determination between the three protocols were found to be 0.4% and for electrons it was 1.5%.

Alfonso et al. [5] introduced a new formalism for small and non-standard fields. This paper outlines the small and composite fields dosimetry based on absorbed dose to water.

2.4. Accuracy of treatment Planning System

Accuracy of out of field dose prediction by treatment planning system (TPS) had been studied by many researchers as modern treatment plan accuracy is highly depends on the algorithms and planning systems. TPS are modeling the treatment fields to deliver adequate dose to the target. Many planning algorithms are developed for accurate dose predication in in-field dosimetry, while it shows poor out-of-field dose predictions.

Huang et al. [20] evaluated the accuracy of out of field dose calculation by a commercially available treatment planning system, using rando phantom and TLD. The data was compared with the results of Monte carlo simulation and TPS predictions. It was concluded that TPS underestimates the out of field dose and this under estimation worsened for increasing distance from the field edge. Michael L. Taylor and Tomas Kron [27] investigated the accuracy of the out-of-field dose

calculated by the Eclipse TPS (AAA algorithm) using 6mv photons for a clinical treatment delivered with a Varian 2100 Clinac. The data was compared with the TLD-measured dose. The results show that in comparison with measured data, the calculated dose underestimated the actual dose by 40% ± 20%. They also found that calculated doses at a given distance from the treatment field varied substantially with depth, while measured doses remained constant. The accuracy of TPS calculations for out-of-field dose may also be affected by beam angle, field size and delivery technique.

Heuvel et al. (83) investigated the dosimetry involved in the out-of-field contributions for IMRT and VMAT using gafchromic films and TLD at 10 cm depth. The data was compared with calculations using a superposition/ convolution based TPS. It is found that, in both cases, the treatment planning system underestimated the doses far from the field.

Measurement of out-of-field dose for 6 MV CSIs in two clinical settings was conducted by Phillip J Taddei,Wassim Jalbout, Rebecca M Howells [59]. Using Anthropomorphic phantom and TLD. The TPS predictions agreed poorly with measurements in regions of sharp dose gradient, e.g., near the field edge. At distances greater than 1 cm from the field edge, the TPS underestimated the dose by an average of 14% to 24% and 44% to 19% in the MD Anderson and AUBMC clinics, respectively. The in-field measured dose values of the measurement at AUBMC matched the dose values calculated by the TPS to within 2%. Dose algorithms in TPSs systematically underestimated the actual out-of-field dose.

Alexandra Bourgouin et al.[60] assessed the potential of using Plastic scintillator dosimeters (PSDs) for surface dose measurement. CC04 ion chamber also used for the measurement. Measurements were performed with a Varian Clinac iX (SSD was fixed at 90 cm for 6 MV and 23 MV beams with a field size of 15 × 15 cm^2 and at 100 cm for electron beams having 6 MeV and 18 MeV except for PDD m easurements). Out of field measurements were done at different distances (3-15 cm). It is observed that before d_{max}, the TPS doses strongly differ from the measurement (between 25% and 80%). The dose measured by PSD was higher than that measured

by IC (5% and 9% for 6 MV and 23 MV, respectively). For the 6MeV beam, there is a large difference between IC and PSD measurement due to the collecting diameter of the IC, This large difference is not observed with photon beams because the out-of-field distance is larger. For larger out-of-field distance, the differences between IC and PSD are in agreement with results obtained with photon beams. The out-of-field dose decreases with the increase of the size of field and this result is observed for both dosimeters.

Cyriac et al. [61] calculated the out-of-field photon dose on TPS (Oncentra V4.3) for 3D-CRT and IMRT treatment techniques, using photon beam of 6MV and size 10x10 cm^2 from Elekta Synergy linear accelerator. Results are compared with the measurement of TLD and ionization chamber, at 5 cm depth in PMMA slabs. It is seen that as distance from field edge increases overall underestimation increases from 5 % to 65 % at a distance of 23 cm. Phantom scatter component was in good agreement in near field edge. An increase of 50 % underestimation is observed for a distance of 10 cm far from the field edge. Collimator scatter was underestimated by TPS in near field (15%) and increases as the distance increases .IMRT plans underestimate out-of field dose more than 3D-CRT plan.

2.5 Introduction of Flattening Filter Free beams.

Introduction of flattening filter beams are reportedly able to reduce the out of field dose. Following are some reviews on the same.

Yue Yan et al. [62] studied Dosimetric differences in flattened and flattening filter-free beam treatment plans using true beam machine. They evaluated Plans three cancer sites performed using flattened and flattening filter-free (FFF) beams and observed similar target coverage and improved OAR dose sparing compared to FF beams mainly in Head and Neck Site.

Zhuang et al [63] investigated the dosimetric characteristics of volumetric modulated arc therapy (VMAT) with flattening filter-free (FFF) beams and assessed the role of VMAT in the treatment of advanced nasopharyngeal carcinoma (NPC).

They concluded that RA with conventional beams has a greater dosimetric superiority than RA-FFF.

A treatment planning and delivery comparison of volumetric modulated arc therapy with or without flattening filter for gliomas, brain metastases, prostate, head/neck and early stage lung cancer by D. Gasic et al. [64] found that They found that it was generally possible to produce FFF-VMAT plans with the same target dose coverage and doses to organs at risk as STD-VMAT plans. Target dose homogeneity tends to be somewhat inferior for FFF-VMAT for the larger targets investigated. For stereotactic radiotherapy, FFF-VMAT resulted in a considerable time gain while maintaining similar plan quality compared to standard beams.

Comparison of treatment plan quality of VMAT for esophageal carcinoma with FF beam versus FFF beam by sun et al. [22] concludes that the treatment plans with FFF beams could get comparable dose distribution in targets and could significantly reduce the peripheral dose around targets compared to the plans with FF beams.

Nicolini et al. [21] in their feasibility study performed to evaluate Rapid Arc (RA), and the potential benefit of flattening filter-free beams, on advanced esophageal cancer against IMRT and three-dimensional conformal radiotherapy 3D-CRT suggests FFF beams might play an important role in the reduction of the dose to the OARs and the general healthy tissue.

Vassiliev et al. [65] conducted study to assess the feasibility of stereotactic radiotherapy for early stage lung cancer using photon beams from a Varian Clinac accelerator operated without a flattening filter. The study concludes that radiotherapy with unflattened beams is feasible and requires substantially less beam-on time, facilitating breath-hold and gating techniques.

Eventhough many mediums like air, water, water equivalent phantoms ,films etc were used for the out of field dose measurements in the above described studies, we have decided to finalize the measurements using films considering its accuracy in the same. This is well described by pierluigi Casolaro in his review [66]

discussing a large number of publications using radio chromic film indicating the remarkable interest in film dosimetry. Niroomand et al. [67] describes the application, data collection, and analysis of radiochromic films in the AAPM task group .

2.6 Moliere Multiple scattering Theory

Experiments and analysis on my thesis work leads to Moliere multiple scattering theory, through which I could explain on scattering and out of field dose. Film measurement was adopted to generate the theoretical modeling based on Moliere scattering. Again in this new era, attention is directed to Moliere multiple scattering theory, which stood the basis for all calculation models which we currently follow.

Midhun et al [68] provides a precise knowledge of the bremsstrahlung spectrum. With the help of recoiled Compton electrons they have measured the energy distribution of high-intensity bremsstrahlung. The spectrum has been reconstructed using Compton cross sections retrieved from the ENDF/B.VIII.0 library and further validated using theoretical simulation by the Geant4 code with incorporating ENDF/B-VIII.0–recommended cross sections.

E. J. Williams [69] published a simple theory of multiple scattering of charged particles in which the result of deflections arising due to the collisions of fast particles with atoms of the medium and the calculations based on the Rutherford law for the interaction of unscreened Coulomb charges with a Gaussian distribution of the probabilities of deflection by an angle theta (θ).

The Goudsmit and Saunderson [70] theory of multiple scattering of electron suggests that the particle path in a layer of the medium and the thickness of this layer are identical. This theory holds good for all scattering angles. It is believed that the largest inaccuracy remaining in the results given is due to uncertainties in the single scattering law.

H. S. Snyder and W T. Scott (71) worked on the theory of multiple scattering of charged particles. They extended the theory in the small-angle approximation

valid for thin foils and fast particles. The extension consists of an exact solution of the integral diffusion equation for the correlated probabilities of lateral and angular displacements, and the numerical integration of the resulting expression for the angular distribution. These studies were mathematically close to each other and to the Goudsmit and Saunderson theory.

Voskresenskaya. O and A. Tarasov [72] revisited Moliere multiple scattering theory concerning the determination of the screening angular parameter. A universal form of the Coulomb corrections, to the screening angle, the exponential part of the distribution function, and the angular distribution, is discussed within the small-angle approximation of this theory. Also the accuracy of the Moliere theory in determining the screening angle is estimated.

Bethe.H.A [73] has derived Moliere's theory of multiple scattering of electrons and other charged particles in a mathematically simpler way. According to Moliere multiple scattering theory, the differential scattering law enters the theory only through a single parameter, the screening angle $\chi a'$, and the angular distribution, except for the absolute scale of angles, depends again only on a single parameter *b*, the impact parameter. Bethe re-investigated the transition to single scattering and an asymptotic formula is obtained which agrees essentially with that of Moliere.

The generally accepted Moliere theory of multiple scattering, which employs the small angle approximation, is used by V. I Yurchenk [74] and derived a kinetic equation for the distribution function in the variable $q= \sin(\upsilon/2)$, (where variable q determines the momentum transfer) for the case of a scattering cross section of general form under the assumption that the region of multiple scattering is small. The limits of the kinetic equation are discussed, with no restrictions imposed on the scattering angles. It is found that the equation has a solution in the form of an integral. Also, it is established that the solution is applicable over the entire range of angles, from 0 to 180° The accuracy of the results were verified by the Monte Carlo method over the entire range of angles.

A. A. Bednyakov [75] went through the misconceptions regarding the Moliere multiple scattering theory and its application in the analysis of experimental results made from several other works. In this article Bedndyakov comments that the critics of this theory misinterpreted the Molière method for determining the cross section of particle scattering by atoms with the screening of their nuclear fields by electron shells, described by the Thomas–Fermi statistical model. Also he confirms that if the original Moliere method is applied consistently, the obtained scattering cross section generally agrees with the results of later classical calculations carried out by Lindhard and his collaborators and other authors. Paper concludes that Molière theory of multiple scattering of fast charged particles is applicable for any value of α, especially since it may be corrected rather easily when more accurate values of the parameters of the multiple scattering process are required.

CHAPTER 3
METHODS AND MATERIALS

3.1Medical Linear Accelerator

The Medical linear accelerator (Linac) is a device that uses high-frequency electromagnetic waves to accelerate charged particles such as electrons to high energies. The high-energy electron beam itself can be used for treating superficial tumours, or it can be made to strike a target to produce x-rays for treating deep-seated tumours.

Out of different accelerator designs available, the linear accelerators used in radiotherapy uses either by traveling or stationary electromagnetic waves in the frequency of microwave region. In the case of the standing wave structures the terminator provide maximum reflection to provide maximum reflection of the waves at both ends of the structure, so that the combination of forward and reverse traveling waves will give rise to stationary waves. In the standing wave design, the microwave power is coupled into the structure through side coupling cavities. Such a design tends to be more efficient than the traveling wave designs since axial, beam transport cavities, and the side cavities can be independently optimized.

Fig 3.1 is a block diagram of a medical linear accelerator showing major components and auxiliary systems. Direct current (DC) power from the power supply is directed to the modulator, which includes the pulse-forming network and a switch tube known as hydrogen thyratron. High-voltage pulses from the modulator section are flat-topped DC pulses of a few microseconds in duration. The high voltage pulses from the modulator are delivered to the magnetron or klystron and simultaneously to the electron gun. Pulsed microwaves produced in the magnetron or klystron are injected into the accelerator tube or structure via a waveguide system. At the proper instant electrons, produced by an electron gun, are also pulse injected into the accelerator structure The accelerator waveguide, is evacuated to a high vacuum consists of a copper tube with its interior divided by copper discs or diaphragms of varying aperture and spacing. The electrons injected into the

accelerator structure interact with the electromagnetic field of the microwaves. The high-energy electrons exit from the accelerator window they are in the form of pencil beam of about 3 mm in diameter. In the low-energy linacs (up to 6 MV) with relatively short accelerator tube, the electrons are allowed to proceed straight on and strike a target for x-ray production. In the higher-energy linacs, however, the accelerator structure is too long and, therefore, is placed horizontally or at an angle with respect to the horizontal. The electrons are then bent through a suitable angle (usually about 90 or 270 degrees) between the accelerator structure and the target. The precision bending of the electron beam is made possible by the beam transport system consisting of bending magnets, focusing coils, and other components.

Linacs are usually isocentrically mounted and the major components are, Gantry, gantry stand, modulator cabinet, patient support assembly (treatment table), and the control console.

The main beam forming components of a modern medical linac are given by, RF power generating system, injection system, accelerating waveguide, auxiliary system, beam transport system, beam collimation and beam monitoring system.

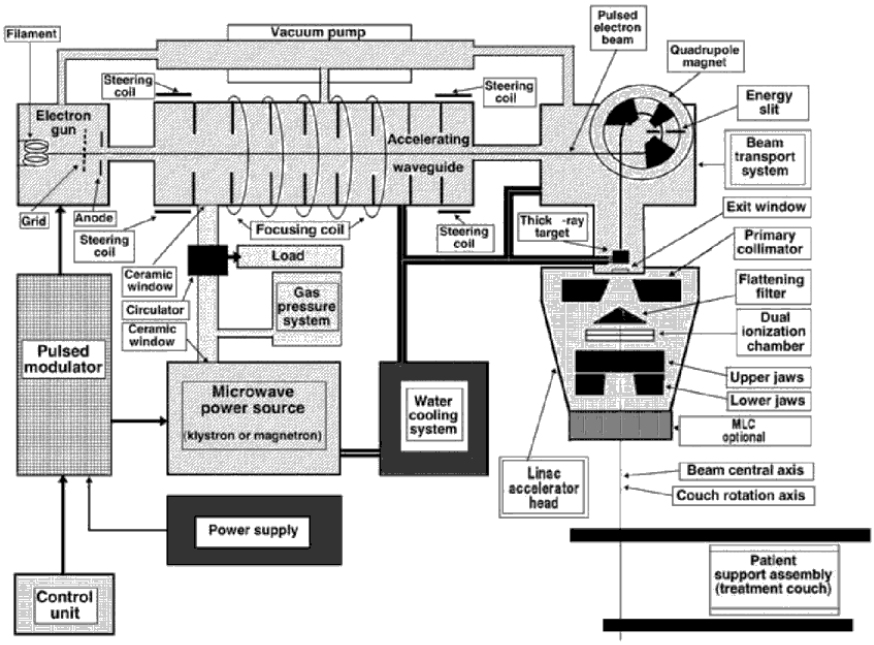

Fig 3.1:Block diagram of medical linear accelerator [podgosark 2006]

For this research work, Elekta Versa HD Machine and Varian Clinac ix linear accelerator machines [Fig 3.2 A and B respectively] at department of Radiation Oncology, Malabar Cancer Centre, Thalassery, Kannur, India were used.

Specifications of Elekta Versa HD :

- Photon energies: 6MV, 10MV, 15MV, 6MVFFF, 10MVFFF
- Electron energies: 4Mev, 6MeV, 8 MeV, 10 MeV, 12 MeV, 15 MeV
- MLC: Agility
- Flattening filter: Aluminium
- Imaging systems: iViewGT and XVI
- It is equipped with hexapod couch, and ABC automatic breath control system

Specifications of Varian Clinac iX

- Photon energies – 6MV and 15MV
- Electron energies - 4Mev,6Mev,9Mev,12Mev,15Mev,18Mev
- MLC- 120 MLC with maximum static field size of 40cm*40cm^2 (0.5 cm leaf resolution at isocenter for the central 20 cm of the 40 cm x 40 cm field)
- Imaging Systems: On Board Imaging System with EPID- Portal vision.
- Respiratory gating facility available.

(A) **(B)**

Fig 3.2 Linear accelerators. (A) Varian Clinac iX (B) Elekta Versa HD

3.2 Interactions

Electrons and photons interact differently with matter.

3.2.2 Electron Production

Electrons are widely used in radiotherapy for treatment of the superficial tumors. The electron beam, as it exits the window of the accelerator tube is a narrow pencil beam of about 3 mm in diameter. In the electron mode of linac operation, this beam, instead of striking the target, is made to strike an electron scattering foil to spread the beam as well as get uniform electron fluence across the treatment field.

The scattering foil consists of a thin metallic foil, usually of lead. The thickness of the foil is such that most of the electrons are scattered instead of suffering bremsstrahlung. However, a small fraction of the total energy is still converted into bremsstrahlung and appears as x-ray contamination of the electron beam [76].

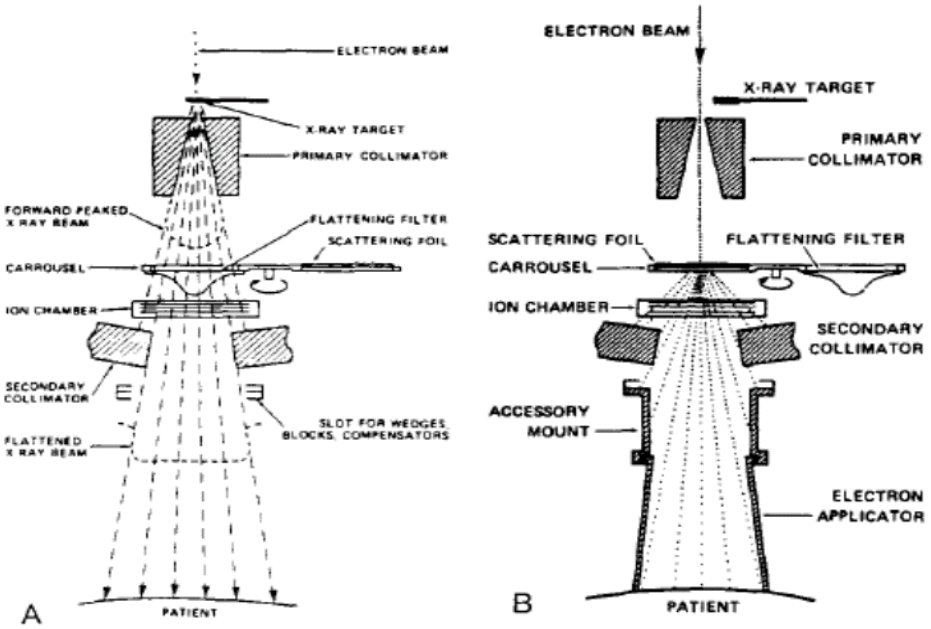

Fig 3.3 Components of treatment head (A) X-ray therapy mode (B) Electron therapy mode(F M Khan 2013)

3.2.3 Electron interaction with matter

As electrons travel through a medium, they interact with atoms by a variety of Coulomb force interactions that may be classified as follows: The interacting electron is known as the incident electron. Incident electrons may interact with:

(a)The nucleus of an atom

When the electron passes near the nucleus of an atom the negatively charged electron is attracted towards the positively charged nucleus. This sudden deceleration from the original path of electron results in energy loss. This kinetic energy lost by the electron is emitted in the form of x-ray photons and the radiation produced is called bremsstrahlung radiation or braking radiation.

(b)The orbital electrons of an atom

When an electron with sufficient energy higher than the binding energy of orbital electron interacts with atom, usually with the inner orbital electron and ejects the orbital electron from the atom leaving the atom positively ionized. To return to the normal state the atom emits excess energy in the form of x-ray photon and is

called characteristic radiation or characteristic x-rays, as the wavelength of produced x-rays are characteristic of the atom. Another way to attain normal state by the atom is ejection of an orbital electron by absorbing the excess energy. This electron is called auger electron.

Interactions may be

(a) Elastic, resulting in no loss of energy

(b) Inelastic, where the kinetic energy of the incident electron changes

3.2.3.1 Electron Scattering

When a beam of electrons passes through a medium, the electrons suffer multiple scattering due to Coulomb force interactions between the incident electrons and, predominantly, the nuclei of the medium. As a result, the electrons acquire velocity components and displacements transverse to their original direction of motion.

The scattering power varies approximately as the square of the atomic number and inversely as the square of the kinetic energy. For this reason, high Z materials are used in the construction of scattering foils. Scattering foils spread out the electron beam that emerges from the accelerator tube and are made thin to minimize x-ray contamination of the electron beam.

3.2.3.2 Moliere Scattering

In Linear accelerators, the high energy charged particle passes through and interacts with different thickness of the incident material. This led to multiple scattering by the atoms of the interacting medium. Hence theory of multiple scattering is always important in high energy interactions. Moliere derived multiple scattering in a mathematically simpler way. The Moliere method is independent of the exact form of the single scattering law, but contains a model-dependent parameter representing the atomic screening, and is called ‘screening angular parameter’ χ_a. The theory was developed for the case of multiple scattering of fast charged particles within small angles in a disordered medium that consist of atoms

described by the Thomas–Fermi statistical model. He obtained an approximate expression for his screening parameter,

$$\chi_a \approx \sqrt{1 + 3.34(\frac{Z\alpha}{\beta})^2} \quad (3.1)$$

$\chi_a$represents the influence of atomic electron shells on the interaction potential of the colliding particles and acts essentially as a "lower cut off angle" that eliminates the angles producing no substantial contributions to the total angular distribution of scattered particles [75].

E. J. Williams [69]; Goudsmit and Saunderson [70] published their work on multiple scattering theory. This two are considered as important earlier work in multiple scattering theories.

3.2.4 Photon Production

X-rays produced by interaction of highly accelerated electrons with high Z target material includes Bremsstrahlung and the Characteristic X-rays. The target is water cooled and is thick enough to absorb most of the incident electrons. As a result of bremsstrahlung-type interactions the electron energy is converted into a spectrum of x-ray energies with maximum energy equal to the incident electron energy. Bremsstrahlung X-rays gives a continuous spectrum. Hence X-ray spectrum includes continuous spectrum of bremsstrahlung photons superimposed by characteristic X-ray spectrum (Fig-3.4).

The X-ray spectrum exiting the bottom of the X-ray target is forward peaked, so the flattening filter is required to provide a more uniform intensity across the treatment field. The beam passes through a series of collimators to adjust its shape for treatment purposes. These collimators are again generally composed of high-Z materials in order to adequately block the radiation Faiz M Khan [76]; Podgorsak.B [77]. X-ray therapy mode of a linear accelerator is given in Fig-3.3

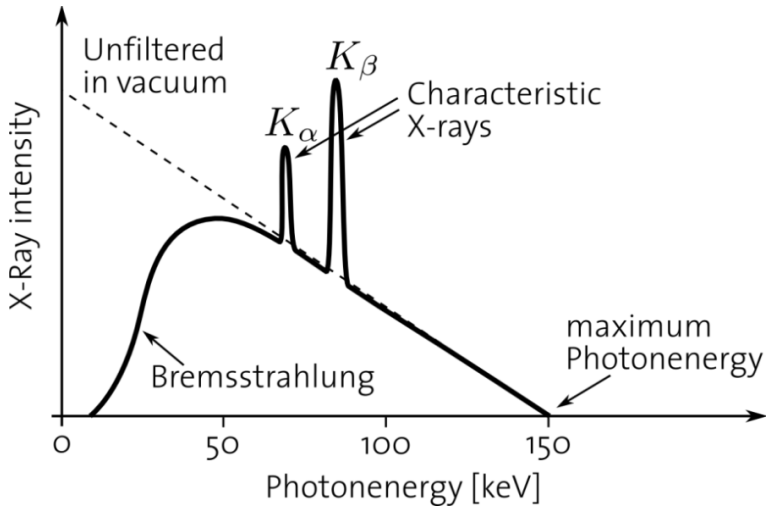

Fig 3.4 - X-ray Spectrum.

3.2.5 Interactions of Photons with Matter

Photon interaction processes are generally classified into Scattering and Absorption. These processes lead to the partial or complete transfer of the photon energy.

3.2.5.1 Scattering

Scattering is a process in which particle is forced to change in direction of motion due to one or more localized non-uniformities in the medium through which it passes. Scattering can be classified in to two types, elastic and inelastic.

3.2.5.2 Primary and Scattered Dose Components

Primary and Secondary particle in a beam equally contributes to dose (ie, photons and electrons). Extents of this contribution are different in different tissues, and differ with the in homogeneities and beam boundaries Papanikolaou N et al. [78].

The photons will undergo different interactions when passing through matter. The main interactions are; the Photoelectric effect, Compton scattering and Pair production. In linear accelerators, most of these interactions are Compton-scattering events, which generate secondary electrons in addition to scattered

photons. Pair production can occur if the incident photon has energy above 1.02 MeV, resulting in the generation of electron-positron pairs and subsequent generation of photons of 0.51 MeV from positron annihilation. Other interactions are Rayleigh scattering, Thomson scattering and photonuclear reactions and most importantly the less discussed Moliere scattering etc.

3.3 Detectors for Measurement

3.3.1 Ionization Chamber

Ionization chamber is a gas filled cavity surrounded by a conductive outer wall and having a central electrode. In a medical LINAC, the radiation output or output of the machine is measured by ionization chambers placed in the photon beam. The ionization chambers measure the amount of charge released by the photon beam, and is a measure of the photon beam's ability to ionize matter. The response from the ionization chambers is given in units of MU (Monitor Units). Various types of ionization chambers are there according to geometry and construction like cylindrical ion chamber, Parallel plate ion chamber, Extrapolation chamber and well type chamber. Cylindrical ion chambers are used in this study.

A cylindrical ion chamber is a gas filled cavity surrounded by an outer wall and having a central collecting electrode (Fig 3.5). The wall and the collecting electrode are separated with a high quality insulator to reduce the leakage current due to very high applied potential. There is a guard electrode usually inserted between the collector and the high voltage electrode whose potential is same as that of collector. The active volume of an ionization chamber is the volume of the gas, where the ions or electrons can be drawn to the collector. The guard electrode can define the active volume of the ionization chamber because some of the ions formed in the gas are drawn to the guard electrode and can't contribute to the signal from the collector. The nominal cavity volume is 0.6 cm^3. The cavity length is 24 mm with an inner diameter of 6.25 mm. The graphite outer wall is 0.5 mm in thickness. Most cylindrical chambers are supplied with a build-up cap. This is placed around the chamber wall in order to achieve Charged Particle Equilibrium.

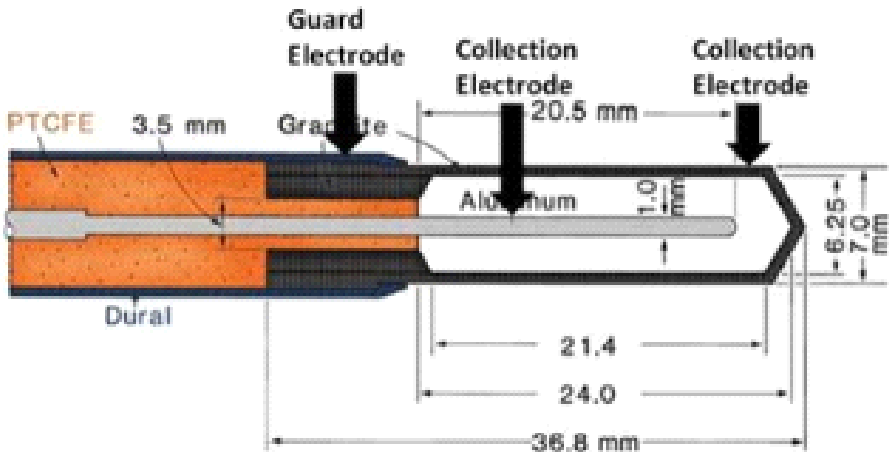

Fig 3.5 Components of a cylindrical ionization chamber (Oncology medical physics)

High degree of fidelity and a wide dynamic range of the electrometers enable them to use with a water phantom scanning system.

3.3.1.1 Semiflex ion chamber

Fig 3.6 Semiflex ion chamber

Fig 3.6 shows PTW cylindrical ion chamber type 31010 with volume 0.125 cm^3 with waterproof and semiflexible design. It has got a spherical sensitive volume, which results in a uniform spatial resolution and a flat angular response along all three axes of a water phantom. It can easily mounted in the water phantom for measuring the profiles and depth doses with minimized directional response. It has got a uniform spatial resolution along all three axis of a water phantom. The nominal useful energy range is from 140kV to 50 MV photons and 6MeV to 50MeV

electrons. The wall material is graphite with protective acrylic covering and inner diameter of the chamber is 5.5 mm. Since the measuring volume is approximately spherical results in a flat angular response over an angle of ±160º. Scanning Setup using Semiflex chamber and Radiation field analyser is shown in Fig 3.10.

3.3.1.2. PinPoint ion chamber

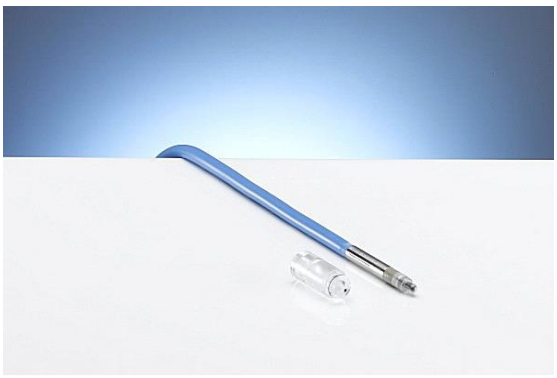

Fig 3.7. PinPoint chamber

Fig 3.7 shows PTW Pin-point ion chamber of type 31014 with sensitive volume 0.016 cm^3. It is a waterproof chamber with high spatial resolution and is suitable for dose measurements in small fields in water. The PinPoint ionization chambers inner diameter is of only 2mm diameter and is ideal for small field dosimetry. It has a flat angular response, since the measuring volume is approximately spherical. It can be used for both depth dose and absolute dose measurements. The wall material is graphite with a protective acrylic cover and fully guarded up to the measuring volume. The nominal energy range is up to 50MV photons and the voltage of the chamber is +400V- 500V

3.3.2. Diode detector

Fig 3.8 Diode detector

Fig 3.8 shows s a PTW P-type Si diode detector of type 60016. They have extremely small sensitive volume of 1mm^{2}circular and are waterproof. It is suitable for scanning stereotactic and IMRT fields because of their superior spatial resolution and suitable for use in remote controlled water phantom. It has got a favorable signal to noise ratio and are suitable for high precise dose distribution measurements. It needs to be cross-calibrated against any other chamber with identical condition and setup. The dosimetry diodes are to be irradiated in axial direction. Reference point of this detector is on detector axis, 2mm from detector tip. For measurement purposes the voltage of the chamber needs to be kept at zero voltage.

3.3.3. microDiamond detector

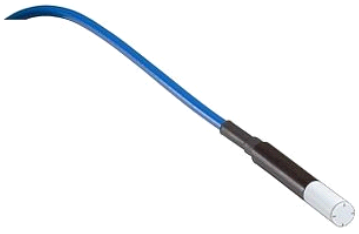

Fig 3.9 microDiamond detector

Fig 3.9 shows a PTW microDiamond detector of type 60019 and is the first commercially available single crystal diamond detector worldwide suitable for

clinical dosimetry. It combines the advantages of natural diamond detectors and silicon diode detectors. Due to its spatial design and material property microDiamond detector shows almost no deviations in absorbed dose to water. It has a very small sensitive volume of 0.004mm^3 and suitable for small field sizes. With the diamond detector precise and accurate measurements in photon, electron and proton fields are possible. The radius of the chamber is 1.1mm and thickness 1.1µm. Reference point is on detector axis, 1mm from detector tip, marked by ring. Similary as in the case of diode detector the voltage of the detector must to keep at 0V.

Fig 3.10 Experimental setup for the out of field dose measurements using radiation field analyzer (RFA) with semi flex ionization chamber.

3.3.4 Octavious 4D Phantom and 2D-array

Fig 3.11. Octavius phantom

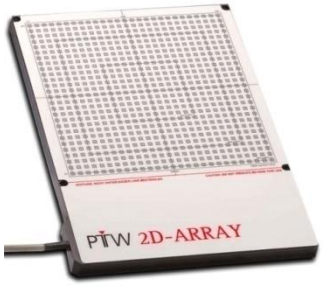

Fig 3.12. PTW 2D-Array

Plans generated using the treatment planning system is verified before executing the treatment as part of the quality assurance. 2D dosimetry system is used for static, dynamic and rotational patient plan verification. It measures the composite dose in one plane (coronal or sagittal depending on phantom setup), acquired at different gantry positions. The Octavius phantom (Fig.3.11) has an octagonal shape in its cross section, and is designed to allow composite rotational IMRT plan verification.

The 2D-array detector 729 (PTW, Freiburg, Germany) is a two-dimensional detector array with 729 equally spaced ionization chambers with a distance of 1 cm (centre to centre) and covering an area of 27 × 27 cm^2. Each chamber has a size of 0.5 × 0.5 × 0.5 cm^3.

The physical dimensions of the 2D-array detector 729 are 2.2 cm (thickness) × 30.0 cm (width) × 42.0 cm (length) with the effective reference point located 0.75 cm below the surface of the array. Plan verification is done using PTW-verisoft software (version 6.0.2.8).

The verisoft software used with the 2D-array is based on the gamma index. Passing criteria of 3mm distance to-agreement and 3% dose difference with reference to the selected dose where used for the study. The gamma index combines dose difference and distance difference to calculate a dimensionless metric for each

point in the evaluated distribution. Dose is reconstructed for each gantry angle and sum of the different angular contributions reconstructed to obtain the total dose.

3.3.5 EDR2 Films

The extended Dose Range EDR2 film (Kodak Extended Dose Range 2: Eastman Kodak, Rochester, NY) was used as a reference two-dimensional (2D) dosimeter. The small size and very fine mono dispersed-grain cubic microcrystal used in the EDR2 structure makes it a very slow-speed film as compared with other conventional films; it is nearly energy independent for dose values of less than 5 Gy [84-86]. For rapid-processing purposes, the EDR2 film is covered with double emulsion layers on a 0.18-mm ester base. Its large area, low cost and wide response range makes it unique.

In radiation treatment, current goal is to make sure that the dose variability obtained by the patient does not exceed 5 percent. This implies that the dose at the segmentation analysis of a LINAC needs to be understood as being within 2 percent, given all sources of error.

3.4 Phantoms

They are used to measure radiation under different conditions. Appropriate phantom material needs have the same effective atomic number, number of electrons per gram as that of tissue or water.

3.4.1 Water Phantom

Water is the standard phantom used for the dosimetry of both electron and photon beams due it its tissue equivalency. Water is widely used as the phantom material as human body contains majority of water and closely approximates the radiation absorption and scattering properties of muscle and other soft tissues. It is universally available with reproducible radiation properties and can make the measurement accurate. It is used for the output calibration in Radiotherapy as recommended by IAEA TRS-398. It has a groove to insert the chamber.

However, it is not always possible to perform dosimetry in a water phantom. In such

conditions plastic phantoms are used. Plastic phantoms are more suitable when films are used for dosimetry. For the phantom to be water equivalent for photon dosimetry, it must have the same linear attenuation coefficient and same linear absorption coefficient, whereas for electron dosimetry it must have same linear stopping power and same angular scattering power. For this condition to be satisfied by the phantom, it should have same electron density and same effective atomic number as water.

3.4.2 Radiation field Analyser (RFA):

Fig 3.13 Radiation Field Analyser (RFA)

A Water phantom that in which detector scanning is possible with the computer controlled measuring system and is essential for commissioning of a linear accelerator machine. Profile measurements and depth dose measurements are possible with RFA. The system consist of a Perspex tank with moving mechanism, a positioning device which allows the tank to be aligned, using the field indicator and laser system of the accelerator and the lines on the walls of the tank, a TBA CONTROL UNIT interface that connects the water phantom to the PC. It supplies power for the stepper motors and controls the detector movement. It has a TBA CONTROL PENDANT hand held terminal, a dual channel electrometer TANDEM. The software used is MEPHYSTO software. The water tank should be at least 10 cm larger than the scan in each dimension. The RFA should be filled with water and then positioned with the radiation detector cantered on the central axis of the radiation beam. It allows the scanning of the radiation field in orthogonal directions

without changing the phantom setup. A 3D scanner of an RFA should be able to scan 50 cm in both horizontal dimensions and 40 cm in the vertical dimension with 1mm movement accuracy.

3.4.3 Plastic Phantom

Acrylic Phantom Material is a clear plastic with the chemical formula (C5 H8 O2)n, polymethyl metha crylate (PMMA). It is also known under the trade names Lucite, Plexiglas and Perspex. Acrylic has a density of 1.185 g/cm3. It is available in 30 x 30 cm sections of varying thicknesses.

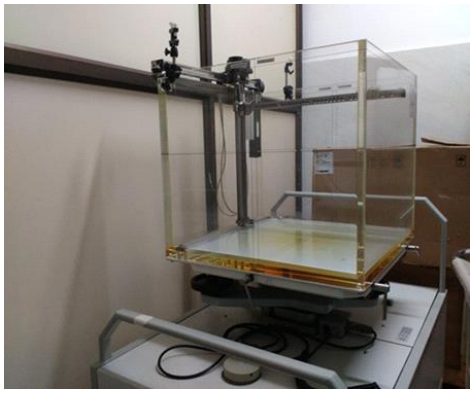

Fig 3.14 Water Phantom **Fig 3.15 Plastic phantom**

3.5. Treatment Planning System

The Treatment planning system simplifies the developments of complex treatment plans. It's comprehensive toolset to provide the infrastructure for increased consistency and efficiency in our planning process. Once image datasets are loaded and the tumors are contoured by the radiation Oncologists, the systems helps to develop a complex plan. Once the plans are approved it is transferred to treatment machine. Eclipse treatment planning system (version 13.7) and Monaco treatment planning system (Version 5.2) were used for the study.

3.5.1 Eclipse Treatment Planning System

Eclipse Treatment planning system has comprehensive clinical protocol templates that speed the planning process. Eclipse uses a very fast optimization

algorithm to converge rapidly to a good plan. While the plan evolves, the clinician can see real-time updates to the dose-volume histogram (DVH), objective function, and fluence matrices. The best plan can be created quickly by interactively modifying the dose constraints during optimization. The user can restart any previous optimization from where it ended, even using different image sets, to efficiently adapt treatment plans during the course of treatment. The leaf motion calculator (LMC) converts optimal fluence to a deliverable leaf motion sequence and fluence while reducing treatment time and monitor units. The LMC incorporates the physical limitations, leakage, and dosimetric effects of the multileaf collimator into the leaf sequence calculation. Varian uses the trade name RAPID ARC for the volumetric modulated arc therapy technique.

3.5.2 Monaco Treatment Planning System

Monaco system offers treatment planning for modalities like 3DCRT, IMRT, VMAT and SBRT. Monaco features innovative biological cost functions with multi-criteria constrained optimization, a leaf sequence optimizer and a robust Monte Carlo dose calculation algorithm [82]. It has Montecarlo and collapsed cone algorithm with the Monte Carlo algorithm, Monaco achieves high accuracy and speed. This improves overall efficiency of the planning system. Monaco uses biologically constrained optimization for VMAT and IMRT. Elekta uses the term VMAT for the volumetric modulated arc therapy technique.

CHAPTER 4

MEASUREMENT AND ANALYSIS OF OUT OF FIELD DOSE

Modern radiotherapy treatment techniques entirely depend upon the treatment planning system. Accuracy of treatment planning system is highly important. The present treatment planning algorithms simulate the dose distributions based on statistical or empirical models**.** This chapter discuss on the studies conducted to know about the treatment planning system accuracy in out of field dose measurement.

4.1 Out of field photon dose measurement using 2D-array detector and comparison with treatment planning system calculated values.

Many studies were conducted to check the treatment planning system accuracy [18-20, 83, 84]. Most of the studies used detectors like, TLD, Ion camber, OSLD, gafchromic film, plastic scintillators etc. In this section initial work done in the measurement of out of field photon dose using 2D-array detector and comparison made with treatment planning system is discussed. 2D-array detector is mainly used for the fluence comparison and point dose measurement for pre-treatment patient plan verification. Evaluation of the dose in this done based on gamma passing criteria suggested by low et al. [85].

4.1.1 Materials and methods

Fifty-one patients diagnosed with pharyngeal cancer and planned for Volumetric Modulated Arc Therapy (VMAT) using the Eclipse treatment planning system were selected for the study. The key study variables include the out of field photon dose (in Gray) using two equipments: (i) 2D-array detector with 729 ion chamber and 4D Octavius phantom and (ii) treatment planning system (Eclipse version 10.0) at 5, 8, 10 and 12 cm distances from the field centre along X and Y axes as shown in Figure 4.1.

Other variables collected include age, sex of the patient and site of cancer.

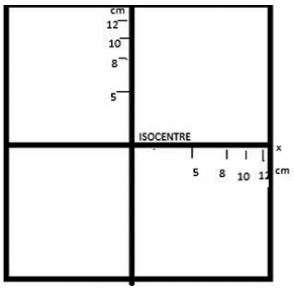

Fig 4.1: Schematic diagram (not to scale) Measurement plane for out of field dose setup for pharyngeal cancer planned for volumetric modulated arc therapy (VMAT).

4.1.1.1 Collection of Data:

Verification plan was created for each treatment plan in Eclipse treatment planning system (version10.0) using the analytical anisotropic algorithm[AAA][86-88] with the 2D- array ionization chamber and the 4D octavius phantom[89,90]. All the plans were done using 6MV photon energy. In conventional radiation therapy treatments, out-of-field organs are defined by the field border. However, for modern radiation therapy techniques like intensity modulated radiation therapy (IMRT) and volumetric modulated arc therapy, where fields are defined by modulated beam intensities, it is difficult to definitively define a field border [91].

In the present study, the out of field dose were measured from the isocenter (centre of the planning target volume). Doses were measured along the +X and +Y axes of the 2D-array plane. Measurements were taken at 5,8,10 and 12 cm distances away from the isocenter along the above- said axis in the treatment planning system. All measurements were performed on a Varian Clinac iX linear accelerator equipped with a millennium 120 leaf collimator (Varian oncology systems, Palo Alto, CA) and the results were cross compared with the fluence obtained from the treatment planning system and is shown in Fig 4.2 and Fig 4.3 respectively. Evaluation for the 2D-array measurements was done using PTW versoft software by keeping the passing criteria as 3mm distance to agreement(DTA), 3% dose difference(DD), for 95% of the evaluated dose points [92,85].

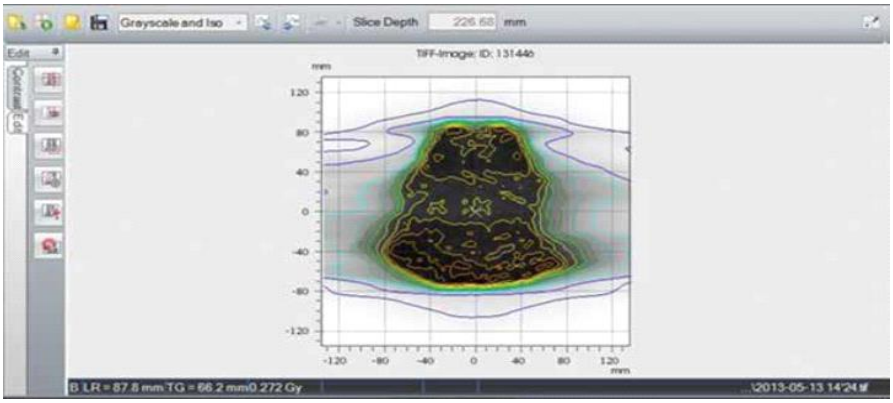

Fig 4.2: Fluence from 2D-array measurement of patients diagnosed with pharyngeal cancer and planned for volumetric modulated arc therapy (VMAT)

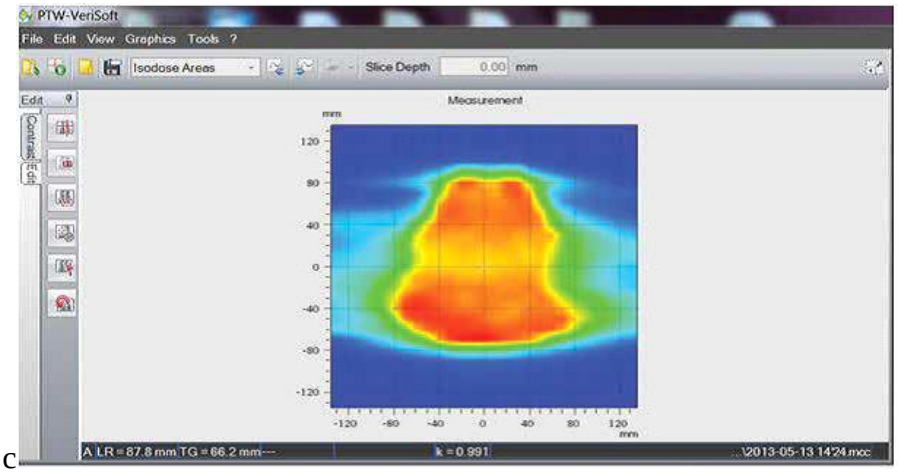

C

Fig 4.3: Fluence from radiotherapy treatment planning systems measurement of patients diagnosed with pharyngeal cancer and planned for volumetric modulated arc therapy (VMAT)

4.1.2 Data Analysis and Statistics:

Data were entered into EpiData entry version 3.1 and analyzed using EpiData analysis version v2.2.2.182 (EpiData Association, Odense, Denmark). Mean (standard deviation) was used to summarize doses of radiation at varying distances from the field edge. Out of field dose was compared across both methods: the TPS and the 2D- array detector using a t-test or Kruskal-Wallis test depending on the distribution of the data. Ethics Considerations: Ethics approval to conduct the study was obtained from the institutional review board (IRB) and institutional ethics

committee (IEC) of Malabar Cancer Centre. Additional ethics approval was also obtained from the Ethics Advisory Group of the International Union against Tuberculosis and Lung Disease (The Union), Paris, France. The present study does not involve any human participant.

4.1.3 Results:

Table 4.1 shows the mean and standard deviation for each of the calculated ($\mu calc \pm \sigma$) and measured ($\mu meas \pm \sigma$) doses at varying distances from the isocenter along the positive X and Y axis. At all distances, the calculated and measured doses were found to being in good agreement. From the table, it is observed that the deviation increases as the distance increases. A maximum deviation of 28.6% along the Y-axis and 5.1% along X-axis was observed at 12 cm. Table 4.2 shows that the out of field dose (both measured and calculated) is significantly associated with the site of cancer, highest in nasopharyngeal cancer. Figure 4.4 shows the variation of out of field dose with the distance from the isocenter. The plot clearly indicates that at distances near the isocentre the 2D-array measured dose and TPS calculated dose are in good agreement, whereas there is some variation as the distance away from the isocenter increases.

Table 4.1: Mean measured doses (μmeas ± σ) and mean TPS-calculated doses (μcalc ± σ) along both X and Y axes and at varying distances from the isocentre of patients diagnosed with pharyngeal cancer and planned for volumetric modulated arc therapy (VMAT)

Axis	Distance from Isocentre (cm)	Count	μmeas ± σ(2D array detector) (Gy)	μcalc ± σ(TPS) (Gy)	Difference (%)[[(μcalc-μmeas)/μmeas] *100
X	5	51	1.12 ± 0.29	1.14 ± 0.25	1.8
X	8	51	0.69 ± 0.23	0.70 ± 0.23	1.4
X	10	51	0.50 ± 0.15	0.52 ± 0.14	4
X	12	51	0.39 ± 0.12	0.41 ± 0.13	5.1
Y	5	51	1.42 ± 0.25	1.42 ± 0.24	0
Y	8	51	1.01 ± 0.46	1.05 ± 0.44	3.9
Y	10	51	0.44 ± 0.41	0.46 ± 0.39	4.5
Y	12	51	0.14 ± 0.09	0.18 ± 0.17	28.6

σ stands for standard deviation; TPS=Treatment Planning System; μmeas and μcal are expressed in Gray

Table 4.2: Association of demographic and clinical characteristics of pharyngeal cancer patients with the measured and calculated TPS dose and planned for volumetric modulated arc therapy (VMAT)

Characteristics	μmeas(Gy)	p-value	μcalc(Gy)	p-value
Sex				
Male	0.73	0.36	0.74	0.5
Female	0.67		0.7	
Site of cancer				
Nasopharynx	0.82	<0.001	0.84	0.002
Hypopharynx	0.61		0.65	
Oropharynx	0.75		0.75	

TPS = Treatment Planning System; μmeas and μcal are expressed in Gray

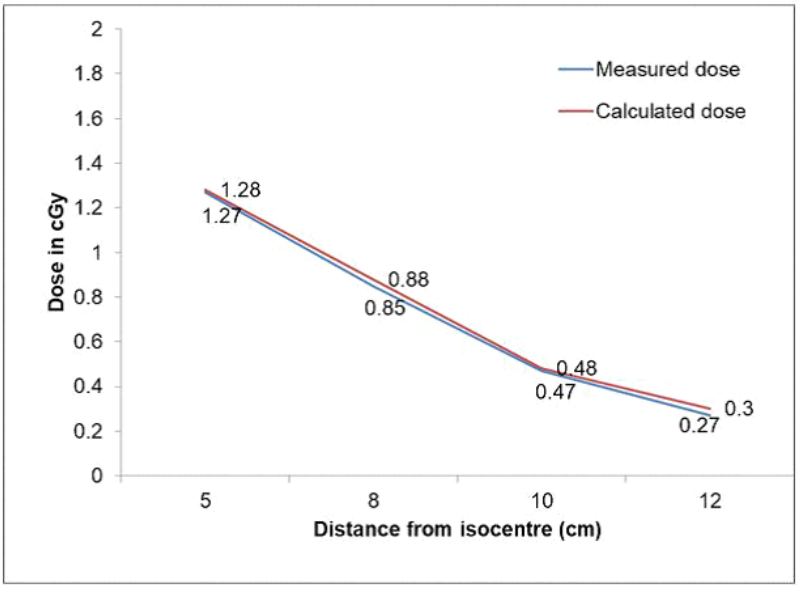

Fig 4.4: Variation of out of field dose with the distance from the isocentre of patients diagnosed with pharyngeal cancer and planned for volumetric modulated arc therapy (VMAT).

4.1.4 Discussion

In this study, we quantified the accuracy of the out of field dose calculated by the Eclipse TPS (version 10.0 using AAA algorithm) for a clinical treatment delivered with a Varian Clinac iX linear accelerator. The results show that in comparison with measured data, the calculated dose is in good agreement, although the small difference was observed at larger distances (12 cm).

'Study showed that, the percentage variation increases with increasing distance from the isocentre 'with a maximum value of 28.6% at 12 cm distance from the isocentre along the Y-axis. For smaller distances away from isocentre measured and calculated values are in good agreement.

In the present study, 2D-array detector was used with passing criteria of 3mm 3% and shows good agreement with TPS obtained values. A 2D-array consists of 729 ion chamber detectors. Detector characteristics will affect the measurement; like low resolution results in dose points in those regions appearing to have an artificially lower dose than the TPS dose. Energy response and detector position and size are crucial for measurement accuracy in the intensity modulated treatment

deliver. After 10cm distance from isocentre, there is a slight variation for the measured and calculated values. The out of field dose was highest in nasopharyngeal cancers probably due to the large volume of cancer compared to the other two cancer types. Out of field doses increases with large field size due to increase in the scattered doses.

4.1.5 Conclusion

2D-array detector shows good agreement between the measured and calculated out of field dose. The limitation of the study using 2D-array detector is that the maximum field size available for the detector is only 27x27 cm^2 for out of field measurements. Since the comparison study was conducted using 2D-array detector, it is difficult to compare with the other TPS studies using TLD and films. The results were specific to the Eclipse TPS version 10.0 (AAA algorithm) and Varian Clinac iX with 2D-array. Out of dose with TPS and linac combination depends on the particular algorithm and commissioning data. Further research is required to examine several commercially available TPS and linac combinations.

Due to the limitation of out of field measurement distance with a 2D-array detector, further study needs to be conducted to evaluate the out of field calculation accuracy of TPS.

4.2 Out of field dose measurement using ion chamber and comparison with treatment planning system calculated values

2D-array measurements were limited with its available area (27x27 cm^2) and hence in this work radiation field analyser (40x40x40 cm^3) was used which helps to make comparatively larger distance measurements and to get more accurate values. Since percentage depth doses at different distances from we have evaluated percentage depth doses at different distances from field edge were evaluated, a detector which is also accurate for surface dose measurements. Usually plane parallel chambers are preferred over cylindrical chambers for measurements in build up region, to achieve the CPE. The cylindrical chambers will not satisfy the CPE at higher dose gradient regions, due to its cavity effect. However in the case of PDD

measurements parallel plate chamber is not recommended by many authors [88] due to its volume effect. This is the reason in choosing the semiflex chamber for primary measurements, of which buildup region measurements are comparable with parallel plate chamber.

Also in this chapter flattening filter (FF) beams and flattening filter free (FFF) beams are compared in the out of field dose measurements.

4.2.1 Methods

Effect of out of field dose for different shielding condition were studied and compared with the treatment planning system. Also FF beams were compared with FFF beams, to check advantage of FFF beams in out of field dose reduction.

4.2.1.1 Data deduction and Analysis

The depth doses were calculated using Eclipse treatment planning system (version 10.0) for different field sizes (5x15, 10x15, 15x15 cm^2) and different shielding conditions (Jaw only, MLC only and Jaw+MLC) using energy 6 and 15MV. Longitudinal field size was fixed to 15 cm and lateral field size was kept asymmetrically as half beam, to make measurements under different shielding conditions. A dose of 200 cGy was used to generate the plans. Data was taken at different out of field positions (1, 2, 3, 5 and 10 cm away from the field edge), for depth up to 16cm on water phantom. Measurement of the depth doses were performed, using Varian Clinac iX linear accelerator equipped with a millennium 120 leaf collimator, under the same condition, with semiflex ionization chamber (0.125cc) as the detector. As a typical case, the percentage out of field depth doses thus measured at distance of 3 cm away from the field edge is estimated and compared with TPS predicted values in Fig: 4.5. As can be seen from this figure the measured depth dose shows a variation from the calculated depth dose for depths beyond 3cm. It is interesting to note that the depth dose shows a uniform variation beyond the depth of 10 cm. This may be due to the saturations in the multiple scattering. In order to estimate the variation between calculated and measured values of percentage depth doses, the variation is calculated at different depths for each out of field points and the average of the same, ($D_{calc} - D_{meas}$) averaged from 0 to 16 cm

depth, is taken as the mean value of relative variations for that particular out of field point. In this way the mean variation is calculated for each out of field points mentioned above and are tabulated in table 4.3. The uncertainity indicates the maximum deviation. In order to see the out of field dose distribution in the same plane at given depth, PDD was plotted for different out of field positions at a depth of 5cm , for 6MV and 15 MV beams and are shown in Fig: 4.6 and 4.7 respectively. The study was also extended using Elekta Versa HD machine. Measurements were carried out for the same distance and field sizes using 6MV and 10MV flattened and unflattened beams. Compared the out of field doses for flattened and flattening filter free beams. The results are shown through Fig 4.8(a)- 4.8(d).

4.2.1.2 Result and Discussion

Table 4.3 Difference between the measured and TPS calculated Percentage out of field depth doses at various out of field points, averaged over the range of 0-16 cm depth.

CONDITION	ENERGY	Field Size(cm^2)	Out of field position away from field edge				
			1cm	2 cm	3 cm	5 cm	10 cm
JAW ONLY	6 MV	5 X 15	1.2±4.48	4±4	6.2±6.4	12±3	5±2
		10 X 15	8.4±3.3	10±6	16±9	3±13	15±5
		15 X 15	3.5±3.8	1.4±3	6±4	13±10	4±6
	15 MV	5 X 15	-1.9±6.3	-13±7.9	2.9±10	14±17	5.9±12
		10 X 15	-3.9±4.8	5±7	6±8.8	-6±13	6±10
		15 X 15	1.3±2.8	-5.6±5	-3.5±8	11±15	10±5
JAW + MLC	6 MV	5 X 15	1.3±2.4	-10±16	-8.6±9.3	-7.5±11	1±5
		10 X 15	5±5.3	-8±6	4.3±5.3	3±12	5±10
		15 X 15	-1.1±1.8	-13±6	9.4±10	18±15	8±10
	15 MV	5 X 15	-5.8±5.5	-12±10	-6.4±11	-8±7	15±15
		10 X 15	-4.4±4	-6±6	-0.13±11	15±16	9±10
		15 X 15	1±3	-9.5±5.4	-1.9±5	18±5	6±5
MLC ONLY	6 MV	5 X 15	-28±0.82	-1.2±.6	-1.5±5	-19±9	10±12
		10 X 15	-3.9±1.1	0.01±1	-0.7±.7	6±4	-25±7
		15 X 15	-3±.47	0.5±2	-0.9±.9	8±2	-7±5
	15 MV	5 X 15	18±.53	-1.2±1.3	-5±4	-15±8	10±12
		10 X 15	-22±3.2	1±4	0.08±.6	15±11	-3±14
		15 X 15	23±1.5	1.1±3	0.4±.8	0.8±1	-5±5

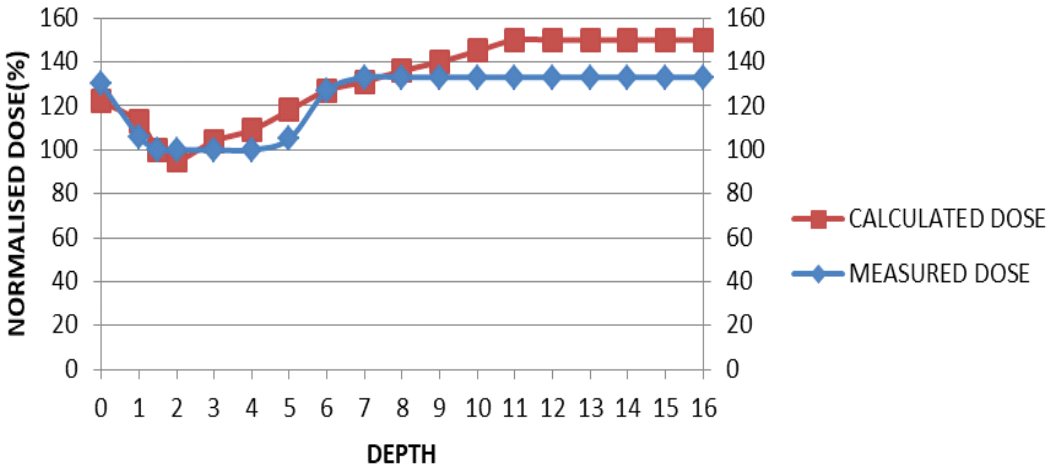

Fig 4.5 Percentage out of field depth dose, calculation and measured, at a point 3 cm away from the field edge, for jaw-defined field size of 5x15 cm^2 for a 6 MV photon energy.

Up to build up region the measured and calculated doses are in good agreement after the build-up region the dose difference increases with depth.

Similar observation for all field sizes and distances except for dose at 1cm distance due to detector positional errors.

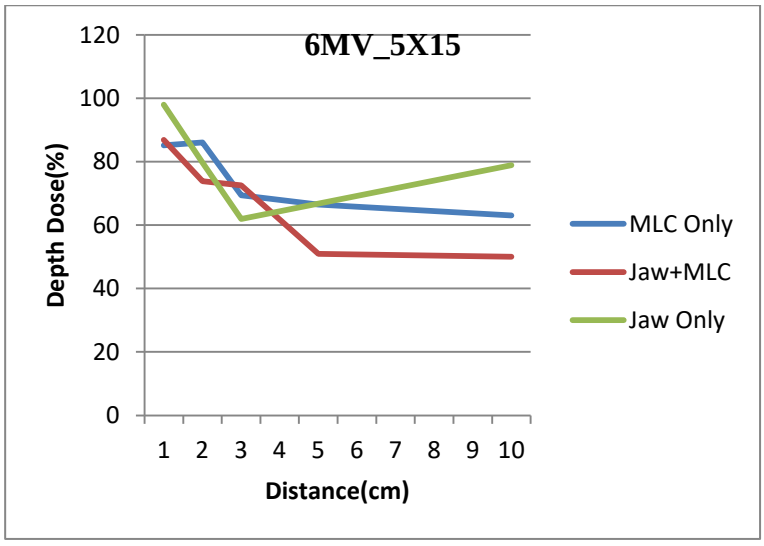

Fig 4.6: Beam profiles for different shielding conditions at various distances from the beam edge with fixed field size of 5 x15 cm^2 for 6MV photon beam at 5cm depth.

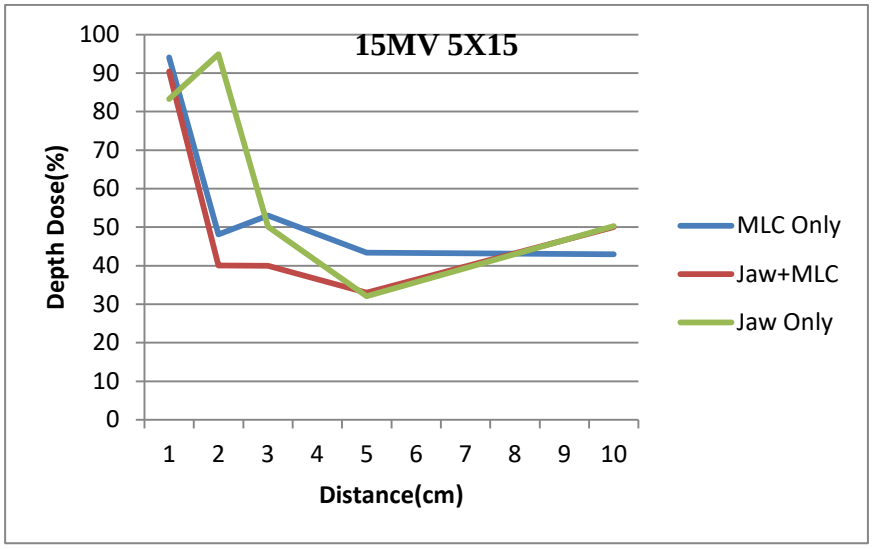

Fig 4.7: Beam profiles for different shielding conditions at various distances from the beam edge with a fixed field size of 5x15 cm^2 for 15 MV photon beam at 5 cm depth.

Fig. 4.6, 4.7 shows out of field dose profiles of 6MV and 15 MV respectively, under three shielding conditions (jaws only, MLC only, both jaws and MLC), as a function of distance from the field edge. The pattern is slightly different from the expected one for Jaw defined shielding conditions, especially for 15MV. This variation is observed at greater distance from the field edge. Measurement uncertainity at larger distance may be a reason for the same.

Fogliata et al. [84], reports uncertainty for very near and far distances from field edge. According to Kry S F et al. [97], the ability of the FFF beam to reduce the out of field dose was less for larger fields. With flattening filter removed, the head leakage substantially reduced, the collimator scatter was reduced, particularly very close to the field edge. Countering these benefits, patient scatter was increased, the reduction in the out of field photon dose was more pronounced with smaller fields than with larger. This study cannot be related to the studies by Howell et al and Heuvel et al, in which approximately 40% variation between measured and calculated is reported [18,83].

4.2.1.3 FFF Measurements

FFF beams are reported to be good in sparing the normal tissues by reduced out of field dose [62]. Out of field doses at 1cm and 5 cm away from the field edge were measured using FFF beams and FF beams and compared. Results of 6MV and 10 MV X-rays are shown in Fig 4.8(a) to Fig 4.8 (d). Fig 4.8 (a) represents depth dose for 6MV FF and FFF beams at 5 cm away (out) from field edge, figure 4.8 (b) represents depth dose for 6 MV FF and FFF beams at 1 cm away (out) from field edge. Similarly plots 4.8 (c) and 4.8 (d) give depth dose values for 5cm and 1cm away from field edge for 10 MV FF and FFF beams.

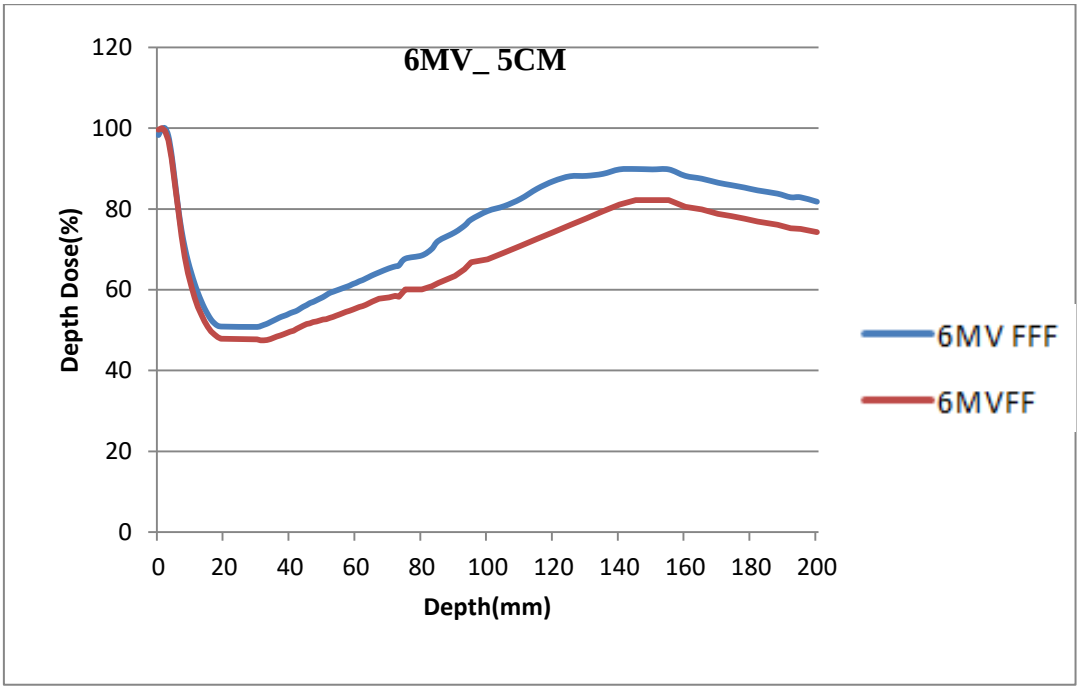

Fig 4.8 .(a). Dose difference between calculation and measurements for 6 MV FF and 6MV FFF beams for 10 × 15 cm^2 field at 5cm distance from the field edge.

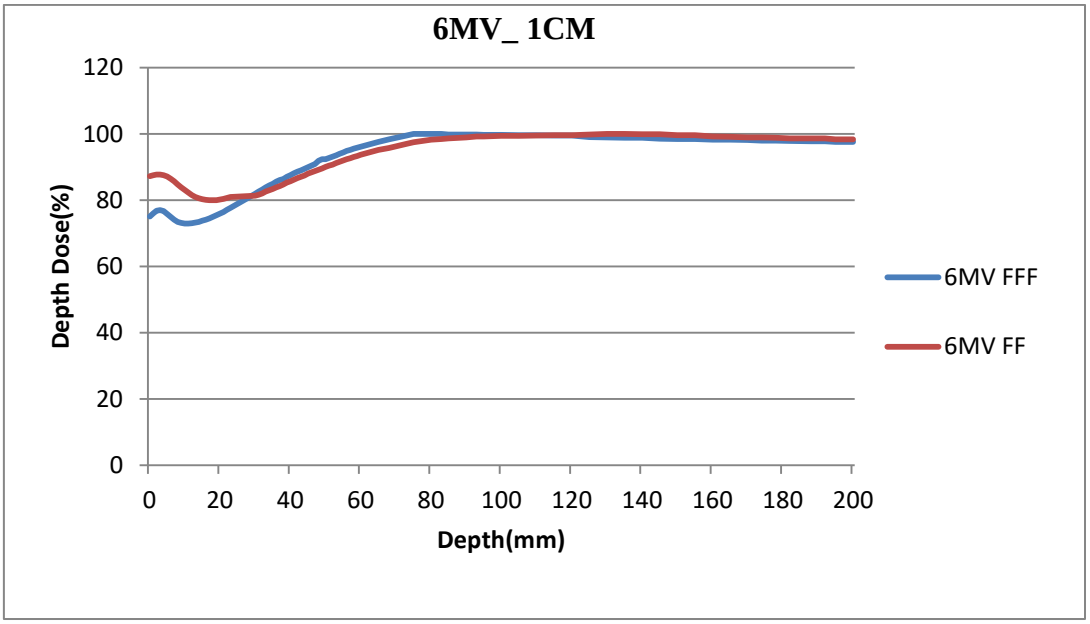

Fig 4.8 (b). Dose difference between calculation and measurements for 6 MV FF and 6MV FFF beams for 10 × 15 cm^2 field at 1cm distance from the field edge.

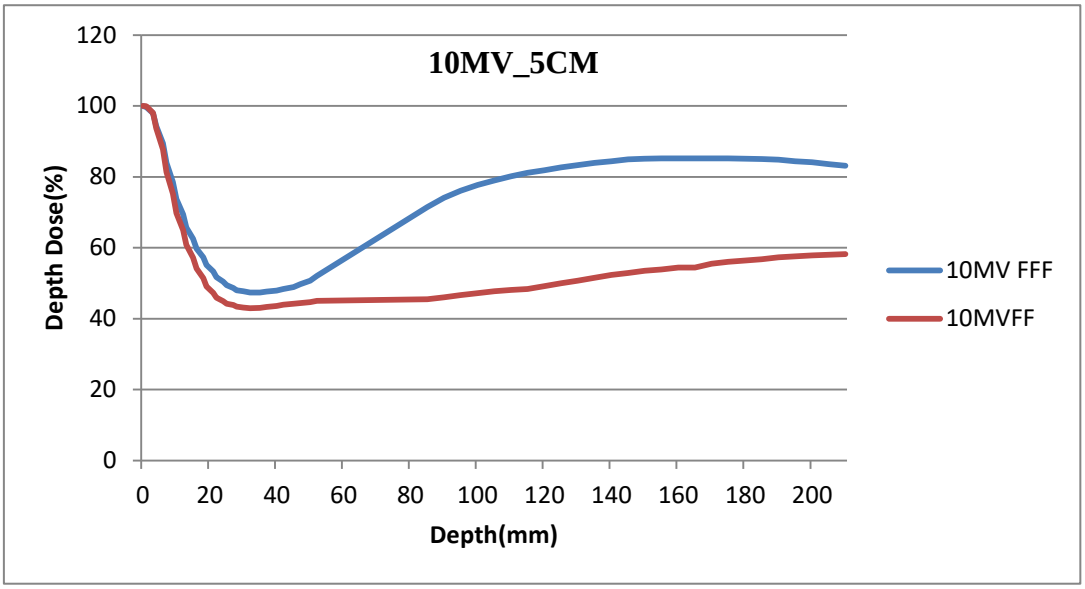

Fig 4.8 (c). Dose difference between calculation and measurements for 10 MV FF and 10 MV FFF beams for 10×15 cm^2 field at 5cm distance from the field edge.

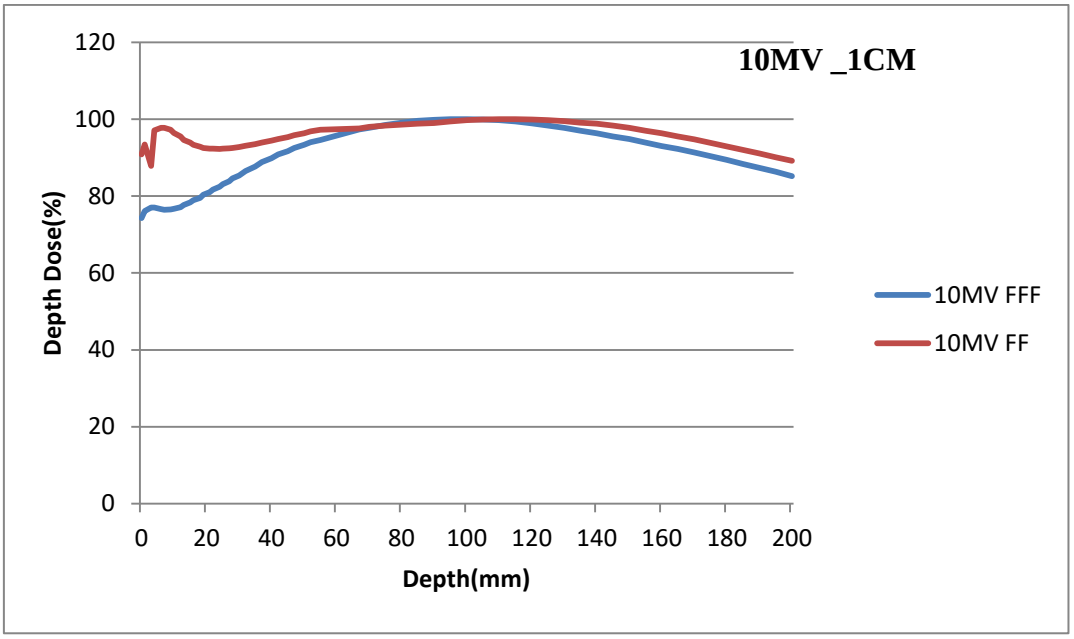

Fig 4.8 (d). Dose difference between calculation and measurements for 10 MV FF and 10MV FFF beams for 10 × 15 cm^2 field at 1cm distance from the field edge.

On evaluation it is found that up to a few centimeters depth, the dose from flattened and unflattened beams shows small difference for I cm distance away from the field edge. As the depth increases both FF and FFF shows same behavior. For 10 MV beams, at 5cm distance away from the field edge, FFF beams shows a higher dose as the depth increase compared to FF beams. It may be due to the fact that in FFF relatively larger components of lower energy beam will be available which is more bound to scattering in phantom. However, this is to be verified with more data for various fields and energies.

4.2.3 Conclusion

The study conducted using semiflex chamber shows more variation between measured and calculated values at larger depths and lesser variation near surface for larger distance away from field edge. Near the field edge, comparatively larger variation near surface and less variation as depth increases. The measurement uncertainity observed in this study suggests to carry out the out of field measurement with different dosimeters for larger distances away from field edge.

4.3 Dosimetric comparison of FF and FFF beams in VMAT treatment plans of Head and Neck Oral Cavity Cancers.

As already discussed, among the head and neck cancers oral cavity cancers are prominent one. About 70% of the reported cases of head and neck cancers are found to be oral cavity cancer. Radiotherapy remains to be an integral part of many oral cavity treatments and established as an important part of the overall management of many of these tumours. Flattening filters are introduced in the beam path to make it uniform. Flattened beams are widely used in radiotherapy. Modern radiotherapy machines are facilitated with FFF beams. VMAT and IMRT plans using FFF beams has several potential advantages, such as increased dose rate, reduced collimator scatter, reduced head leakage, and reduced out-of-field doses to the patient [21-24,93,94]. We aim to compare the dosimetric effects during treatment delivery using Flattened and unflattened (FFF) beams in head and neck oral cavity cancers. Oral cavity cancers are selected for evaluating benefits of FFF in this study.

Vassiliev et al [65] studied the case of lung cancer and opined that FFF beams mitigate dose loss at tumour periphery and that the current clinical practice fails to capture this under dosing at the tumour periphery. Spruijt et al. [95] reported that the OAR doses for breast IMRT is comparable for FF and FFF beams. Further, lower delivery time for FFF reported in most of the studies [19-20].

4.3.1 Materials and methods

4.3.1.1 Patient Selection

Dosimetric data of 50 patients already treated for head and neck cancer (planned with FF and FFF beams) were randomly retrieved from the MONACO treatment planning system. CT simulations were performed using a GE 4DCT machine (OPTIMA580W). Slice thickness of 2.5mm were reconstructed and transferred to MIM contouring work station (version 6.8.6). Contouring of target volumes and OARs were performed by Radiation Oncologist. Contoured structures were transferred to the MONACO treatment planning system for treatment planning.

Flattened and FFF beam plans were quantitatively compared in terms of coverage of planning target volume (PTV), conformity index, homogeneity index, the organ at risk (OAR) doses, peripheral dose and the monitor units (MU).

4.3.1.2 Radiation Therapy Planning

FF and FFF Plans were generated using the Monaco treatment planning system (version 5.2, Elekta Medical Systems Pvt. Ltd) for 6MV. The maximum dose rate was set to 600 MU/min for FF and 1400 MU/min for FFF. VMAT technique was used for planning. Prescribed dose (PD) was 30 x 2 Gy (60 Gy) to PTV high risk and 30 x1.5 Gy (54Gy) to PTV low risk. The optimization was performed inversely using the same plan parameters such as position of isocenter, beam angle, arc number and field size. Doses were calculated using Monte Carlo (MC) algorithm with 3% of statistical uncertainty per control point and 3mm of voxel grid size. All original VMAT plans used single full arc of 360° gantry rotation from -180 to 180 in the clockwise direction and with a couch angle of zero degrees. To exclude the bias of treatment plan skills of different individuals, in the final results, all treatment plans were designed by the same person. The planning objectives are tabulated in Table 4.4.

4.3.1.3 Treatment Plan Evaluation

Homogeneity index and conformity index are calculated as

$$\text{Homogeneity index (HI)} = (D2\% - D98\%)/D50\% \quad (1)$$

where D2%, D98% and D50% are dose to 2% , 98% and 50% volume of the PTV respectively.

$$\text{Conformity index (CI)} = (TVPI)^2 / (PI \times TV), \quad (2)$$

Where TVPI is the volume of target covered by the prescription isodose line (95%), PI is the volume of tissue covered by the prescription isodose line (95%) and TV is the total target volume. The coverage volumes of 45Gy, 30Gy, and 20Gy outside targets (V45Gy, V30Gy, and V20Gy) were used to compare the peripheral dose. OAR dose of the spinal cord, esophagus, and parotids was also evaluated from

Dose Volume Histogram (DVH).

Table-4.4 the planning objectives for VMAT plans.

Structures	Planning Objectives
PTV60 PTV54	V60 Gy≥95% V54 Gy≥95%
Spinal Cord	Max 50Gy (full end cross section)
Parotid	D50% < 30 Gy, Dmean< 26 Gy
Esophagus	V95Gy<33%
Brainstem	Entire brainstem<54 Gy, V59Gy<1-10CC
Eye	Mean<35Gy,Max 54Gy
Lens	Max7Gy
Chiasm/Optic Nerves	Max 55Gy
Mandible	Max 70Gy, V75<1CC
Normal Tissues	As low as possible

PTV = planning target volume;VxGy = volume receiving at least x-Gy dose

4.3.2 Statistical Analysis

To determine the statistical significance of the differences among the techniques, the Mann-Whitney U test was performed, with a p-value of < 0.05 considered to be significant, using SPSS version 20 software.

4.3.3 Results

Adequate coverage of target volume has been obtained for all the fifty cases, evaluated in this VMAT plans, on using FF and FFF beams. Dose distributions of the two plans (FF and FFF), for a typical case, are shown in Figure- 4.9. Result of statistical analysis of high dose PTVs, for all the cases under study, is given in Table-4.5. It is observed that dosimetric differences in FF and FFF plans are not statistically significant for the target volume covering 95% of the prescribed isodose. The average DVHs for the PTVs are plotted in Figure 4.10. Similarly, the result of statistical analysis of MU, CI and HI, for both FFF and FF plans, are given in Table-

4.6. It is seen that the MU shows significant difference for FF and FFF with $p < 0.05$, while no substantial differences were observed in homogeneity, or conformity.

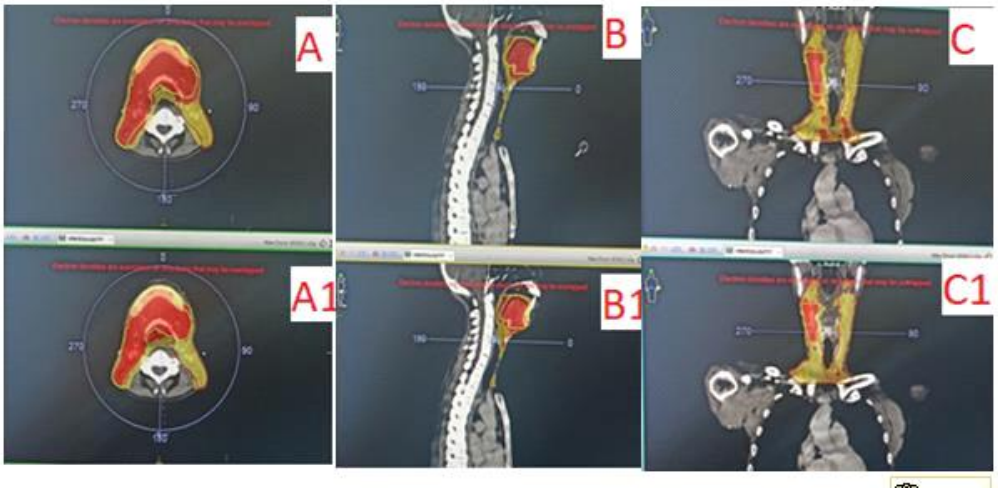

Fig. 4.9 Distribution for 60Gy covering high-risk PTV and that for 54Gy covering low-risk PTV (A, B, C represents distributions of plans with FF beam in the three planes; A1, B1, C1 represents plan distributions with FFF beams).

Table-4.5 statistical data of the high dose PTVs (Target volume covering 95% of the prescribed dose)for all studied cases.

Modality	N	Mean	Std. Deviation	P-value
FF	50	307.10	149.332	0.85
FFF	50	303.00	147.441	

N-number of studied cases, FF-beams with flattening filter, FFF-flattening filter-free beams

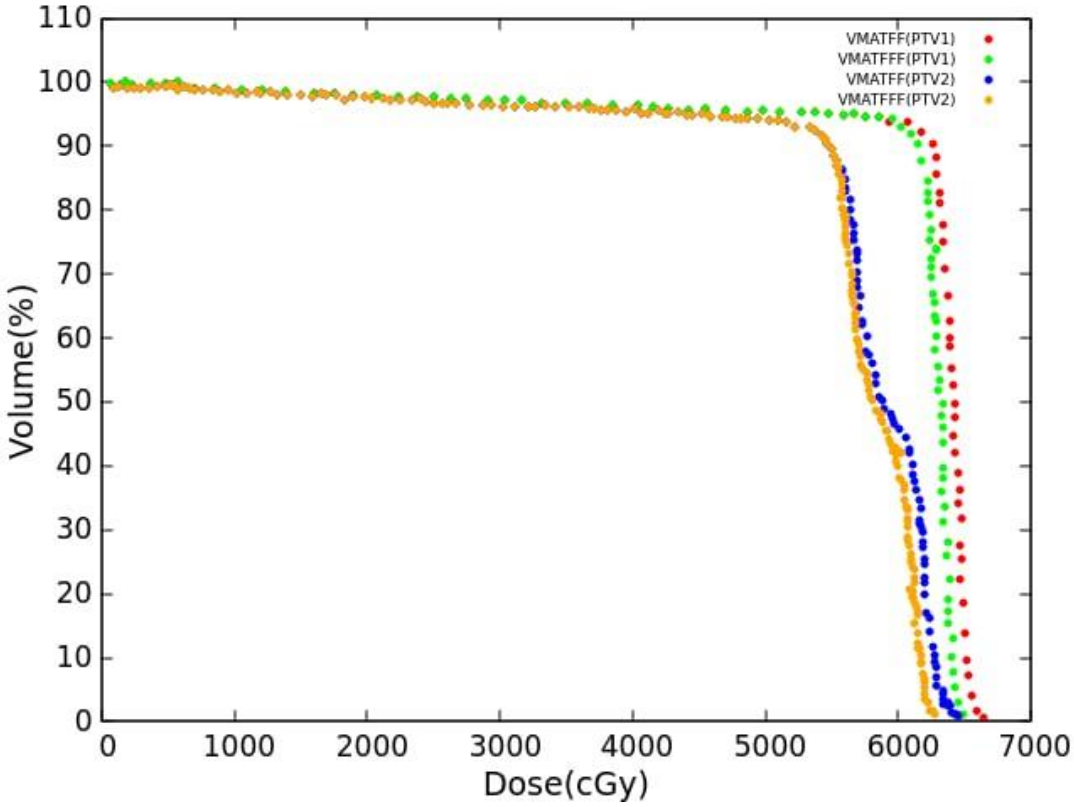

Fig. 4.10. DVH of PTV 60Gy (PTV1) and that of PTV 54 Gy (PTV2).

Table 4.6.Comparison of Monitor Units, Conformity Index (CI), and Homogeneity Index (HI)

	N	**FF Mean ± SD**	**FFF Mean ± SD**	**P Value**
Monitor Units	50	1008 ± 16	1280.7 ± 17	0.00
Conformity Index(CI)	50	0.54 ± 0.09	0.55 ± 0.13	0.15
Homogeneity Index(HI)	50	0.07 ± 0.02	0.09 ± 1.21	0.01

N –number of studied cases, FF- beams with flattening filter, FFF- flattening filter-freen beams

Results of statistical analyses of D98%, D50% and D2% are given in Table 4.7.

Table-4.7 Comparison of PTV Doses for the FFF and FF Plans for PTV (PTV 60Gy)

Variables	N	FF Mean ± SD	FFF Mean (SD)	P-Value
D98%(cGy)	50	5912 ± 99	5911 ± 75	0.003
D50%(cGy)	50	6147 ± 63	6135 ± 19	0.004
D2%(cGy)	50	6313 ± 81	6329 ± 5	0.12

N – number of studied cases, P Value - Wilcoxon test p value between VMATFF-VMATFFF, D98% = Dose received by 98% of the PTV volume.

The coverage volumes receiving 45 Gy, 30 Gy, and 20 Gy outside target volume (V45Gy, V30Gy, and V20Gy) were used to compare the peripheral dose. Result of the statistical analysis of peripheral dose is shown in Table-4.8. The mean doses for FFF beams shows slightly lesser value compared to FF beams, however, no statistical significance observed.

Table-4.8 Dosimetric Parameters for the FFF and FF Plans

Variables	N	FF Mean ± SD	FFF Mean ± SD	P-Value
V45(cGy)	50	1375 ± 29	1356 ± 31	0.79
V30(cGy)	50	2212 ± 46	2157 ± 49	0.65
V20(cGy)	50	2723 ± 59	2698 ± 59	0.79

N – number of studied cases, P-Value = Wilcoxon test p-value between VMATFF-VMATFFF. V_D = the percentage volume of the PTV at the prescribed dose and D was the prescribed dose.

Figures 4.11.-4.13 represent the DVH for the three organs at risk, namely, Esophagus, Spinal cord and Parotid respectively. The doses to the critical organs were comparable in both plans. The result of the statistical analysis on dose to OARs is given in Table 6. Here also it is seen that there is no significant difference of doses to organs at risk, due to FF and FFF plans.

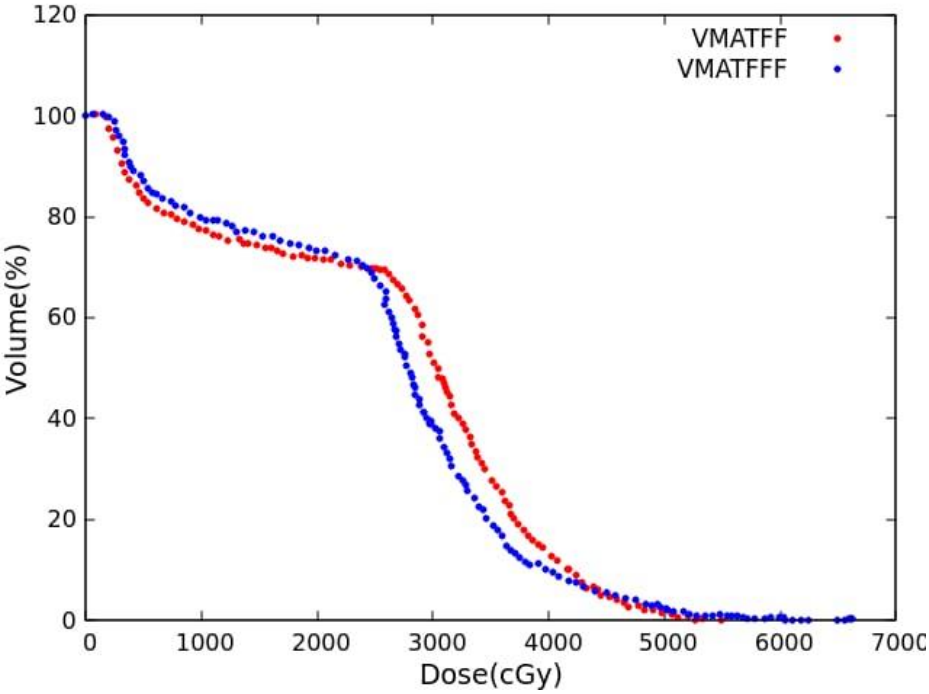

Fig 4.11 Dose volume histogram of Esophagus

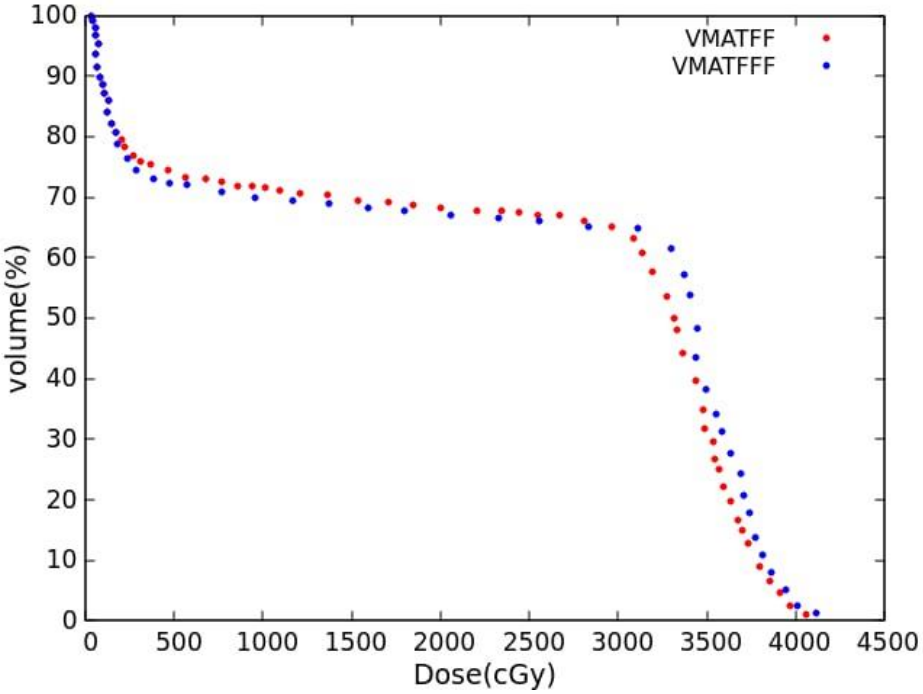

Fig.4.12 Dose volume histogram of Spinal cord

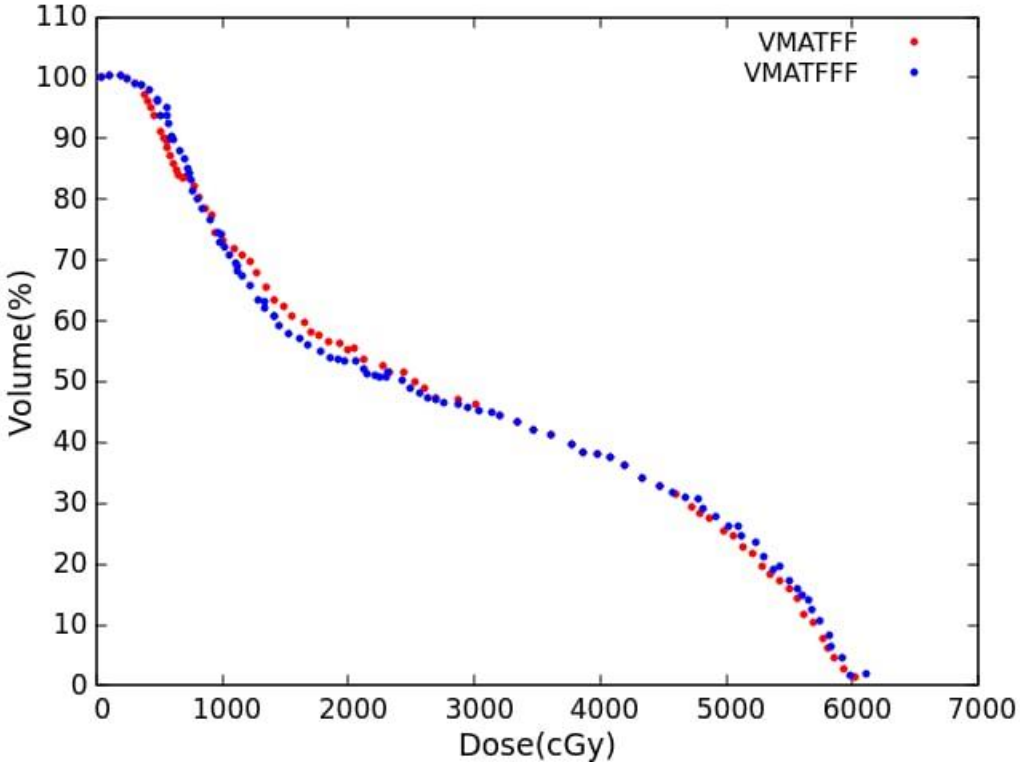

Fig 4.13 Dose volume histogram of Parotid

Table 4.9.Comparison of OAR Doses among FFF and FF plans

	N	FF Mean ± SD (cGy)	FFF Mean ± SD (cGy)	P-Value
Spinal Cord	50	3990 ± 250	4106 ± 345	0.056
Esophagus	50	2771 ± 285	2776 ± 271	0.927
Parotid	50	2874 ± 809	2843 ± 830	0.848

N – number of studied cases, P Value - Wilcoxon test p value between VMATFF-VMATFFF

4.3.4 Discussion

Owing to the increased dose rate compared to flattened beams, introduction of FFF beams in clinical use helps to reduce the long delivery time required for SRS treatments and hence the immobilization time for patients. Similar comment is made by Thomas et al. [96]. Further, reduction in delivery time reduces the machine ON time and hence the treatment cost. Kry S F et al.[97] also opined that removal of

flattening filter results in reduced out of field dose, sparing the nearby critical organs. This also leads to a faster treatment with reduced out-of-field dose exposure and hence reducing the long term risk of secondary cancer.

Present analyses show that, in the case of Oral Cavity Cancer, there is no significant changes for PTV mean dose and dose coverage. Also there is no substantial differences in homogeneity and conformity indices for FF and FFF plans. Still, it is a good indication that FFF VMAT plans provide comparable results with FF VMAT plans.

Though the calculated dose to the periphery was slightly less for FFF beam plans, it was not statistically significant. This may be due to the fact that the PTV for oral cavity is relatively larger and hence the effect of conical nature of the beam may produce a radial variation of dose over the target volume. This is in line with the observations of Zhuang et al.[59] for Nasopharyngeal carcinoma and Gasic et al.[60] for, prostate,lung and larynx.

Unlike esophageal cases which were reported with reduced OAR dose [22, 24, 93] we observed statistically not significant. OAR mean dose value for FFF-VMAT plans than FF-VMAT plans, except that there is a slight reduction in the mean doses of all treated cases. This may be due to the FFF property in reducing the out-of-field dose by reducing the collimator scatter, electron contamination and head leakage as reported by Kry S F et al. [97].

MU obtained in FFF –VMAT plans were higher than FF-VMAT plans. This can be due to the modulation required in the case of FFF Beams to deliver uniform doses in large volume tumors, which will result in increased Monitor units. However due to the increase in dose rate the overall beam delivery time can be reduced.

4.3.5 Conclusion

In the current era, VMAT techniques with flattened beams are commonly utilized for the treatment of head and neck cancers. This treatment planning comparison study of oral cavity cases demonstrates that FF and FFF treatment plans are, in general, comparable in quality. Hence, for moderately larger PTV, FFF plans

are beneficial from the point of view of treatment time and energy conservation. Further studies with optimization of different planning parameters are desired to be performed with higher accuracy and over wide range of cases, to confirm the clinical significance of FFF beams for large PTV Volumes. However advantages like reduction in treatment time, immobilization time and out of field dose make the FFF technique beneficial in Radiotherapy treatment.

CHAPTER 5

SMALL FIELD ANALYSIS AND PERFORMANCE OF DETECTORS

Considering the fact that the detectors with very small volume shows better performance in small field dosimetry [98-100], it is logical to expect that the sensitive volume and cross sectional area will be sensitive parameters for the performance of the detectors. Small field dosimetry needs to be accurate in infield and out of field as current treatment methods are concerned [101,102]. In order to see the dependence of variation of point dose with respect to various parameters of the detector, the deviation of measured dose with that of treatment planning system is evaluated as a function of detector volume and cross-sectional area of the detectors.

In this work, plans for small field sizes, 1x1cm^2 to 7x7 cm^2, were generated using a virtual water phantom in Eclipse TPS version 10.0. RFA was used to make the measuring setup easier and accurate, with convenient detector positioning. The point doses were measured using four different detectors i.e, semi-flex ionization chamber, pin-point ionization chamber, diode detector and microDiamond detector. All measurements were performed on Varian Clinac iX linear accelerator equipped with millennium 120 leaf collimator.

5.1 Materials and methods

In this work, plans for small field sizes, 1x1cm^2 to 7x7 cm^2, were generated using a virtual water phantom in Eclipse TPS version 10.0, at a specific depth of 10 cm as shown in Fig 5.1. For continuous evaluation purpose, higher field sizes also selected in this study. These plans were transported to the treatment machine and delivered using a radiation field analyzer (RFA) at 100cm SSD. RFA was used to make the measuring setup easier and accurate, with convenient detector positioning. The point doses were measured using four different detectors i.e., semi-flex ionization chamber, pin-point ionization chamber, diode detector and microDiamond detector. All measurements were performed on Varian Clinac iX linear accelerator

equipped with millennium 120 leaf collimator (Varian oncology systems, Palo Alto, CA), as shown in Figure 5.2, and the outputs were cross-compared with the treatment planning system. Further, the detector efficiencies of each detectors were verified using IMRT plans. The variation in the measurement, of point dose, with respect to the calculated dose is expressed as percentage variation(% variation) as follows.

% variation = (TPS dose – measured dose)/TPS dose *100 (5.1)

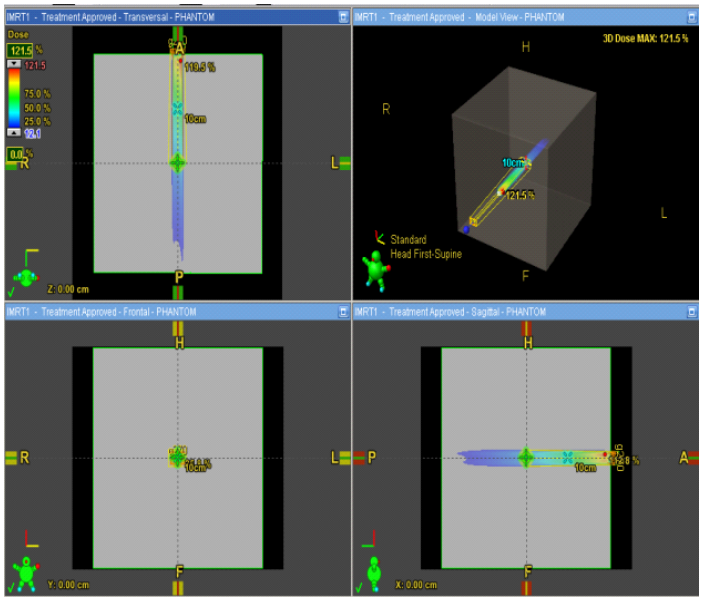

Fig 5.1. Eclipse Treatment planning system window of the small fields created in the water phantom.

Fig 5.2 Experimental setup for the point dose measurements using radiation Field analyzer with detector

Five small field IMRT plans that were created on small volume PTV of already treated brain cases, taken from the TPS are used for the verification of the data. The following plans were taken for verification (i) IMRT Plan 1 brain case with field size of 4x3 cm^2,(ii) Plan2 brain case with field size of 5x4cm^2,(iii) Plan3 brain case with field size 7x4cm^2, (iv)Plan4 brain case with field size 8x4 cm^2 and (v) Plan5 brain case with field size 7x5 cm^2 . The verification plans were created accordingly as shown in Fig 5.3. The gantry angles of all plans were reset to zero and corresponding dose to be delivered was calculated. Then the verification plans were delivered to the radiation field analyzer. Measurements corresponding to the above five plans were made using each of the four detectors, semi-flex ionization chamber, pin-point ionization chamber, diode chamber, and microDiamond detector. The data generated for each detector, with various field sizes, are tabulated through Table5.1-5.4. The percentage variations of each measurement with TPS are also shown in the respective tables. Similarly, the data for verification plans are tabulated in Table- 5.5

Data for detector volume and sensitive cross-sectional area are taken from the technical specifications of the detectors, provided by the respective manufacturers. The details of specifications of interest are tabulated in Table 5.6.

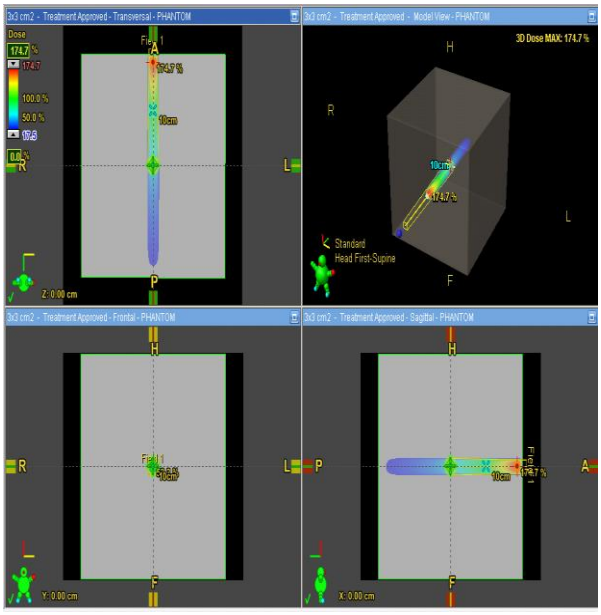

Fig. 5.3 Verification plan window of the TPS for small field IMRT

5.2 Results

Analyzing tables 5.1-5.4 it can be seen that the point doses measured using different detectors for different field sizes 1x1 to 7x7 cm^2 shows large variation up to 6.7%, compared to TPS data, for semiflex ionization chamber with a field size of 2x2 cm^2, and minimum variation of 0.8% for microDiamond detector for a field size of 6x6 cm^2. However for this detector the point dose for 2x2 cm^2 field is 1.3%. The mean variation for semiflex detector, averaged over the measured field sizes, is 5.9% and that for pinpoint chamber, diode detector and microDiamond detector are 1.89%, 1.47%, and 1.1% respectively. From the mean variation for different detectors it is seen that the microDiamond detector shows minimum deviation. Whereas, the mean value for pinpoint chamber is approximately twice the value of that of microDiamond detector and variation of semiflex is 6 times with that of microDiamond detector. Variation of diode detector is comparable with that of microDiamond detector. A comprehensive information of the above observation is plotted in Fig 5.4. It can also see that field sizes 3x3, 4x4 and 5x5 cm^2 shows minimum variation for pinpoint chamber. For the diode detector, the variations were almost comparable in all the cases. microDiamond detector shows minimum variation for the field sizes, 3x3, 4x4 and 6x6 cm^2. From Fig 5.4 it is also clear that pinpoint chamber, diode detector and microDiamond has a larger variation at 1x1 cm^2.

Considering the case of verification plans, as tabulated in tables 5.5. It can be observed that the semiflex detector shows larger variation compared with other detectors, for all the field sizes. Whereas, microDiamond detector gives minimum variation for all the cases. Semiflex chamber shows maximum variation of 6.2% for plan1 and minimum variation of 2.5% for plan2. Pinpoint detector shows a maximum variation of 2.4% for plan 4 and minimum variation of 1.8 for plan 3 and plan5. Diode detector shows a maximum variation of 1.1% for plan 1 and 5 and minimum variation of 0.8% for plan 4. microDiamond detector shows maximum variation of 0.6% for plan 1 and 4 and minimum variation of 0.4 for plan 2 and plan 5. The comprehensive data is summarized in Fig 5.5. It is interesting to note that the semiflex detector shows relatively larger variation of point dose for plan1 having

minimum field size out of the measured cases. Diode detector and microDiamond detector shows comparable variations for all the cases, followed by pinpoint chamber.

Considering the effect of the sensitive volume of the detector, as shown in Fig 5.6, it is observed that microDiamond detector with lowest volume (0.004cc) shows consistently lowest variation for all field sizes. Diode detector (0.03cc) shows comparatively less variation with pinpoint chamber (0.016cc) for all field sizes except for $3x3cm^2$. Semiflex chamber (0.125cc) having comparatively large volume shows the maximum variation for almost all the field sizes. Analyzing the above result, the detector accuracy is found to be directly related to the sensitive volume of the detector. Similarly in order to see the effect of cross sectional area, an attempt is made to find the correlation of efficiency with the cross-sectional area of the detector that determines the fraction of the radiation passing through the detector. Hence the variation of the point dose is plotted against the sensitive cross-sectional area of the detector for all the measured fields and the results are plotted in Fig.5.7. In this case, it is interesting to note that the microDiamond detector with comparatively larger area gives good result. Diode detector having comparitively minimum cross sectional area shows comparable performance with the microDiamond detector. Whereas the pinpoint chamber having cross sectional area comparable to that of micro-diamond detector shows higher variation. Hence it may be concluded that it is not a major sensitive parameter in deciding the performance of the small volume detectors in small field dosimetry.

Table 5.1. Comparison TPS calculated and semi-flex ionization chamber measured point doses for small fields created in the water phantom and percentage of variation.

Detector	Field Sizes cm^2	Point Dose from TPS (cGy)	PointDose measured Mean(SD) (cGy)	Variation (%)
Semiflex chamber	1x1	54.2	50.7(±0.1)	6.4
	2x2	55.8	52(±0.29)	6.7
	3x3	56.2	52.6(±0.1)	6.2
	4x4	56.9	53.8(0.05)	5.4
	5x5	58.1	55(±0.1)	5.2
	6x6	59.8	56.3(±0.06)	5.7
	7x7	60.1	56.6(±0.06)	5.7

Table 5.2. Comparison TPS calculated and Pinpoint Chamber measured point doses for small fields created in the water phantom and percentage of variation.

Detector	Field Sizes (cm^2)	Point Dose from TPS (cGy)	Point Dose measured Mean(SD) (cGy)	Variation (%)
Pinpoint Chamber	1x1	54.2	55.6(±0.01)	2.6
	2x2	55.8	57(±0.1)	2.1
	3x3	56.2	57(±0.06)	1.5
	4x4	56.9	57.7(±0.01)	1.4
	5x5	58.1	57.2(±0.27)	1.5
	6x6	59.8	56.6(±0.06)	2.0
	7x7	60.1	58.1(±0.05)	2.1

Table5.3. Comparison TPS calculated and diode detector measured point doses for small fields created in the water phantom and percentage of variation.

Detector	Field Sizes (cm^2)	Point Dose from TPS (cGy)	Point Dose measured Mean(SD) (cGy)	Variation (%)
Diode Detector	1x1	54.2	55.3(±0.03)	1.5
	2x2	55.8	56.5(±0.06)	1.3
	3x3	56.2	57.1(±0.01)	1.6
	4x4	56.9	57.6(±0.17)	1.3
	5x5	58.1	57.4(±0.06)	1.1
	6x6	59.8	58.6(±0.15)	1.9
	7x7	60.1	59.1(±0.12)	1.6

Table 5.4. Comparison TPS calculated and micro-diamond detector measured point doses for small fields created in the water phantom and percentage of variation.

Detector	Field Sizes (cm^2)	Point Dose fromTPS (cGy)	Point Dose measured Mean(SD) (cGy)	Variation (%)
microDiamond detector	1x1	54.2	53.4(±0.12)	1.4
	2x2	55.8	55.0(±0.12)	1.3
	3x3	56.2	55.6(±0.06)	0.9
	4x4	56.9	56.3(±0.1)	0.9
	5x5	58.1	57.4(±0.06)	1.1
	6x6	59.8	59.2(±(0.21)	0.8
	7x7	60.1	59.4(±0.18)	1.1

Table 5.5. Comparison of TPS calculated and pin-point ionization chamber measured point doses for small fields created in the water phantom and percentage of variation.

Plan	Detectors	Plan Fields (cm^2)	Pointdose fromTPS (cGy).	Pointdose measured (cGy).	Variation (%)
IMRT plan 1	Semiflex ionization chamber	4x3	199.3	211.6	6.2
	Pin-point ionization chamber	4x3	199.3	203.3	2.0
	Diode Detector	4x3	198.5	200.9	1.1
	microDiamond detector	4x3	199.3	197.9	0.6
IMRT Plan2	Semiflex ionization chamber	5x3	340.5	331.6	2.5
	Pin-point ionization chamber	5x3	340.0	336.5	1
	Diode Detector	5x3	340.6	337.4	0.9
	microDiamond detector	5x3	340.6	339.1	0.4
IMRT Plan3	Semiflex ionization chamber	7x4	355.0	342.1	3.6
	Pin-point ionization chamber	7x4	355.0	348.4	1.8
	Diode Detector	7x4	355.0	351.3	1.0
	microDiamond detector	7x4	355.0	353.0	0.5
IMRT Plan 4	Semiflex ionization chamber	7x5	351.8	339.6	3.4
	Pin-point ionization chamber	7x5	351.8	343.3	2.4
	Diode Detector	7x5	353.2	350.0	0.8
	microDiamond	7x5	353.2	351.1	0.6

IMRT Plan 5	Semiflex ionization chamber	8x5	292.7	284.1	2.9
	Pin-point ionization chamber	8x5	291.5	286.2	1.8
	Diode Detector	8x5	293.5	290.7	1.1
	microDiamond detector	8x5	292.7	291.5	0.4

Table 5.6. Detector Details

Detector Type	**Detector Volume(mm^3)**	**Detector Cross Sectional Area(mm^2)**	
Microdiamond	0.004	3.8	
pinpoint chamber	15.0	3.14	
Diode Detector	0.03	0.318	
Semiflex	125.0	23.746	

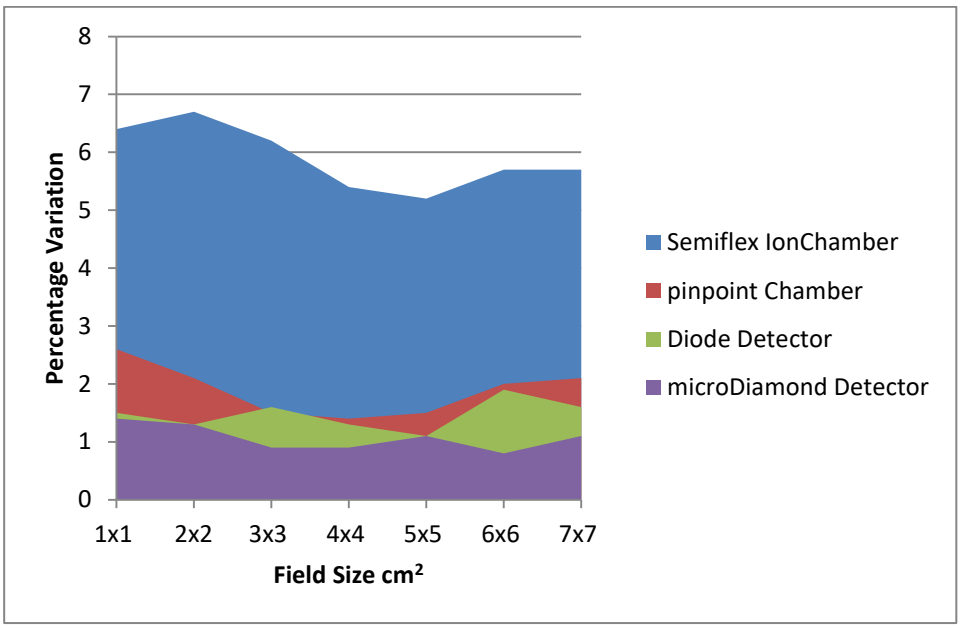

Figure 5.4. Comparison of different detector accuracy for different field sizes.

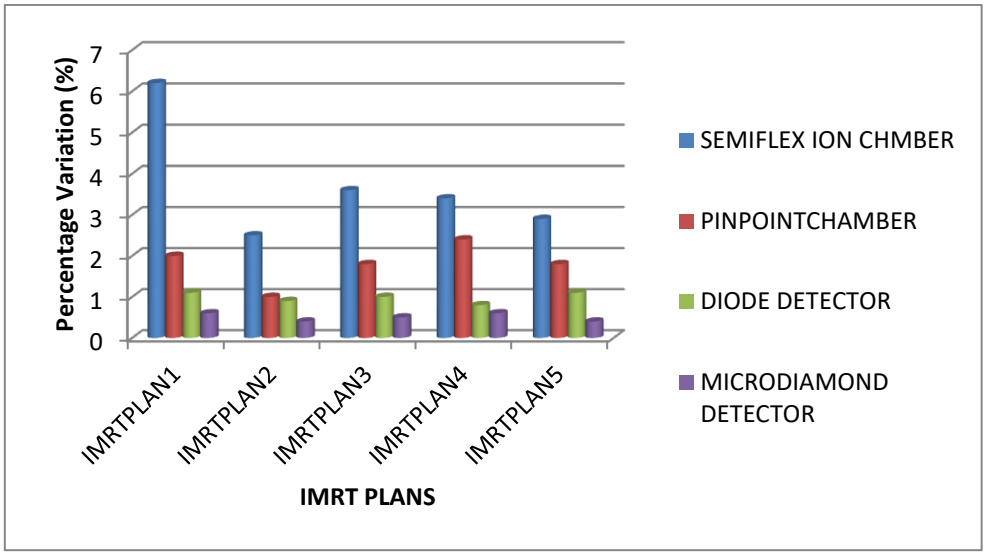

Figure 5.5. Verification of different detector efficiency in determining point dose for different intensity-modulated radiation therapy plan.

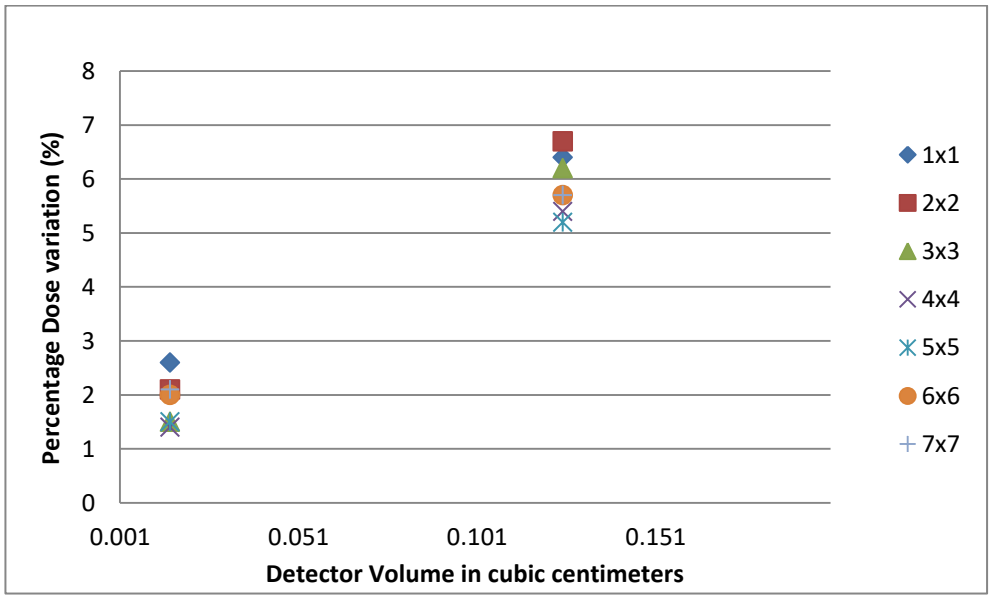

Figure 5.6. Percentage dose variation Vs detector volume for different field size.

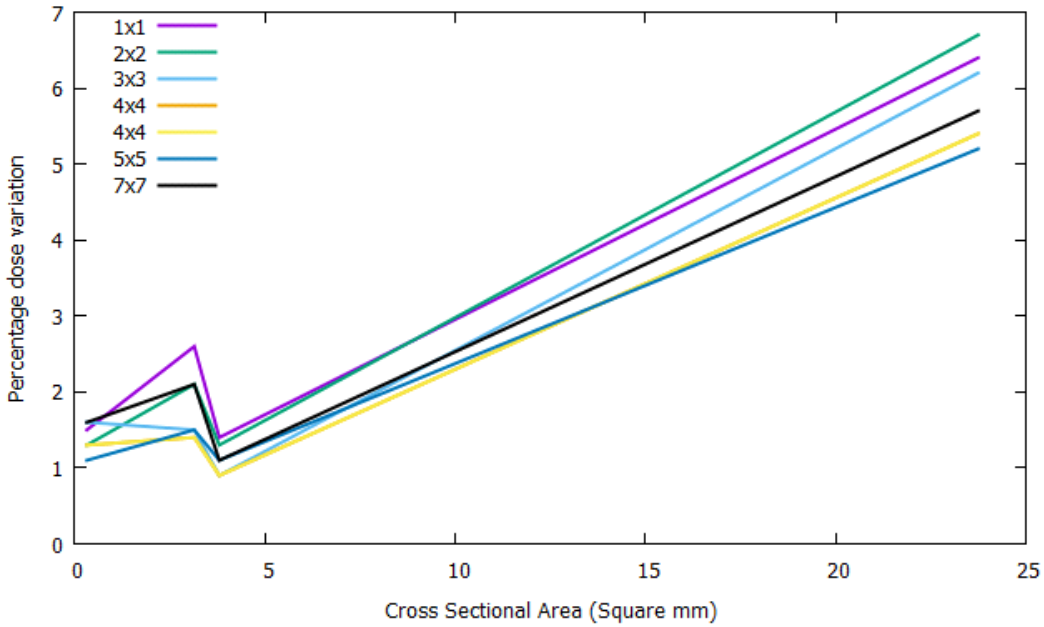

Fig.5.7: Percentage dose variation Vs detector Cross sectional area for different field sizes.

5.3 Discussion

Analyzing the dose measurements using various detectors such as semi flex ion chamber, pinpoint chamber, diode detector and microDiamond detector, it is obvious that the semi flex shows large variation from the dose calculated using Eclipse. Table 5.1- 5.4 gives the comparison of point dose calculated from the Eclipse treatment planning system version 10.0 and measured point dose from the four commercial detectors available in our center using radiation field analyzer (RFA). From this data it is seen that between the detectors large variation is present in measuring the point dose. The comparison study shows a maximum variation of 6.7% for semi flex chamber and minimum variation of 0.8% for microDiamond detector. Because of their excellent dose response, dose rate independence, low directional dependence ion chambers are widely used in Radiotherapy. Maximum variation observed with semi-flex chamber due to the comparatively large volume of the semi-flex chamber, which leads to volume averaging effect and lack of lateral electronic equilibrium. W. U. Laub and T. Wong reports under estimation of correct output factor results from lateral electronic disequilibrium is more pronounced with ion chambers compared to volume effect [103].This could lead to inaccurate

conclusions upon clinical verification of IMRT plans. Large variation is observed for 2x2cm^2 field size compared to the maximum field size (7x7 cm^2) used in the study, which may be due to the volume effect. For 7x7 cm^2 variation is 5.7%. Variation observed with semi flex chamber for 2x2 cm^2 is 5 times more than that with microDiamond detector. This indicates the increasing accuracy with increasing field size in case of semi flex chamber. This large variation of semi flex detector for small field size shows the chamber is not a good choice for small field dosimetry. Mean variation calculated for the chambers gives their accuracy in the increasing order for small field dosimetry, viz, semiflex chamber, pinpoint chamber, diode detector and microDiamond detector. This order is comparable with corresponding chamber volume. Pinpoint diode and microDiamond detectors gives minimum variation for 6x6 cm^2 field size and larger variation at 1x1 cm^2.

Considering the case of verification plan of actually implemented cases, as tabulated in Table-5.5, plans delivered using semiflex maximum variation (6.2%) among all the five IMRT plans. This variation is observed in the 4x3 cm^2 field size plan, this again strengthens above statement on the comparatively large volume of semiflex chamber, which makes it inaccurate for smaller field sizes. Maximum variation observed with microDiamond is 0.6% for plan 1 and plan 4, also microDiamond has a minimum variation of 0.4 % for plan 2 and plan 5.This indicates the available small volume chamber is highly accurate and stable in predicting the point dose. Diode detector also shows stable results for the plan verification with a maximum variation of 1.1% for plan 1 and plan 5. Whereas pinpoint shows a maximum variation of 2.4% for plan 4 and minimum variation of 1.8% for plan 3 and plan 5.

Analyzing the comparable performance of these three detectors viz, microDiamond, diode and pinpoint chamber detectors, microDiamond shows a slight superiority of performance followed by diode detector however considering the cost effectiveness of the detectors it may be concluded that all these three detectors provide satisfactory performance as detector for point dosimetry in small fields. It is also important to note that both diode and microDiamond has the variations of ~1 %.

Like previously reported [104-106], microDiamond detectors will be able to give more accurate results and is proved in the detector and plan comparison (Figure 5.5 and Figure 5.6).

5.4 Conclusion

The performance of microDiamond, diode, pinpoint chamber and semiflex ion chamber are evaluated as detectors for point dosimetry in small fields. The study concludes that the sensitive volume is the most sensitive parameter while selecting the detector for measurement of point dose in small fields. Diode and pinpoint detectors give comparable performance with microDiamond detector. In general, detectors with very small volume are found to be ideal for small field measurements.

CHAPTER 6

MATHEMATICAL MODELLING OF OUT OF FIELD DOSE

6.1 Introduction

This chapter discusses the development of mathematical model of out of field dose in terms of Moliere scattering. Measured the out of field dose of small fields experimentally using EDR2 film. Large area, low cost and wide response range makes EDR2 film unique. In the case of small field radiation therapy the secondary dose due to the scattering of electrons or leakage photons, are not properly accounted. This produces high uncertainty in determining the out of field dose. For pencil beams, having very small size, the simple photon interaction process like compton processes, photo electric effect, pair production and triplet production, cannot define the true electron spectrum at the region of interest. This may be due to multiple scattered photons, effect of the uncertain boundaries, density variations etc. [63, 96, 97]. The contribution of secondary electrons, scattered from the high intense fields to the out of field region is also to be accounted.

Moliere approach of multiple scattering of electrons is adapted in addressing this out of field doses [106, 107]. This multiple scattering is fairly general in nature and may easily be applied in calculations. This made the Moliere theory for wide acceptance. Moliere scattering includes all types of electron interactions. With the help of Moliere multiple scattering theory, a phenomenological model for calculating out of field dose, has been developed for small fields.

Theoretical predictions were generated through multigroup solution to the diffusion equation. The primary source distribution function is derived as the uniform pencil beams spread over the field size. This is binned to energy intervals for accounting the multi-group solutions. The diffusion operator for each group is calculated using Moliere scattering. The multigroup equations were solved for an appropriate boundary from the centre point of the beam, depending on the field size. The solution produces the electron spectrum at each voxel, and which is then

converted to dose. The spatial variation of the dose is taken as the profile. The multigroup solution has been performed through in-house developed code to solve diffusion equation.

6.2 Measurement of out of field dose for small fields using EDR2 Film

In order to generate a precise reference beam profiles of smaller size field, small fields (0.4x40, 1x40, 2x40 and 3x40 cm^2) were recorded in an EDR-2 dosimetry film (Eastman Kodak Company Rochester, NY), having fine grain size. Slit for 0.4 x 40 cm^2 is given in Fig. 6.1. The film was positioned at a depth of 1.5 cm in the PMMA phantom having density 1.04 gm/cm3. 6MV beam from, Varian Clinac-iX was used for irradiation. In order to maintain the entire distribution in the linear response region of the machine dose was set to 1000 MU. The larger size along the Y direction is selected to avoid the edge effect and hence the profile can be approximated in to a line spread function distribution, (LSF(x)). The film was processed in the automatic processor (Promax ADC, CGPR 12, chayagraphics) and scanned using film scanner (Dosimetry PRO Advantage, M/S Vidar Systems Corporation with software Ray 4.0) [108-111]. Dose profile in the X direction has been generated from inversion of the scanned image of the exposed film using Image J software [112,113]. The pixel to millimeter (mm) calibration has been generated by scanning an ordinary scale and using a graticule. The beam profile is generated as distance - intensity plot. The scanned image of processed film is shown in Fig.6.1. For the sake of comparison, the measured dose profile is compared with the dose profile for TPS, Eclipse 13.7, which was generated with AAA algorithm [114]with grid size of 1mm.

In the case of film measurement analysis, the primary beam intensity function (g1(x)) and secondary intensity function (g2(x)) corresponds to a Gaussian fit. A term y_0 is introduced to incorporate film fogging effect (base+fog+leakage).

$$f(x)= g1(x)+ g2(x)+y0. \quad - \quad (6.1)$$

Fig 6.1. Slit for 0.4x40 cm^2 field size

Beam profile for the above measurement is shown in Fig 6.2 (shown in red colour). For the sake of comparison, the beam profile for the same field size ($0.4x40cm^2$) had been generated in the Eclipse treatment planning system using AAA algorithm. The same is also been plotted in Fig-6.2 (shown in black, smooth line) along with the measured profile. The sensitivity analysis shows a significant deviation of TPS calculated dose distribution about the significance region of secondary can be observed in the out of field region. To reproduce this measured distribution, a novel theoretical background has been developed.

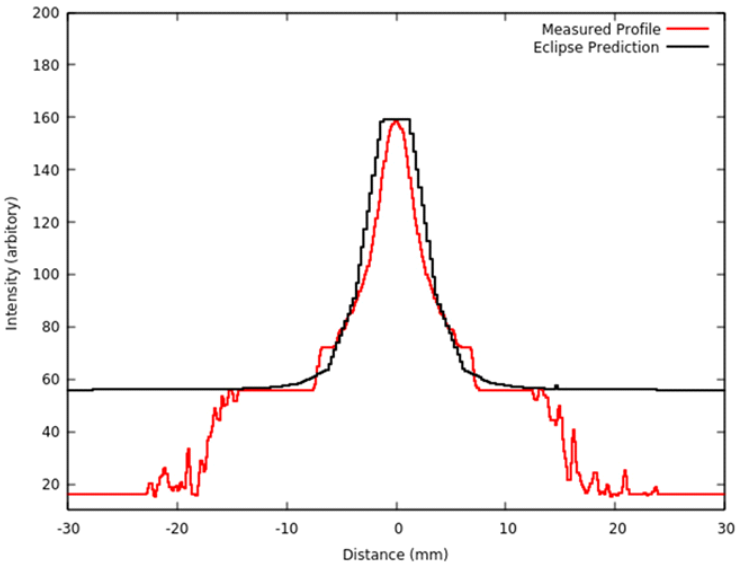

Fig 6.2. Measured profile to Eclipse prediction comparison

6.3 Theoretical background

This theory is implemented for measuring the energy distribution provided by the photon beam. A beam of photon, having energy distribution in the range of 1 to 6 MeV as a bremsstrahlung beam, on interacting with the medium, transfers its energy to the electrons through the process of Compton scattering. Hence the angular distribution of scattered photon and electron depends upon energy of the incoming photon. The double differential cross section for the angular distribution of photons follows the Klein -Nishina formalism stated as,

$$\frac{d\sigma}{d\Omega} = \frac{1}{2}\alpha^2 r_0^2 P\left(E_{\gamma,\theta}\right)^2 [P\left(E_{\gamma,\theta}\right) + \left(P\left(E_{\gamma,\theta}\right)\right)^{-1} - \sin^2(\theta)] \text{ - (6.2)}$$

Where, $\frac{d\sigma}{d\Omega}$ is the differential cross section, E_γ is the incident gamma energy,

r_0 *is* the classical electron radius and α is the photon energy in terms of rest mass energy of electron, given as,

$$\alpha = \frac{E_\gamma}{M_0 C^2} \text{ - (6.3)}$$

P ($(E_\gamma$,θ)is the ratio of photon energies after and before collisions and is calculated as,

$$(\left(E_\gamma, \theta\right) = \frac{1}{1+\alpha(1-\cos\theta)}, \text{ where}\alpha \text{ is obtained from equation (6.3)}$$

To quantify the energy distribution of scattered flux, for a particular angle the scattered photon energy distribution obeys the compton scattering equation,

$$E_{Scattered} = \frac{E_\gamma}{1+\alpha(1-cos\theta)} \text{ - (6.4)}$$

Further scattered flux is calculated for angle -90^0 to $+90^0$. Angular distribution and yield were calculated for each bremsstrahlung energy bin, and summed over the angular range. Corresponding yield for each energy and standard scattering flux are tabulated in Table-1 and 2 of appendix-1 respectively.

Further average electron energy for each scattered photon is calculated by multiplying with corresponding continuous slowing down approximation (CSDA) range. The Standard deviation is estimated from this distribution. This standard deviation for each energy is summed and tabulated in table-3 of appendix-1.

6.4 Mathematical Modeling of the Interaction

A mathematical model for the theoretical approach is obtained using diffusion equation. To estimate the contribution at each point, it has been assumed as the solution for diffusion equation. At this point electrons are produced from the photon interaction. These electrons are scattered and absorbed within these volume element. Hence the primary dose deposition within this volume element is due the energy loss of the secondary electrons, which are capable of depositing further low energy electrons. These low energy electrons are produced through different generations which are originated primarily from the interaction of photons. The photons produced from the interactions are energetically being reduced through absorption, collisions and scattering. Hence all these are cumulatively undertaken in the diffusion equation and hence the formalism. Hence, for the sake of reproducibility of dose distribution by the small fields, a solution of diffusion equation has been developed and attributed.

The dose deposition in the volume element dV($\vec{r}$) is considered purely by the electrons, produced by the photon interaction. Hence the dose at the volume dV($\vec{r}$)is taken as

$$D(\vec{r}) = \int_E \phi_{ele}(E)\left(\frac{dE}{\rho dx}\right)_{E\bar{Z}} dE \qquad \text{- (6.5)}$$

Where $\bar{Z}$ is the average atomic number of the volume element, ϕ_{ele} (E) is the electron flux of energy E, $\left(\frac{dE}{\rho dx}\right)_{E\bar{Z}}$is the stopping power for electrons having energy E, in the material.

Here the electron flux at every volume element dV($\vec{r}$) is estimated as a solution to the diffusion equation,

$$D\nabla^2(\vec{r}) - Z_a(\vec{r}) - S(\vec{r}) = 0 \quad \text{- (6.6)}$$

Here, r is the position vector of the volume element dV($\vec{r}$)which can be represented as, is the absorption cross section which contributes to D is the diffusion coefficient defined as,

$$D = \frac{Z_s}{3Z_t} \quad \text{- (6.7)}$$

where Z_s is the macroscopic scattering cross section for electrons, which is calculated from the Moliere scattering cross section. Z_t is the total cross section for the electron which is the sum of the cross section $Z_{scattering}$, Z_{brem} (bremsstrahlung) and, the, Z_{ab} absorption cross section S($\vec{r}$) is the source distribution function, which are contributed from the first,second,third and higher order generations of electrons. So S($\vec{r}$) can be written as sum of the respective contributions.

$S(\vec{r}) = [S_0(\vec{r})\phi_0(E_\gamma)] + [S_1(\vec{r})\phi_1(E_\gamma') + S_2(\vec{r})\ \phi_2(E_\gamma'')] + [\text{third generation}] + [\text{Fourth generation}] + \text{etc}$ (6.8)

The first generation electrons is given by $S_0(\vec{r})\phi_0(E\gamma)$, where $S_0(\vec{r})$ is electrons produced in the volume element at r, due to the Compton scattering of primary photons, and $\phi_0(E\gamma)$ is the spectrum of primary photons, the bremsstrahlung spectrum. The second generation of electrons are produced from the Compton scattering of secondary photons, the Compton scattered photons, given by $S_1(\vec{r})\phi_1(E_\gamma')$ and the electron produced from the compton scattering of secondary bremsstrahlung produced by the first generation of electrons in the medium given by $S_2(\vec{r})\phi_2(E_\gamma'')$. Higher generation electrons will be accounted in the continuity equation. Accordingly S($\vec{r}$) can be represented, in the continuity equation, as $(\vec{r},E,E\gamma,E')$.

Since all the parameters like flux, cross sections etc., are having energy dependence, the same has been introduced in the diffusion equation as

$$D\nabla^2(E)\phi(\vec{r},E) - Z_a\phi(\vec{r},E) - S(\vec{r},E,E\gamma,E') = 0 \quad \text{- (6.9)}$$

Further to solve the diffusion equation, the energy domain has been divided

into a number of groups, having a constant width Δ E .Thus an electron, corresponds to a group, interacting in a volume dV ($\vec{r}$) results in an energy reduction from E to E' (E'= E- Δ E). It is treated as the electron got absorbed in the volume from group E, simultaneously generating new group of electrons with energy E', due to secondary compton scattering. The multi-group solution of the continuity equation makes n_{ele} x n_{γ} number of continuity equations to be solved for the estimation of $\phi_{ele}(\vec{r}, E)$.

Now from the solution of diffusion equation we can estimate the dose at volume dV($\vec{r}$) using equation (6.1),

For the present study, the primary source distribution function $S_0(\vec{r})$ is taken as 2D lorentzian in x and y, and exponentially falling in z. S_1 and $\phi_1(E)$ are generated using compton scattering [115-117] and Klein-Nishina formalism [118].

In the current analysis the width of electron energy group and that of photon group are selected to be 0.5 MeV uniformly, from 1MeV up to 6MeV of bremsstrahlung beam, producing a set of 10 x10 differential equations . The group averaged cross sections for,, has been taken from ENDF/B .Vlll.0 evaluated nuclear data library based on EPICS- 2017 report. The calculation and analysis are performed for the present experimental geometry.

6.5. Result and Discussion

Dose profile is generated corresponding to a bremsstrahlung photon beam 0.4x 40cm^2 size, using the above approximation, and is shown in Fig-6.3. Measured profile from the film, Moliere approximated profile and the profile generated for the first generation secondary and the combined primary plus secondary profile (total) measured are shown separately for the analytical purposes. The primary and secondary component of the profile from the film is reproduced using Klein-Nishina formalism and Moliere approximation. It is clear that theoretically calculated profile, based on Moliere multiple scattering formalism, exactly matches with the

total profile. Further for the sake of completeness, the measurement and analysis were extended to higher fields of sizes 1x40 cm^2, 2x40cm^2 and 3x40 cm^2 as representative case. Analysis was carried out, by combining the measured and calculated profiles, for 1x40 cm^2 field, and is plotted in Fig 6.4 indicating various contributions of primary scattering, secondary scattering, total distribution, the measured distribution and the base plus fog correction. There is a perfect matching of measured profile and calculated profile on proper accounting of contributing factors as mentioned above. Similarly calculation was performed for field sizes of 2x40 cm^2. The result is plotted, as the sum profile (Klein -Nishina+ Moliere) along with measured profile and base plus fog correction, in Fig-6.5. Calculation is also extended for field size of 3x40 cm^2 and the result is plotted, along with measured profile, in Fig 6.6. Excellent matching of the theoretical prediction with the measured profile , over wide range of small fields, justifies the success of this approach for treating the out of field dose and that the theory is well validated for higher field sizes.

As can be seen from Fig 6.3, accounting primary and secondary contributions of electron scattering can represent the total dose deposited, in each voxel, moderately well. The curve representing total dose deposition is corrected for the base plus fog term by introducing a correction term y_0 in the final calculation. Measured profile from the film, Moliere approximated profile, first generation secondary, the combined primary plus secondary profile (Total) and the base plus fog correction factor are to be accounted. Theoretically calculated profile based on Moliere multiple scattering formalism [119-122] could successfully reproduce with the total profile over wide range of field sizes. In the present analysis, dose deposition due to scattering of primary photons in terms of Compton scattering of bremsstrahlung and the scattering of Compton scattered electrons are accounted for the dose calculations. Higher orders of scattering will automatically be accommodated through diffusion equation.

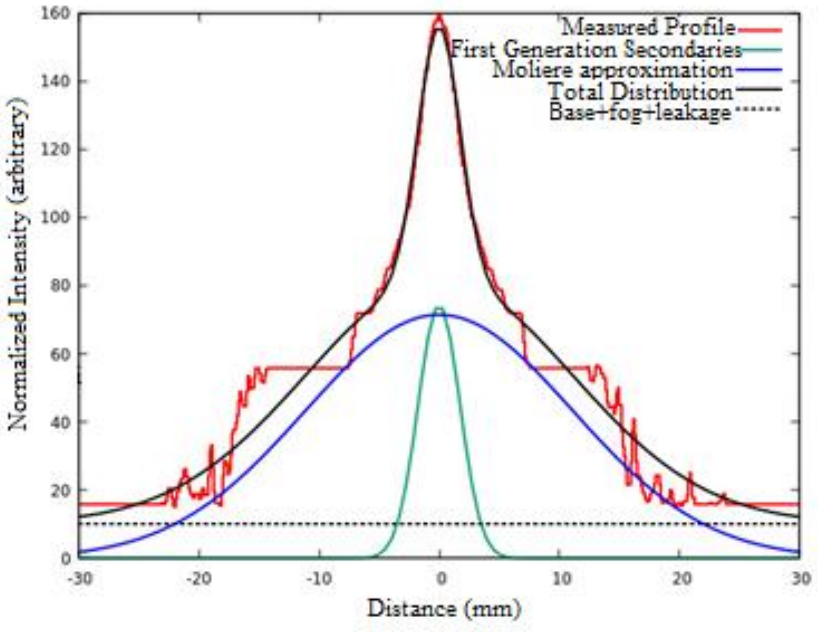

Fig 6.3. Combined experimental and theoretical distribution, 0.4x40 cm^2

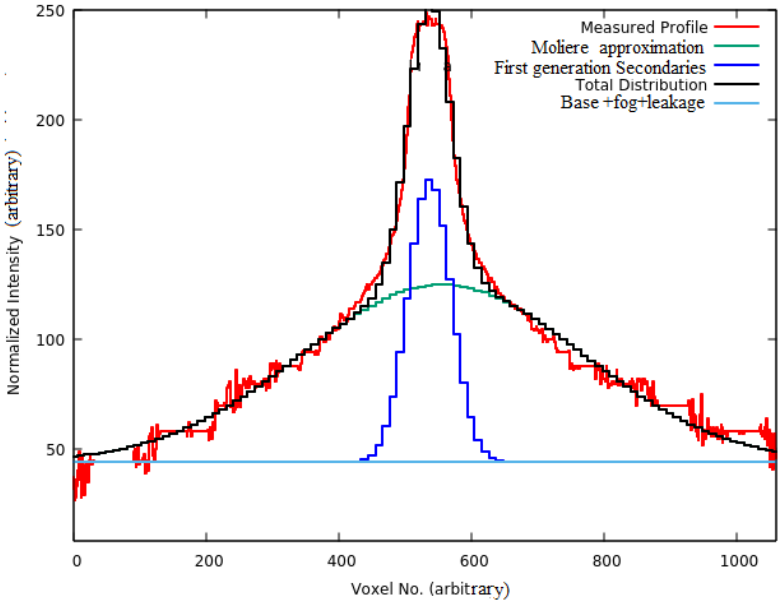

Fig 6.4.Combined experimental and theoretical distribution, 1x40 cm^2

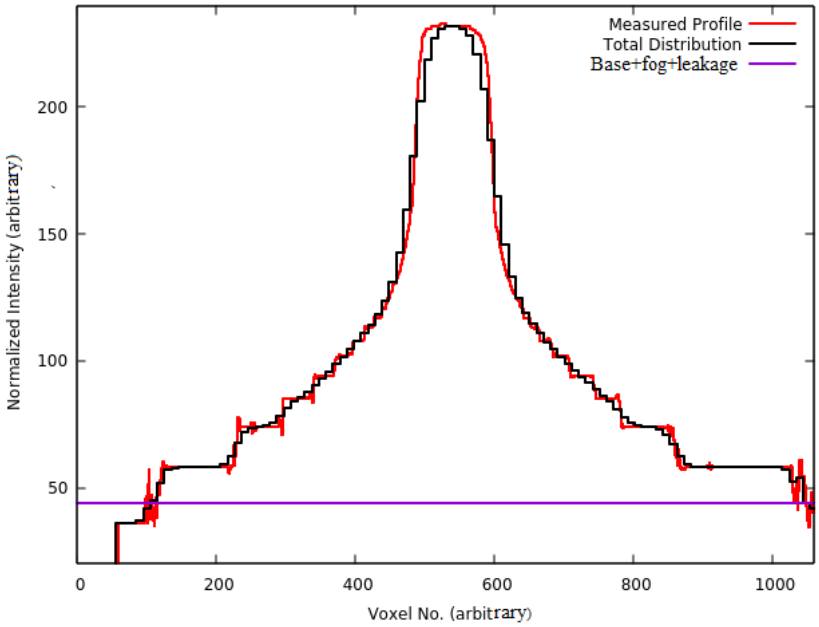

Fig 6.5.Combined experimental and theoretical distribution,2x40 cm^2

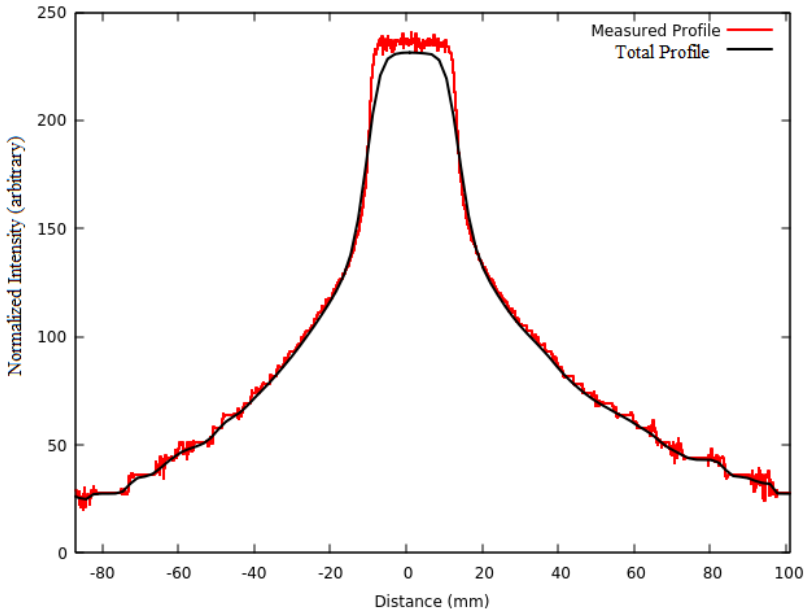

Fig 6.6.Combined experimental and theoretical distribution, 3x40 cm^2

6.6 Conclusion

Present work has taken efforts, to derive an analytical formalism for dose distribution outside the field with the help of diffusion equation and Moliere multiple scattering.

Summary of the work

In cancer treatment, radiotherapy treatments plays major role. Out of field dose or non-targeted organ dose remains a major concern in the treatment of radiation therapy. These non-target dose are never accounted in radiotherapy treatment evaluation or in the planning system. Out of field dose is always important to consider, as this reportedly increases the secondary cancer risk. Out of field measurements are widely done to access the dose and to check the possibility of secondary cancer induction. Analysis of these results provide a basis for the reduction of out of field dose in current radiotherapy treatment.

Modern treatment techniques available in radiotherapy depend highly on the accuracy of treatment planning system. Out of field photon dose measurements were carried out for the better understanding of the accuracy of commercially available treatment planning systems. Primary measured out of field dose was done using 2D-array detector and 4D octavious phantom. Further measurement was extended to water phantom considering availability of larger distance out of field dose. Ion chamber was used for the measurement. Analysis were performed to check effect of different field defining shielding conditions like jaw defined fields and MLC defined fields and jaw plus MLC defined fields. Flattening Filter Free (FFF) beams setting is expected to reduce the out of field dose as compared to Flattening Filtered (FF) beams. In order to evaluate the relative contribution of out of field dose due to FF and FFF, measurements of out of field doses were performed for FF and FFF beams for different field sizes at different distances away from the field edge using water phantom and semiflex ion chamber. Analysis of FF and FFF were performed in monaco TPS for the case of oral cavity cancer. It is observed that notable organ sparing could not be achieved with FFF beam.

Small fields and small field dosimetry are most discussed in modern treatment techniques. Small field dosimetry is different from the established large field dosimetry to which current treatment planning systems accounts very precisely. Even though techniques are developed as to accommodate small field dosimetry, the proper detectors and protocols are still under discussion. In order to calculate the accuracy of detector dependence, small field dose measurements were analyzed using various detectors, Viz semi flex ion chamber, pinpoint ion chamber, diode detector and microDiamond detector. Detector accuracy is found to depend initially on the sensitive volume and cross sectional area of the detector.

It is necessary that a methodology be developed to calculate the out of field dose precisely and account this out of field dose in the treatment planning system in the case of small field dosimetry. To address this issue, a phenomenological model was developed for predicting the out of field dose accurately by solving diffusion equation for electron scattering on the basis of Moliere scattering approach. In order to generate a precise beam profiles of smaller size field, small fields (0.4x40, 1x40, 2x40 and 3x40 cm^2) were recorded in an EDR-2 dosimetry film, having fine grain size. These profiles were used as the reference profile for developing the mathematical model. Klein - Nishina equation and Moliere scattering approximation were used for generating the primary and secondary components of the profile respectively. Moliere approximated total profile was generated for various field size, thereby validating the model for wide range of small fields.

Conclusion

Even though a number of studies had conducted for measurement of out of field dose, till there is no incorporation of out of field dose. Especially in the case of radiotherapy treatments, this entirely depends on treatment planning systems. For this reason current study measured out of field, using the different mediums and finally using film. Profiles were generated from film, treatment planning system for absolute analysis. We realized the importance of point - to point validation in calculating out of field dose. The point-to-point validation requires an analytical formalism. Also analytical models developed by many authors are limited to some

empirical formalism. Hence the compound of multiple scattering is generally neglected. Considering the scenario, efforts are taken in the present work, to derive an analytical formalism for dose distribution, from the diffusion equation, with diffusion operator from Moliere scattering cross sections. This will take in to account multiple scattering within the medium and hence better representation of data.

Future Work

The present model could reproduce the measured profile to a very high extent, by accounting source distribution function generated from the measured primary profile. The effect of leakage and external scattering from the treatment head are assumed to be accounted base plus fog term, which is an approximation correction. Incorporation of these factors is expected to account for the edge correction in the higher order components that involves complex calculations.

Suggestions

Treatment protocol has to accommodate secondary and higher generation scattering contribution properly to account the actual absorbed dose.

APPENDIX

Calculation tables used for theoretical modeling of out of field dose using Moliere scattering theory.

Table 1 - Energy and corresponding yield

Energy(MeV)	Yield
1	0.416332
1.5	0.262405
2	0.169362
2.5	0.1200659
3	0.0846626
3.5	0.0621291
4	0.0448277
4.5	0.0343159
5	0.0238273
5.5	0.0137053
6	0.00270522

Table 2 Standard deviation multiplied by all energies for different angles for 0.4x40cm2

Angle	(dσ/dΩ)Y1	(dσ/dΩ)Y1.5	(dσ/dΩ)Y2	(dσ/dΩ)Y2.5	(dσ/dΩ)Y3	(dσ/dΩ)Y3.5	(dσ/dΩ)Y4	(dσ/dΩ)Y4.5	(dσ/dΩ)Y5	(dσ/dΩ)Y5.5	(dσ/dΩ)Y6
-90	2.82E-07	2.14E-07	1.15E-07	6.99E-08	4.28E-08	2.79E-08	1.81E-08	1.26E-08	8.03E-09	4.3E-09	7.82E-10
-80	3.23E-07	2.44E-07	1.31E-07	8.04E-08	4.96E-08	3.24E-08	2.12E-08	1.48E-08	9.41E-09	5.0E-09	9.20E-10
-70	3.84E-07	2.89E-07	1.56E-07	9.60E-08	5.94E-08	3.91E-08	2.56E-08	1.79E-08	1.14E-08	6.1E-09	1.12E-09
-60	4.79E-07	3.62E-07	1.95E-07	1.20E-07	7.46E-08	4.91E-08	3.22E-08	2.26E-08	1.45E-08	7.7E-09	1.43E-09
-50	6.41E-07	4.83E-07	2.61E-07	1.60E-07	9.91E-08	6.52E-08	4.29E-08	3.01E-08	1.93E-08	1.0E-08	1.91E-09
-40	9.12E-07	6.82E-07	3.71E-07	2.29E-07	1.42E-07	9.38E-08	6.14E-08	4.32E-08	2.79E-08	1.5E-08	2.76E-09
-30	1.37E-06	3.80E-06	5.59E-07	3.51E-07	2.21E-07	1.47E-07	9.68E-08	6.83E-08	4.41E-08	2.4E-08	4.38E-09
-20	2.09E-06	1.31E-06	8.49E-07	5.56E-07	3.62E-07	2.47E-07	1.67E-07	1.20E-07	7.86E-08	4.3E-08	8.01E-09
-10	2.91E-06	1.88E-06	1.18E-06	8.19E-07	5.60E-07	4.01E-07	2.82E-07	2.10E-07	1.42E-07	8.0E-08	1.54E-08
-8	3.16E-06	1.95E-06	1.237E-06	8.654E-07	5.97E-07	4.3024E-07	3.0514E-07	2.2967E-07	1.56825E-07	8.87291E-08	1.544E-08
-6	3.22E-06	2.01E-06	1.282E-06	9.04E-07	6.28E-07	4.5605E-07	3.2574E-07	2.4687E-07	1.69717E-07	9.66604E-08	1.889E-08
-4	3.27E-06	2.0491E-06	1.316E-06	9.334E-07	6.52E-07	4.7614E-07	3.4196E-07	2.6056E-07	1.80088E-07	1.0311E-07	2.026E-08
-2	3.396E-06	2.0748E-06	1.338E-06	9.518E-07	6.67E-07	4.8892E-07	3.5235E-07	2.6941E-07	1.86842E-07	1.07343E-07	2.116E-08
0	3.31E-06	2.0835E-06	1.345E-06	9.58E-07	6.72E-07	4.93E-07	3.5593E-07	2.7247E-07	1.8919E-07	1.08821E-07	2.148E-08
2	3.396E-06	2.0748E-06	1.338E-06	9.51E-07	6.67E-07	4.89E-07	3.5235E-07	2.6941E-07	1.86842E-07	1.07343E-07	2.116E-08
4	3.26E-06	2.0491E-06	1.316E-06	9.33E-07	6.52E-07	4.76E-07	3.4196E-07	2.6056E-07	1.80088E-07	1.0311E-07	2.026E-08
6	3.218E-06	2.0073E-06	1.282E-06	9.04E-07	6.28E-07	4.56E-07	3.2574E-07	2.4687E-07	1.69717E-07	9.66604E-08	1.889E-08
8	3.153E-06	1.951E-06	1.237E-06	8.65E-07	5.97E-07	4.30-07	3.0514E-07	2.2967E-07	1.56825E-07	8.87291E-08	1.544E-08
10	2.91E-06	1.88E-06	1.18E-06	8.20E-07	5.60E-07	4.01E-07	2.82E-07	2.10E-07	1.42E-07	8.0E-08	1.54E-08
20	2.09E-06	1.31E-06	8.49E-07	5.56E-07	3.62E-07	2.47E-07	1.67E-07	1.20E-07	7.86E-08	4.3E-08	8.01E-09
30	1.37E-06	3.80E-06	5.59E-07	3.51E-07	2.21E-07	1.47E-07	9.68E-08	6.83E-08	4.41E-08	2.4E-08	4.38E-09
40	9.12E-07	6.82E-07	3.71E-07	2.29E-07	1.42E-07	9.38E-08	6.14E-08	4.32E-08	2.79E-08	1.5E-08	2.76E-09
50	6.41E-07	4.83E-07	2.61E-07	1.60E-07	9.91E-08	6.52E-08	4.29E-08	3.01E-08	1.93E-08	1.0E-08	1.91E-09
60	4.79E-07	3.62E-07	1.95E-07	1.20E-07	7.46E-08	4.91E-08	3.22E-08	2.26E-08	1.45E-08	7.7E-09	1.43E-09
70	3.84E-07	2.89E-07	1.56E-07	9.60E-08	5.94E-08	3.91E-08	2.56E-08	1.79E-08	1.14E-08	6.1E-09	1.12E-09
80	3.23E-07	2.44E-07	1.31E-07	8.04E-08	4.96E-08	3.24E-08	2.12E-08	1.48E-08	9.41E-09	5.0E-09	9.20E-10
90	2.82E-07	2.14E-07	1.15E-07	6.99E-08	4.28E-08	2.79E-08	1.81E-08	1.26E-08	8.03E-09	4.3E-09	7.82E-1

Table 3 Electron Normalization data for 0.4x40cm2

Angle	1Mev	1.5Mev	2Mev	2.5Mev	3Mev	3.5Mev	4Mev	4.5Mev	5Mev	5.5Mev	6Mev
-90	0.0006761	0.000856	0.0008566	0.0008566	0.000837	0.0008566	0.001272	0.001272	0.001272	0.001272	0.001272
-80	0.0008366	0.001272	0.001272	0.001272	0.001272	0.001756	0.001756	0.001756	0.001756	0.001756	0.001756
-70	0.001272	0.001756	0.001756	0.001756	0.002306	0.002306	0.002306	0.002306	0.002306	0.002306	0.002306
-60	0.0013395	0.002306	0.002306	0.002919	0.002919	0.002919	0.002919	0.003391	0.003391	0.00432	0.003391
-50	0.001756	0.002914	0.003591	0.00432	0.004333	0.00513	0.00432	0.00594	0.00594	0.00594	0.00594
-40	0.002306	0.00432	0.005103	0.00594	0.007762	0.007762	0.009773	0.00977	0.009773	0.01196	0.009773
-30	0.002919	0.00594	0.007762	0.009773	0.01196	0.01431	0.01431	0.01431	0.0208	0.02083	0.02817
-20	0.00432	0.007762	0.01196	0.01431	0.0208	0.0208	0.02083	0.028177	0.03622	0.024487	0.03588
-10	0.00432	0.0093708	0.01431	0.0208	0.02817	0.03622	0.04487	0.04487	0.04487	0.06372	0.0756042
-8	0.00432	0.00977	0.0144	0.02278	0.030462	0.0379599	0.0464246	0.05574383	0.06372	0.073198674	0.08216
-6	0.00432	0.00977	0.0161	0.02278	0.03322	0.0397142	0.04901107	0.05897263	0.067818	0.0780384	0.08848
-4	0.0051	0.009777	0.01655	0.02817	0.03311	0.04143	0.05096477	0.06963672	0.07107	0.076473	0.0929
-2	0.0051	0.00977	0.01677	0.02817	0.03381	0.0418468	0.05218949	0.06296347	0.07302246	0.080026	0.0959
0	0.0051	0.009773	0.016848	0.02817	0.03405	0.0421189	0.05259631	0.6373	0.073689205	0.08421	0.0968482
2	0.0051	0.0977	0.016779	0.02817	0.033808	0.041847	0.05218949	0.06296347	0.07302246	0.080026	0.0959
4	0.0051	0.0977	0.01655	0.02817	0.03311	0.04143	0.05096477	0.06963672	0.07107	0.076473	0.0929
6	0.00432	0.0977	0.0161	0.02278	0.03322	0.039714	0.04901107	0.05897263	0.067818	0.0780384	0.08848
8	0.00432	0.00977	0.0144	0.02278	0.03322	0.0379599	0.0464245	0.05574383	0.06372	0.073198674	0.08216
10	0.00432	0.0093708	0.01431	0.0208	0.02817	0.03622	0.04487	0.04487	0.04487	0.06372	0.0756042
20	0.00432	0.007762	0.01196	0.01431	0.0208	0.0208	0.02083	0.028177	0.03622	0.024487	0.03588
30	0.002919	0.00594	0.007762	0.009773	0.01196	0.01431	0.01431	0.01431	0.0208	0.02083	0.02817
40	0.002306	0.00432	0.005103	0.00594	0.007762	0.007762	0.009773	0.00977	0.009773	0.01196	0.009773
50	0.001756	0.002914	0.003591	0.00432	0.004333	0.00513	0.00432	0.00594	0.00594	0.00594	0.00594
60	0.0013395	0.002306	0.002306	0.002919	0.002919	0.002919	0.002919	0.003391	0.003391	0.00432	0.003391
70	0.001272	0.001756	0.001756	0.001756	0.002306	0.002306	0.002306	0.002306	0.002306	0.002306	0.002306
80	0.0008366	0.001272	0.001272	0.001272	0.001272	0.001756	0.001756	0.001756	0.001756	0.001756	0.001756
90	0.0006761	0.000856	0.0008566	0.0008566	0.000837	0.0008566	0.001272	0.001272	0.001272	0.001272	0.001272

REFERENCES

[1]. Source: Globocan2020- Global cancer Observatory .2020.

[2]. Siegel RL, Miller KD, Fuchs HE, Jemal A. Cancer Statistics, CA Cancer J Clin. 2021; 71(1):7-33.

[3]. Kumar M, Nanavati R, Modi TG, Dobariya C. Oral cancer: Etiology and risk factors: A review. J Can Res Ther 2016; 12:458-631.

[4] Martens C, De Wagter C, De Neve W. The value of the PinPoint ion chamber for characterization of small field segments used in intensity-modulated radiotherapy. Phys Med Biol. 2000; 45(9):2519.

[5] Alfonso R, Andreo P, Capote R, Huq MS, Kilby W, Kjäll P, Mackie TR, Palmans H, Rosser K, Seuntjens J, Ullrich W. A new formalism for reference dosimetry of small and nonstandard fields. MedPhys.2008; 35(11):5179-5186.

[6]. Cranmer-Sargison G, Weston S, Evans JA, Sidhu NP, Thwaites DI. Monte Carlo modeling of diode detectors for small field MV photon dosimetry: detector model simplification and the sensitivity of correction factors to source parameterization. Phys Med Biol. 2012;57(16):5141-5143.

[7]. Benmakhlouf H, Sempau J, Andreo P. Output correction factors for nine small field detectors in 6 MV radiation therapy photon beams: a PENELOPE Monte Carlo study. Med Phys. 2014;41(4):041711.

[8]. Fenwick JD, Kumar S, Scott AJ, Nahum AE. Using cavity theory to describe the dependence on detector density of dosimeter response in non-equilibrium small fields. Phys Med Biol. 2013;58(9):2901.

[9]. Bouchard H, Kamio Y, Palmans H, Seuntjens J, Duane S. Detector dose-response in megavoltage small photon beams. II. Pencil beam perturbation effects. Med Phys. 2015;42(10):6048-6061.

[10]. Kry, S. F., Bednarz, B., Howell, R. M., Dauer, L., Followill, D., Klein, E., George Xu, X. AAPM TG 158: Measurement and calculation of doses outside the treated volume from external-beam radiation therapy. Medical Physics, 2017;44(10), 391–429.

[11]. Sungkoo C, Seong Hoon KI, Chan Hyeong KI, Jang Guen PARK JH. Secondary cancer risks in out-of-field organs for 3-D conformal radiation therapy. Prog. Nucl. Sci. Technol. 2011; 1:512-4.

[12]. Howell R. Second Primary Cancers and Cardiovascular Disease after Radiation Therapy. NCRP Report No. 170. Medical Physics. 2012; 39(12):7729-7731.

[13]. Takam R, Bezak E, Marcu L, Yeoh E. Out-of-Field Neutron and Leakage Photon Exposures and the Associated Risk of Second Cancers in High-Energy Photon Radiotherapy: Current Status. Radiation Research. 2011; 176(4):508-520.

[14]. Travis L, Ng A, Allan J, Pui C, Kennedy A, Xu X et al. Second Malignant Neoplasms and Cardiovascular Disease Following Radiotherapy. Health Physics. 2014; 106(2):229-246.

[15]. Preston D, Ron E, Tokuoka S, Funamoto S, Nishi N, Soda M et al. Solid Cancer Incidence in Atomic Bomb Survivors: 1958–1998. Radiation Research. 2007;168(1):1

[16]. ICRP. Low-dose extrapolation of radiation-related cancer risk.Oxford: ICRP Publication 99 Ann; 2005.

[17]. Farah J, Mares V, Romero-Expósito M, et al. Measurement of stray radiation within a scanning proton therapy facility: EURADOS WG9 intercomparison exercise of active dosimetry systems. Med Phys. 2015; 42(5):2572-2584.

[18]. Howell RM, Scarboro SB, Kry SF, Yaldo DZ.The Accuracy of out-of-field dose calculations by a commercial treatment planning system. Physics in medicine and biology. 2010 12;55(23):6999.

[19]. Shine NS, Paramu R, Gopinath M, Jaon Bos RC, Jayadevan PM. Out-of-field dose calculation by a commercial treatment planning system and comparison by monte carlo simulation for varian TrueBeam®. J Med Phys. 2019;44(3):156–75.

[20]. Huang JY, Followill DS, Wang XA, Kry SF.Accuracy and sources of error of out-of-field dosecalculations by a commercial treatment planning system for intensity-modulated radiation therapytreatments. Journal of Applied Clinical Medical Physics. 2013;14(2).

[21]. Nicolini, G., Ghosh-Laskar, S., Shrivastava, S. K., Banerjee, S., Chaudhary, S., Agarwal, J. P., Munshi, A., Clivio, A., Fogliata, A., Mancosu, P., Vanetti, E., & Cozzi, LVolumetric modulation arc radiotherapy with flattening filter-free beams compared with static gantry IMRT and 3D conformal radiotherapy for advanced esophageal cancer: A feasibility study. International Journal of Radiation Oncology Biology Physics, 2012; 84(2), 553-560.

[22]. Sun WZ, Chen L, Yang X, Wang B, Deng XW, Huang XY. Comparison of treatment plan quality of VMAT for esophageal carcinoma with: flattening filter beam versus flattening filter free beam. J Cancer. 2018;9(18):3263-3268.

[23]. Cashmore J, Ramtohul M, Ford D. Lowering whole-body radiation doses in pediatric intensity-modulated radiotherapy through the use of unflattened photon beams. Int J Radiat Oncol Biol Phys. 2011;80:1220-1227.

[24]. Huang Y, Siochi RA, Bayouth JE. Dosimetric properties of a beam quality-matched 6 MV unflattened photon beam. J Appl Clin Med Phys. 2012;13(4):3701.

[25]. Palm Å, Johansson K. A review of the impact of photon and proton external beam radiotherapy treatment modalities on the dose distribution in field and out-of-field; implications for the long-term morbidity of cancer survivors. Acta Oncologica. 2007; 46(4):462-473.

[26]. Xu X, Bednarz B, Paganetti H. A review of dosimetry studies on external-beam radiation treatment with respect to second cancer induction. Physics in Medicine and Biology. 2008; 53(13):R193-R241.

[27]. Taylor ML, Kron T. Consideration of the radiation dose delivered away from the treatment field to patient in radiotherapy. Journal of medical physics. 2011 ; 36 (2):59.

[28]. Sánchez-Nieto B, Medina-Ascanio KN, Rodríguez-Mongua JL, Doerner E, Espinoza I. Study of out-of-field dose in photon radiotherapy: A commercial treatment planning system versus measurements and Monte Carlo simulations. Medical Physics. 2020 Jul 16; 47(9):4616–25.

[29]. Harrison,R.Out-of-fielddosesinradiotherapy:Inputtoepidemiologicalstudiesand dose-risk models. Physica Medica, 2017;42, 239–246.

[30]. Hauri P, Radonic S, Vasi F, Ernst M, Marcin Sumila, Mille MM, et al. Development of whole-body representation and dose calculation in a commercial treatment planning system. Zeitschrift Fur Medizinische Physik. 2021 Jul 20;32(2):159–72.

[31]. Jagetic L, Newhauser W. A simple and fast physics-based analytical method to calculate therapeutic and stray doses from external beam, megavoltage x-ray therapy. Physics in Medicine and Biology. 2015;60(12):4753-4775.

[32]. Greene D, ChuGL, Thomas DW. Dose levels outside radio therapy beams. Br J Radiol. 1983;56 (668)543-550.

[33]. Kase KR, Svensson GK, Wolbarst AB, Marks MA. Measurements of dose from secondary radiation outside a treatment field. International Journal of Radiation Oncology*Biology*Physics . 1983; 9(8):1177–83.

[34]. van der Giessen PH. Calculation and measurement of the dose at points outside the primary beam for photon energies of 6, 10, and 23 MV. Int J Radiat Oncol Biol Phys. 1994 Dec; 30 (5):1239–46.

[35]. Fraass B A, van de Geijn J. Peripheral dose from megavolt beams. Med Phys. 1983; 10(6): 809-18.

[36]. Francois P, Beurtheret C, Dutreix A. Calculation of the dose delivered to organs outside the radiation beams. Med Phys. 1988; 15(6):879-83.

[37]. Niroomand-Rad A, Cumberlin R. Measured dose to ovaries and testes from Hodgkin's fields and determination of genetically significant dose. Int J Radiat Oncol Biol Phys. 1993 (4):745-51.

[38]. Hall E, Wuu C. Radiation-induced second cancers: The impact of 3D-CRT and IMRT Int J Radiat Oncol Biol Phys 2003; 56:83-8.

[39]. Wang B, Xu X. Measurements of non-target organ doses using mosfet dosimeters for selected IMRT and 3D CRT radiation treatment procedures. Radiat Protect Dosim 2008; 128:336-42.

[40]. Followill D, Stovall M, Boyer A. Estimates of whole-body dose equivalent produced by beam intensity modulated conformal therapy. Int J Radiat Oncol Biol Phys 1997; 38:667-72.

[41]. Ruben J, Davis S, Evans C, Jones P, Gagliardi F, Haynes M, Hunter A. The effect of intensity-modulated radiotherapy on radiation-induced second malignancies. Int J Radiat Oncol Biol Phys 2008; 70:1530-6.

[42]. Kry SF, Titt U, Followill D, Pönisch F, Vassiliev ON, White RA, Stovall M, Salehpour M. A Monte Carlo model for out-of-field dose calculation from high-energy photon therapy. Med Phys. 2007 ;34 (9):3489-99.

[43]. Kry S, Salehpour M, Followill D, Stovall M, Kuban D, White R,Rosen I. 2005b Out of field photon and neutron dose equivalents from step-and-shoot intensity-modulated radiation therapy. Int J Radiat Oncol Biol Phys 2005b;62:1204-16.

[44] Kry S, Salehpour M, Followill D, Stovall M, Kuban D, White A, Rosen I. The calculated risk of fatal secondary malignancies from intensity-modulated radiaiton therapy. Int J Radiat Oncol Biol Phys 2005a;62:1195-203.

[45]. Kry S, Followill D, White R, Stovall M, Kuban D, Salehpour Uncertainty of calculated risk estimates for secondary malignancies after radiotherapy. Int J Radiat Oncol Biol Phys 2007a;68:1265-71.[47].

[46] Klein E, Maserang B, Wood R, Mansur D. Peripheral doses from pediatric IMRT. Med Phys 2006;33:2325-531.

[47]. Mutic S, Klein E. A reduction in the AAPM TG-36 reported peripheral dose distributions with tertiary multileaf collimation. Int J Radiat Oncol Biol Phys 1999;44:947-53.

[48]. Vlachopoulou V, Malatara G, Delis H, Theodorou K, Kardamakis D, Panayiotakis G. Peripheral dose measurement in high-energy photon radiotherapy with the implementation of MOSFET. World J Radiology. 2010;2(11):434-439.

[49]. Taylor ML, McDermott LN, Johnston PN, Haynes M, Ackerly T, Kron T, et al. Stereotactic fields shaped with a micro-multileaf collimator: Systematic characterisation of peripheral dose. Phy Med Biol 2010b:55 873-81.

[50]. Schönfeld AB, Poppinga D, Kranzer R, et al. Technical Note: Characterization of the new microSilicon diode detector. Med Phys. 2019;46(9):4257-4262.

[51]. Abdelaal AM, Attalla EM, Elshemey WM. Estimation of Out-of-Field Dose Variation using Markus Ionization Chamber Detector. SciMedicine Journal. 2020 Mar 1;2(1):8–15.

[52]. Yoon J, Heins D, Zhao X, Sanders M, Zhang R. Measurement and modeling of out-of-field doses from various advanced post- mastectomy radiotherapy techniques. Phys Med Biol. 2017;62(23):9039-9053.

[53]. Garrett L, Hardcastle N, Yeo A, Lonski P, Franich R, Kron T. Out-of- field dose in stereotactic radiotherapy for paediatric patients. Physics and Imaging in Radiation Oncology. 2021;19:1-5.

[54]. Farhood, B., & Ghorbani, M. Dose calculation accuracy of radiotherapy treatment planning systems in out-of-field regions. Journal of Biomedical Physics & Engineering, 2019; 9(2), 133.

[55]. Schönfeld AB, Poppinga D, Kranzer R, et al. Technical Note: Characterization of the new microSilicon diode detector. Med Phys. 2019;46(9):4257-4262.

[56]. Barnett E, MacKenzie M, Fallone BG. IMRT point dose measurements with a diamond detector. Radiol Oncol. 2005; 39(1).

[57]. Poppinga D, Kranzer R, Ulrichs AB, Delfs B, Giesen U, Langner F, Poppe B, Looe HK. Three-dimensional characterization of the active volumes of PTW microDiamond, microSilicon, and Diode E dosimetry detectors using a proton microbeam. Med Phys. 2019 ;46(9):4241-4245.

[58]. Paliwal B, Yan Y, Yadav P, Bassetti M, Du K, Saenz D et al. Dosimetric differences in flattened and flattening filter-free beam treatment plans. Journal of Medical Physics. 2016;41(2):92.

[59]. Zhuang M, Zhang T, Chen Z, et al. Advanced nasopharyngeal carcinoma radiotherapy with volumetric modulated arcs and the potential role of flattening filter-free beams. Radiat Oncol. 2013; 8:120.

[60]. Gasic D, Ohlhues L, Brodin NP, Fog LS, Pommer T, Bangsgaard JP, Munck Af Rosenschöld P. A treatment planning and delivery comparison of volumetric modulated arc therapy with or without flattening filter for gliomas, brain metastases, prostate, head/neck, and early-stage lung cancer. Acta Oncol. 2014 ;53(8):1005-11.

[61]. Vassiliev ON, Kry SF, Chang JY, Balter PA, Titt U, Mohan R. Stereotactic radiotherapy for lung cancer using a flattening filter-free Clinac. J Appl Clin Med Phys. 2009;10(1):2880.

[66]. Casolaro P. Radiochromic Films for the Two-Dimensional Dose Distribution Assessment. Applied Sciences. 2021; 11(5): 2132.

[67]. Niroomand-Rad A, Chiu-Tsao S, Grams M, Lewis D, Soares C, Van Battum L et al. Report of AAPM Task Group 235 Radiochromic Film Dosimetry: An Update to TG-55. Medical Physics. 2020;47(12):5986-6025.

[68]. Midhun C, Musthafa M, Akbar S, Cyriac S, Sajeev S, Joseph A et al.SpectroscopyofHigh-IntensityBremsstrahlungUsingComptonRecoiledElectrons.NuclearScienceandEngineering.2019;194(3):207-212

[69]. Williams EJ. Multiple scattering of fast electrons and alpha-particles, and“curvature” of cloud tracks due to scattering. Phys Rev. 1940;58(4):292-306.

[70] Goudsmit S, Saunderson JL. Multiple scattering of electrons. II. Phys Rev. 1940;58(1):36-42.

[71]. Snyder H, Scott W. Multiple Scattering of Fast Charged Particles. Physical Review 1949;76(2):220-225.

[72]. Voskresenskaya O, Tarasov A. Molìere’s multiple scattering theory revisited. 2014.

[73] Bethe H. Molière's Theory of Multiple Scattering. Physical Review. 1953;89(6):1256-1266.

[74] Yurchenko VI. On the theory of multiple scattering. J Exp Theor Phys. 1999;89(2):223-231.

[75]. Bednyakov AA. On the Molière theory of multiple scattering of charged particles (1947–1948) and its critique in subsequent years. Phys Part Nucl. 2014;45(5):991-999.

[76]. Faiz M Khan, Physics of Radiation Therapy, 4th Edition, Lippincott Williams & Wilkins, Baltimore, USA 2013, pp. 39-42.

[77]. Podgorsak E.B, Radiation Oncology Physics: A Handbook for Teachers and Students, IAEA, Vienna-Austria, 2005, pp. 136-156.

[78]. N Papanikolaou, J Battista, A Boyer, C Kappas, E Klein, T Mackie, M Sharpe, J Van Dyk Tissue inhomogeneity corrections for megavoltage photon beams. AAPM Report No. 85, Task Group No 65 of the Radiation Therapy Committee of the American Association of Physicists in Medicine, 2004, Task Group No 65. [82]. Clements M, Schupp N, Tattersall M, Brown A, Larson R. Monaco treatment planning system tools and optimization processes. Med Dosim. 2018;43(2):106-117.

[79]. Dogan N, Leybovich LB, Sethi A. Comparative evaluation of Kodak EDR2 and XV2 films for verification ofintensity modulated radiation therapy. Phys Med Biol. 2002;47(22):4121–4130

[80]. Zhu X, Jursinic P, Grimm D, et al. Evaluation of Kodak EDR2 film for dose verification of intensity modulatedradiation therapy delivered by a static multileaf collimator. Med Phys. 2002;29(8):1687–1692.

[81]. Dempsey JF, Low DA. Dosimetry of therapeutic photon beams using an extended dose range film. Med Phys. 2002;29(10):2438–2445.43..

[82]. Clements M, Schupp N, Tattersall M, Brown A, Larson R. Monaco treatment planning system tools and optimization processes. Med Dosim. 2018;43(2):106-117

[83]. Van den Heuvel F, Defraene G, Crijns W, Bogaerts R. Out-of-field contributions for IMRT and volumetric modulated arc therapy measured using gafchromic films and compared to calculations using a superposition/convolution based treatment planning system. Radiotherapy and Oncology. 2012;105(1):127-32.

[84]. Fogliata A, Clivio A, Vanetti E, Nicolini G, Belosi MF,1Cozzi L. Dosimetric evaluation of photon dose calculation under jaw and MLC shielding. Med Phys. 2013 ;40(10):101706.

[85]. Low DA, Dempsey JF. Evaluation of the gamma dose distribution comparison method. Medical physics. 2003;30(9):2455-64.

[86]. Fogliata A, Nicolini G, Vanetti E, Clivio A, Cozzi L. Dosimetric validation of the anisotropic analytical algorithm for photon dose calculation: fundamental characterization in water. Physics in medicine and biology. 2006;51(6):1421.

[87]. Rana SB. Dose prediction accuracy of anisotropic analytical algorithm and pencil beam convolution algorithm beyond high- density heterogeneity interface. South Asian journal of cancer. 2013; 2(1):26.

[88]. Lu L. Dose calculation algorithms in external beam photon radiation therapy. International Journal of Cancer Therapy and Oncology. 2013;1(2).

[89]. Stathakis S. Ionization chamber array for patientspecific VMAT, Tomotherapy and IMRT QA.InJournal of Physics: Conference Series 2010 ; 250(1). 012029.

[90]. Code of practice: OCTAVIUS 4D How to start (Eclipse). Technical Note, D913.200.02/02.

[91]. Teoh M, Clark CH, Wood K, Whitaker S, Nisbet A. Volumetric modulated arc therapy: a review of current literature and clinical use in practice. The British journal of radiology. 2011Nov;84(1007):967-9.

[92]. Low DA. Gamma dose distribution evaluation tool. InJournal of Physics-Conference Series 2010; 250(1),012071.

[93]. Subramanian S, Thirumalaiswamy S, Srinivas C, Gandhi GA, Kathirvel M, Kumar KK, Mallik S, Babaiah M, Pawar Y, Clivio A, Fogliata A, Mancosu P, Nicolini G, Vanetti E, Cozzi L. Chest wall radiotherapy with volumetric modulated arcs and the potential role of flattening filter free photon beams. Strahlenther Onkol. 2012 ;188(6):484-90.

[94]. Yan Y, Yadav P, Bassetti M, Du K, Saenz D, Harari P, Paliwal BR. Dosimetric differences in flattened and flattening filter-free beam treatment plans. J Med Phys. 2016 41(2):92-9.

[95]. Spruijt KH, Dahele M, Cuijpers JP, Jeulink M, Rietveld D, et al. Flattening filter free vs flattened beams for breast irradiation. Int J Radiat Oncol Biol Phys. 2013;85:506-513.

[96]. Thomas E, Popple R, Prendergast B, Clark G, Dobelbower M, Fiveash J. Effects of flattening filter-free and volumetric-modulated arc therapy delivery on treatment efficiency. Journal of Applied Clinical Medical Physics. 2013;14(6):155-166.

[97]. Kry SF, Vassiliev ON, Mohan R. Out-of-field photon dose following removal of the flattening filter from a medical accelerator. Phys Med Biol . 2010;55:2155-2166.

[98]. Barnett E, MacKenzie M, Fallone BG. IMRT point dose measurements with a diamond detector. Radiol Oncol. 2005;39(1).

[99]. Zakaria GA, Schuette W. Determination of absorbed dose to water for high-energy photon and electron beams-comparison of the standards DIN 6800-2 (1997), IAEA TRS 398 (2000) and DIN 6800-2 (2006). J Med Physc AssociatcMedic Physic India. 2007;32(1):3.

[100]. Wrya Parwaie, Soheila Refahi, Mahdieh Afkhami Ardekani, Bagher Farhood. Different Dosimeters/Detectors Used in Small-Field Dosimetry: Pros and Cons J Med Signals Sens. 2018; 8(3): 195–203.

[101]. Podgosark E.B (2006) Radiation Physics for Medical Physicists (Biological and Medical Physics, Biomedical Engineering) (second edi) Heidelberg Dordrecht London New York ,Springer.

[102]. Sharma S. Challenges of small photon field dosimetry are still challenging. Journal of Medical Physics. 2014;39(3):131.

[103]. Laub WU, Wong T. The volume effect of detectors in the dosimetry of small fields used in IMRT. Med Phys. 2003;30(3):341-347.

[104]. Vatnitsky S, Jarvinen H. Application of a natural diamond detector for the measurement of relative dose distributions in radiotherapy. Phys Med Biol. 1993;38(1):173-184.

[105]. Rustgi SN, Frye DM. Dosimetric characterization of radiosurgical beams with a diamond detector. Med Phys. 1995;22(12):2117-2121.

[106]. Moliere G. Theorie der Streuung schneller geladener Teilchen I. Einzelstreuung am abgeschirmten Coulomb-Feld1. Zeitschrift fur Naturforsch - Sect A J Phys Sci. 1947;2(3):133-145.

[107]. Moliere G. Theorie der Streuung schneller geladener Teilchen II Mehrfach-und Vielfachstreuung1. Zeitschrift fur Naturforsch - Sect A J Phys Sci. 1948;3(2):78-97.

[108]. Matney JE, Parker BC, Neck DW, Henkelmann G, Rosen II. Evaluation of a commercial flatbed document scanner and radiographic film scanner for radio chromic EBT film dosimetry. J ApplClinical Med Phys.2010 ;11(2):198–208.

[109]. Zhu XR, Jursinic PA, Grimm DF, Lopez F, Rownd JJ, Gillin MT. Evaluation of kodak EDR2 film for dose verification of intensity modulated radiation therapy delivered by a static multileaf collimator. Med Phys. 2002;29(8):1687–92.

[110]. Mohammadi M, Bezak E, Reich P.The use of extended dose range film for dosimetric calibration of scanning liquid-filled ionization chamber electronic portal imaging device. J ApplClin Med Phys. 2007;8(1):69–84.

[111]. Arnfield M, Otto K, Aroumougame V, Alkins R. The use of film dosimetry of the penumbra region to improve the accuracy of intensity modulated radiotherapy. Medical Physics. 2004;32(1):12-18.

[112]. Zilbergleit M, Temruk V. Package ImageJ. Application for image processing obtained scanning electronic microscopy (paper analysis). Polymer materials and technologies. 2017;3(1):71-74.

[113]. Schneider C, Rasband W, Eliceiri K. NIH Image to ImageJ: 25 years of image analysis. Nature Methods. 2012;9(7):671-675.

[114]. Breitman K, Rathee S, Newcomb C, Murray B, Robinson D, Field C, Warkentin H, Connors S, Mackenzie M, Dunscombe P, Fallone G. Experimental validation of the Eclipse AAA algorithm. J ApplClin Med Phys. 2007;10;8(2):76-92..

[115]. Compton A.A Quantum Theory of the Scattering of X-rays by Light Elements. Physical Review. 1923; 21(5):483-502.

[116]. Breit G.A Correspondence Principle in the Compton Effect.Physical Review. 1926;27(4):362-372.

[117]. High-Intensity Bremsstrahlung Using Compton Recoiled Electrons.Nuclear Science and Engineering. 2019;194(3):207-212.

[118]. NISHINA Y. The Polarization of Compton Scattering according to Dirac's New Relativistic Dynamics. Nature. 1928; 122(3083):843-843.

[119]. Snyder H, Scott W. Multiple Scattering of Fast Charged Particles. Physical Review. 1949;76(2):220-225.

[120]. Hanson A, Lanzl L, Lyman E, Scott M. Measurement of Multiple Scattering of 15.7-Mev Electrons.Physical Review. 1951;84(4):634- 637.

[121]. Nigam B, Sundaresan M, Wu T. Theory of Multiple Scattering: Second Born Approximation and Corrections to Molière's Work. Physical Review. 1959;115(3):491-502.

[122]. Lewis H. Multiple Scattering in an Infinite Medium.Physical Review. 1950;78(5):526-529.